

University of Alberta

Examination of the Building Recommissioning Process inside Variable Air Volume
(VAV) Systems with Direct Digital Control (DDC)

by

Wayne E. Klaczek



A thesis submitted to the Faculty of Graduate Studies and Research in partial fulfillment
of the requirements for the degree of Master of Science

Department of Mechanical Engineering

Edmonton, Alberta
Fall 2004



Library and
Archives Canada

Bibliothèque et
Archives Canada

Published Heritage
Branch

Direction du
Patrimoine de l'édition

395 Wellington Street
Ottawa ON K1A 0N4
Canada

395, rue Wellington
Ottawa ON K1A 0N4
Canada

Your file *Votre référence*

ISBN: 0-612-95785-3

Our file *Notre référence*

ISBN: 0-612-95785-3

The author has granted a non-exclusive license allowing the Library and Archives Canada to reproduce, loan, distribute or sell copies of this thesis in microform, paper or electronic formats.

L'auteur a accordé une licence non exclusive permettant à la Bibliothèque et Archives Canada de reproduire, prêter, distribuer ou vendre des copies de cette thèse sous la forme de microfiche/film, de reproduction sur papier ou sur format électronique.

The author retains ownership of the copyright in this thesis. Neither the thesis nor substantial extracts from it may be printed or otherwise reproduced without the author's permission.

L'auteur conserve la propriété du droit d'auteur qui protège cette thèse. Ni la thèse ni des extraits substantiels de celle-ci ne doivent être imprimés ou autrement reproduits sans son autorisation.

In compliance with the Canadian Privacy Act some supporting forms may have been removed from this thesis.

Conformément à la loi canadienne sur la protection de la vie privée, quelques formulaires secondaires ont été enlevés de cette thèse.

While these forms may be included in the document page count, their removal does not represent any loss of content from the thesis.

Bien que ces formulaires aient inclus dans la pagination, il n'y aura aucun contenu manquant.

Canada

Acknowledgments

I would like to thank Mark Ackerman and Dr. Brian Fleck for their guidance and support throughout the completion of this thesis. Their technical expertise and dedication to their students cannot be over stated. Several others also contributed to the completion of this work. These included Scott Arnold, Dr. Roger Toogood, Dr. Lorenz Sigurdson, Andrew Coward, Terry Nord, Bernie Faulkner and all the people working in the general office, machine shop and 6th floor labs. I would also like to thank Mr. Jeff Woo who assisted on numerous experiments and is an excellent example of a true engineer.

I would also like to thank my family and friends for keeping me going. My parents, Stan and Joan, and my brother, Kevin, have been essential through the course of my education. T.M. Gunderson and Ellen Buchan also deserve many thanks; the three of us have completed our studies together and they have been truly excellent friends. Finally, I would especially like to thank Kristeena Garrah, who has kept me working since my first year of University. Kristeena is an amazing girl who has been my best friend and grown essential to me.

This research was completed with financial support from the American Society of Heating, Refrigeration, and Air-Conditioning Engineers (ASHRAE) and Mark Ackerman. Personal funding was also received from the Natural Sciences and Engineering Research Council of Canada (NSERC), the University of Alberta, the Mechanical Engineering Department, Dr. Brian Fleck and the Provincial Government to ensure that I was able to finish.

Table of Contents

1.0	Background Information.....	1
1.1	The Definition of Building Recommissioning	2
1.2	Variable Air Volume Design and its Role within HVAC	4
1.3	Direct Digital Control Systems Overview... ..	6
2.0	Statement of Objectives	7
3.0	Literature Review and Theory.....	8
3.1	The Commissioning Process	8
3.2	The Benefits of VAV systems with DDC	9
3.3	Energy and Economic Indicators.....	10
3.4	Health and Wellness Indicators (IAQ).....	11
3.5	Comfort Indicators	13
3.6	Airflow Measurement within HVAC Systems.....	14
3.7	VAV Flow Sensors Theory	14
3.7.1	The Diameter, Number, and Spacing of the Total Pressure Ports.....	16
3.7.1.1	Simplified Case: 2 Total Pressure Ports.....	16
3.7.1.2	Three Total Pressure Port Case	21
3.7.2	Static Pressure Port Location: Pressure Coefficient Dependence	23
3.7.2.1	Cylindrical Model	23
3.7.2.2	Review of other Common Shapes.....	30
3.7.3	Summary of VAV Flow Sensor Response to Velocity Profiles.....	31
4.0	Field Research Methodology	33
4.1	Field Test Locations	33
4.1.1	The Cross Cancer Institute	33
4.1.2	The Timms Center for the Arts	34
4.1.3	The Yellowhead Regional Library	34
4.2	Data Collection Techniques	35
4.2.1	Summary of Data Collected	35
4.2.2	Explanation of DDC Data Trends	36
4.2.3	“Tunable” DDC Parameters for Recommissioning	36
4.3	Project Equipment.....	37
4.3.1	Common Instrumentation.....	37
4.3.2	Overview of DAS and Tracer Gas Injection	38
4.3.3	The MIRAN Gas Analyzer and Tracer Gas Selection	39
4.3.4	General Problems with the Tracer Gas Method	42
4.4	Recommissioning Procedure at Each Facility	43
4.4.1	The Timms Center for the Arts	43
4.4.2	The Cross Cancer Institute	44
4.4.3	The Yellowhead Regional Library	44
4.5	Recommissioning Data Analysis	44
4.6	Sources of Error	47
4.6.1	Instrumentation Error	48
4.6.2	Human Error associated with a Pitot Tube Traverse.....	50
4.6.2.1	Experimental Setup	51
4.6.2.2	Theory	52
4.6.2.3	Results.....	53
5.0	Discussion of Field Results	55
5.1	DDC System Errors.....	55
5.2	Improved DDC System Accuracy.....	56
5.2.1	Methodology for DDC Accuracy Analysis.....	57

5.2.2	Sample Calculations for the Yellowhead Regional Library.....	57
5.2.3	Results of DDC Accuracy Analysis.....	61
5.2.4	Limitations and Benefits of the Analysis.....	64
5.2.5	Methodology for DDC Accuracy (with Trend Data).....	64
5.2.6	Results of DDC Accuracy Analysis (with Trend Data).....	65
5.3	Variations in IAQ due to Recommissioning (with Trend Data).....	67
5.3.1	Tracer Gas Analysis to verify minimum O/A.....	68
5.4	Energy Savings due to Re-Commissioning (with Trend Data).....	70
5.4.1	Simple Economic Considerations.....	72
5.4.2	Methodology for EOL Static Pressure Related Savings.....	73
5.4.3	Results of EOL Static Pressure Related Savings.....	75
5.4.4	Methodology for Supply Fan Energy Savings at the Minimum Setpoint.....	77
5.4.5	Results of the Supply Fan Energy Savings at the Minimum Setpoint.....	78
5.5	Temperature Variations due to the Recommissioning Process.....	80
5.5.1	Methodology for Determining Zone Temperature Accuracy.....	80
5.5.2	Sample Results from the Yellowhead Regional Library.....	81
5.5.3	Discussion of Thermal Comfort.....	82
6.0	Methodology for Laboratory Experiments.....	83
6.1	Laboratory Setup.....	83
6.2	Velocity Profile and Sensor Response.....	86
6.3	Flow Visualization Setup.....	86
7.0	Discussion of Laboratory Experiment Results.....	89
7.1	Baseline (C_{40D}) Experiments used to Standardize the Laboratory Results.....	89
7.2	Non-Ideal Geometry observed in the Field Tests.....	92
7.2.1	Two 90° Elbows in Series.....	92
7.2.2	S-Shaped Bends (Two 45° Elbows in Series).....	93
7.2.3	Concentric Reducers and Expanders (with and without Elbows).....	95
7.3	Discussion of Duct Length Prior to the Sensor.....	98
7.4	Discussion of Greater Flow Errors near the Minimum Flow Setpoint.....	99
7.5	Supporting Flow Visualization Results.....	100
7.6	Summary of Coefficients, Independent of Adequate Duct Length.....	104
8.0	Conclusions.....	106
8.1	The Critical Aspect of Building Recommissioning, in Terms of Longevity.....	106
8.2	The Response of VAV Airflow Sensors.....	108
9.0	Recommendations for Future Work.....	110
10.0	Bibliography.....	112
Appendix A: Theoretical Calculations.....		116
1)	Fluid Mechanics for the Case of 3 Total Pressure Ports.....	117
2)	Sample Calculations for the VAV airflow sensor Model.....	123
Appendix B: Sample Calculations and Results of Field Testing.....		129
1)	DDC system accuracy Tables.....	130
2)	Degree-Day Analysis.....	142
Appendix C: Sample Calculations and Results of Laboratory Experiments.....		145
1)	Summary of Laboratory Results.....	146

List of Tables

Table 1: Summary of Other Likely Cylindrical Pressure Coefficients (C_p) for VAV Sensors* ...	30
Table 2: Important Dates for Data Collection at each of the Field Testing Locations	35
Table 3: Summary of the test variables considered for each of the field tests	36
Table 4: List of common Instruments used within the Field-tests.....	37
Table 5: Summary of Results for Human Error associated with a Pitot Tube Traverse.....	53
Table 6: Summary of % Changes*	54
Table 7: Recommissioning Airflow Measurements at the Yellowhead Library*	58
Table 8: Linear Calibration Equations for the Yellowhead Regional Library*	59
Table 9: Flow Error at the midpoint of the VAV range for the Yellowhead Library*	60
Table 10: Improvement for the Yellowhead Regional Library*	61
Table 11: Summary of DDC Accuracy Analysis Improvements for all VAV Terminals	62
Table 12: Results of DDC Accuracy (with trend data) to gauge IAQ*	66
Table 13: EOL Static Pressure Sensor Energy Savings*	75
Table 14: Energy Savings at the Minimum Airflow Setpoint (during heating mode)*	78
Table 15: Improvements at the Minimum Airflow Setpoint (during heating mode)*	79
Table 16: Summary of Equipment needed for the Upstream Laboratory Experiments	83
Table 17: Summary of Equipment needed for the Flow Visualization Experiments	87
Table 18: Baseline (C_{40D}) results for Laboratory test of the VAV Terminals*	89
Table 19: Summary of the most significant Amplification Loss, μ (Average)*	105
Table 20: Summary of the most significant Precision Loss, σ (Standard Deviations)*	105

List of Figures

Figure 1: A simplified schematic of a VAV system, in this case with three zones serviced by three VAV airflow terminals and one supply duct, note the EOL sensor location.....	5
Figure 2: Internals of a typical VAV terminal.....	15
Figure 3: Simple representation of a typical VAV airflow sensor	16
Figure 4: Resistance circuit analogy of the model being considered	18
Figure 5: More realistic representation of a typical VAV airflow sensor with three forward facing velocity pressure ports.	21
Figure 6: Simple representation of fluid flow past identical blunt bodies.....	24
Figure 7: Simple representation of fluid flow past a cylinder with.....	25
Figure 8: Theoretical representation of surface pressure using Laplace's equation.....	27
Figure 9: Theoretical and experimental representation of surface pressure around a cylinder immersed in the flow.	28
Figure 10: Experimental representation of the separation points around a cylinder	28
Figure 11: Simple comparison of the true airflow rate signal versus the signal indicated by a VAV sensor that utilizes a static pressure port located in the wake region.....	29
Figure 12: Theoretical prediction of sensor amplification for a typical 8" VAV airflow sensor using a range of likely pressure coefficients (C_p) and true velocities (V_T)	32
Figure 13: A schematic of the typical tracer gas injection system setup.....	41
Figure 14: An example of the VAV terminal airflow calibration equations from the BC, AC and the AAC trends (VAV Terminal #1 from the Timms Center).....	45
Figure 15: A typical plot of the error in flow rate	46
Figure 16: A plot of the Error in flow rate (Indicated - Set point) versus the flow set point	47
Figure 17: Experimental setup for the pitot tube laboratory study	51
Figure 18: The equal area method for a pitot tube traverse that is recommended by ASHRAE for round ducts.....	52
Figure 19: Normal Distribution fit for the "ideal" location, full traverse.....	54
Figure 20: A simple representation of the DDC error region associated with a linear VAV terminal calibration.....	57
Figure 21: A simple representation of the DDC error region associated with a linear VAV terminal calibration when compared to the true VAV response.....	63
Figure 22: A typical plot of the outdoor air fraction (O/A).....	70
Figure 23: A typical zone temperature plot.....	82
Figure 24: Examples of common non-ideal duct geometry	84
Figure 25: Sample non-ideal duct geometries that were investigated.....	85
Figure 26: Representation of the three duct geometries that were tested in the flow visualization experiments.....	87
Figure 27: A simple representation of typical laboratory results	90
Figure 28: The sample base line results for the first (a) and second (b) brand of VAV terminal (designated as Type A and B in Table 18, respectively) in the 10" size	91
Figure 29: Experimental flow coefficients for the Type B, 6" VAV terminal	93
Figure 30: Results for the Type A and B, 10" VAV terminal for the S-Shape Geometry	94
Figure 31: Simple representation of expected airflow behavior through a concentric reducer (a) and a concentric expander (b).....	95
Figure 32: Results for the Type A, 6" VAV terminal for the 10" to 6" reducer geometry	96
Figure 33: Experimental results for the 8" to 10" expander, Type B VAV terminal.....	97
Figure 34: Results for the Type B, 6" VAV terminal for the 10" to 6" reducer geometry with a 90° elbow	98
Figure 35: Usable operational range of the 10" VAV Terminals within the 40D ideal base line test for Terminal Type A and B.	100

Figure 36: Flow visualization results for the straight duct configuration..... 101
Figure 37: Flow visualization results for the concentric reducer where the damper positions are
fully open or 90° (a), half closed or 45° (b) and nearly closed or 30° (c)..... 102
Figure 38: Flow visualization results for the 90° elbow where the damper positions are fully open
or 90° (a), half closed or 45° (b) and nearly closed or 30° (c)..... 103

Nomenclature

#D – This is a common HVAC reference that refers to the number of straight, unobstructed duct diameters prior to the area of interest

AHU or APU – Air Handling Unit or Air Processing Unit, this refers to the central HVAC system at each facility. Although designs differ, this generally includes supply and return fans and an outdoor air mixing mechanism to ensure that fresh air is provided to the facility.

ASHRAE – The American Society of Heating, Refrigeration, and Air-Conditioning Engineers; this is the primary organization responsible for defining the codes, standards and design principals of the HVAC industry in North America. Among other things, ASHRAE provides research money for projects that are pertinent to the industry; for instance, the vast majority of the field-testing was funded through ASHRAE RP 1137.

Benchmark – This term is used to describe the results prior to any changes in the control variables. For instance, the 40D laboratory trials are often referred to as the benchmark tests.

BC, AC, AAC – These three terms are used to describe the three time intervals of data collected at each facility where BC refers to the 1st or “as found” conditions, AC refers to the conditions immediately following recommissioning and AAC refers to the conditions after a suitable amount of time has passed for the systems to (possibly) deviate. The time-period between the AC and AAC trends varied at each field location, from a minimum value of 7 months to a maximum value of almost 2 years.

BAS – Building Automation System, in the strictest sense a DDC system is a type of BAS. However, DDC systems are the only type of BAS considered within this thesis, thus the terms are interchangeable for our purposes.

CAV – Constant Air Volume, a varying method of design in HVAC systems where, as the name implies, a constant airflow rate is provided to the space at all times when the system is operational.

DAS – Data Acquisition System, this refers to a number of different PC based systems that were installed at the field test location. The DAS systems were set to record system variables in 10-minute intervals. The specific variables were dependent on the DDC system and what points were already monitored but included things like airflow rate, pressure, and temperature.

DDC – Direct Digital Control, a common type of control systems that monitors and adjusts the heating and ventilation systems within a building.

EOL – End of Line, this term is commonly used to describe the location of a static pressure transducer that is used within a control system feedback loop to change the supply fan speed. The transducer is located on the longest duct run, prior to the last VAV terminal, where the static pressure losses are highest. The rationale is that if the supply fans can supply enough air (i.e. static pressure) for the last VAV terminal then all the terminals prior to that should also be able to operate.

FPT – Function Performance Testing, this is quite similar to the TAB (see below) analysis but this slightly older term was also used within the industry to describe the maintenance of HVAC systems.

HVAC – Heating Ventilating and Air Conditioning, a common term used to describe this facet of the building sciences.

IAQ – Indoor Air Quality, for the purposes of this research this term refers chiefly to amount of outdoor air (or the O/A) provided to each zone. Other possible considerations could include factors like possible contaminants, such as mold or chemical recirculation in the HVAC system.

O/A – Outdoor Air Fraction, the amount of outdoor air, as a percentage of the supply air, provided into each zone or to the system. There is typically a minimum O/A set by ASHRAE Standard 62-1999, which is based on zone occupancy. O/A is also a chief factor in the consideration of IAQ.

Performance Indicators – This term is used to describe things such as energy efficiency, Indoor Air Quality (IAQ), thermal comfort and other factors that can be used to gauge the performance of each VAV system. These indicators were specifically chosen to because they are factors that can be monitored accurately over time, which was a major requirement of the field research.

RP – Research Project, a common descriptor for previous ASHRAE funded research.

TAB – Testing and Balancing, this refers to a portion of the commissioning or recommissioning procedure where the system components are calibrated and tested to ensure that they are accurate. This is an essential component of the commissioning procedure.

VAV – Variable Air Volume terminals or systems, a VAV terminal typically consists of an airflow sensor that is based on differential pressure prior to a damper that is allowed to fluctuate between a minimum and maximum set point position to control ventilation. If a system predominantly uses VAV terminals (VAV boxes) it is referred to as a VAV system.

Symbols

A	=	Cross Sectional area (m^2)
B, m	=	Various linear equation coefficients ($B = y$ -intercept, $m =$ slope)
C	=	Flow Coefficient, the ratio of Q_{VAV}/Q_{TRUE}
C_p	=	Pressure Coefficient (dimensionless)
C_{40D}	=	Pressure Coefficient from the 40D Benchmark experiments (dimensionless)
D, d	=	Various diameter terms (m)
f	=	Pipe Friction factor, function of Re_D (dimensionless)
g	=	Gravitational Constant, $9.81 m/s^2$
K, k	=	Loss Coefficient: K , and the orifice coefficient: k (dimensionless)
L	=	Length (m)
M_{air}	=	Molecular weight of air, simplified mixture (kg/kmol)
N	=	Fan speed (RPM)
O/A	=	Outdoor air fraction (%)
P	=	Air Pressure (Pa)
P_{atm}	=	Local atmospheric pressure (Pa)
P_R	=	Pressure Ratio (dimensionless)
P_S	=	Static Air Pressure (Pa)
P_{STP}	=	DDC system setpoint of EOL static pressure transducer (Pa)
P_T	=	Total Air Pressure (Pa)
P_V	=	Velocity Air Pressure (Pa)
P_∞	=	Air Pressure far from the area of interest (Pa)
Q_I	=	The DDC “indicated” air flowrate (m^3/s , L/s)
Q_M	=	The actual, or “measured” flowrate during field testing (m^3/s , L/s)
Q_S	=	The DDC setpoint airflow rate (m^3/s , L/s)
Q_{TRUE}	=	The “true” airflow rate from a standard measurement (m^3/s , L/s)
Q_{VAV}	=	The VAV sensors indicated airflow rate (m^3/s , L/s)
R	=	Radius (m)
Re_D	=	Reynolds Number, based on diameter (dimensionless)
T	=	Air temperature ($^{\circ}C$)
T_{ERROR}	=	Absolute difference between DDC indicated and true temperature ($^{\circ}C$)
U_C	=	Centerline Velocity (m/s)
U_∞	=	Air Velocity far from the area of interest (m/s)
V	=	Air Velocity (m/s)
V_T	=	True Air Velocity (m/s)
W	=	Power, typically fan power (watts)
z	=	Relative Elevation (m), third component of polar coordinates
\dot{m}	=	Air Mass flow rate (kg/s)
ϕ	=	Velocity Potential (m/s)
∇	=	Gradient Operator
θ	=	Angle measurement ($^{\circ}$ or radians)
ρ	=	Air Density (kg/m^3)
ΔP	=	$(P_1 - P_2)$, change in air pressure between points 1 and 2 (Pa)
ΔP_{EOL}	=	Difference between the actual and the DDC systems indicated EOL pressure (Pa)
ΔQ	=	$(Q_I - Q_M)$, difference between indicated and measured airflow rate (m^3/s , L/s)
μ	=	Mean of a normal distribution
σ	=	Standard Deviation of a normal distribution
ε	=	Difference or Error, this is commonly used to represent the % change

1.0 Background Information

Variable Air Volume (VAV) systems with Direct Digital Control (DDC) are a common form of Heating Ventilation and Air Conditioning (HVAC) system implemented in commercial and institutional buildings. This is largely due to the economic benefits that can be realized with a VAV system responding to varying loads with the flexibility of digital control. However, the complexity of these systems has brought into question the efficiency of VAV systems in real buildings. Thus, these systems can result in poor energy efficiency, compromised comfort, and poor Indoor-Air-Quality (IAQ) that must be addressed during the commissioning, or recommissioning stages.

VAV systems with DDC rely on digital control to adjust the system response and deal with varying environmental conditions; therefore, the proper response of the system is highly influenced by the accuracy of the various control sensors. If the sensors are not calibrated correctly, the DDC system will quickly deviate from the design intent (the design intent simply refers to the expected building operation when it is first constructed). Thus, many building occupants suffer from poor air quality or uncomfortable conditions; furthermore, many building owners are not realizing the savings that were promised by their newly installed or renovated VAV systems. Often these problems are associated with implementing digital controls, whether the problem stems from programming errors, faulty controllers, or even conceptual problems related to how mechanical systems actually operate.

For the last 20 years it has been recognized that a building commissioning procedure, or a recommissioning procedure (for existing facilities), is beneficial to ensure that VAV systems with DDC operate as they were intended. The exact definitions of commissioning, or recommissioning (within existing facilities), are well established; however, the scope and magnitude of a commissioning procedure can vary considerably. There is no universal recommissioning procedure because of the large variations that exist in HVAC designs (including VAV systems with DDC) and building conditions. There are also conflicting thoughts on the consequences and most importantly, the procedure involved with recommissioning. In order to outline a universal VAV recommissioning procedure that will be useful to the HVAC industry, it is first necessary to complete additional research into these systems. There is a need for objective research on the recommissioning process of VAV systems with DDC. This thesis explores aspects of VAV systems equipped with DDC; specifically, this includes the approximate longevity of recommissioning. Secondary objectives of this research deal with the response of

VAV airflow sensors, focusing on the accuracy and precision that can be expected from a typical recommissioning procedure. The Literature Review (Section 3.0) has indicated that recommissioning is a worthwhile exercise purely from an economic standpoint; it has also been recognized that benefits to factors such as IAQ, thermal comfort, and improved zone control can often exceed the economic benefits. Past research has shown that VAV systems with DDC are prone to poor sensor calibrations, control errors and mechanical breakdowns due to the increased complexity of the components; this dramatically reduces energy efficiency and economic benefits while compromising zone control, occupant comfort, and DDC accuracy. The consequences of poor system operation will only continue to grow more importance as societal concerns over environmental and economic issues continue to increase¹.

1.1 The Definition of Building Recommissioning

It has been consistently shown that the commissioning process is critical in ensuring that VAV systems with DDC operate to the intended design (this point is further discussed in the Literature Review, Section 3.0). Commissioning is a broad term in the building sciences that has grown in complexity and scope over the years. The original term was developed in 1984 when ASHRAE started a committee in response to industry demands; the first guideline was developed several years later in 1989. Originally, the term applied only to new developments and was often confused with Functional-Performance-Testing (FPT), which is a verification of system equipment. Since that time, the term commissioning has evolved into a very complicated and detailed procedure, which when done correctly, can provide substantial economic and health benefits to occupants of new and existing buildings. When completed correctly, a commissioning, or even a recommissioning procedure is often justified by only the economic benefits, in addition to the obvious improvements in health and comfort. “Total building commissioning” is the broadest and most commonly used term; it involves checking every system related to the operation of a building, including the HVAC systems. This process would begin prior to the design phase and continue after the building was occupied. It usually requires a team of professionals including engineers, managers, technicians, system experts, and a commissioning authority that leads and manages the team while representing the building owners. The ASHRAE (2003) HVAC Applications Handbook describes the commissioning process as:

¹ Recent environmental initiatives continue to focus on the building sciences, such as the Canadian Government’s Federal Building Initiative (FBI) department, which funds R&D to improve building energy efficiency.

Commissioning is a quality assurance process for buildings from predesign through design, construction, and operations. It involves achieving, verifying, and documenting the performance of each system to meet the building's operational needs within the capabilities of the documented design and equipment capabilities, according to the owner's functional criteria.... Commissioning can be applied to the building as a total system, which includes structural elements, building envelope, life safety features, electrical systems, communication systems, plumbing, irrigation, controls, and HVAC systems.

The term recommissioning, or the more recent term retrocommissioning, refers to the application of a commissioning process to an existing facility that is already occupied. The scope of recommissioning work is often confused with a Testing-and-Balancing (TAB) procedure, which involves only operational checks of the system and equipment, similar to FPT. Retrocommissioning involves the evaluation of all building systems, which are compared to the original design intent; thus, if the space usage has changed over time the design is actually altered to conform to the new requirements. It is agreed by most sources, including ASHRAE, that the recommissioning process is beneficial; however, the recommissioning process is also significantly more expensive and difficult than simply commissioning the building at the start of the project. The ASHRAE (2003) HVAC Applications Handbook definition of retrocommissioning is:

Retrocommissioning involves systematically investigating, analyzing, and optimizing performance of existing equipment, systems, and assemblies that have not been recently commissioned, and ensuring their continued performance over time....
retrocommissioning has broad application to virtually every building type and vintage with excellent cost-benefit and ratios...

The formal recommissioning process is a very detailed process and is typically quite expensive. For the purposes of this research, it is important to note that a full systems recommissioning process was never completed, at least not in the entirety of the definition. First, the focus of this research was on HVAC systems (specifically VAV systems with DDC) and did not consider other building factors. This is acceptable because the HVAC systems are of primary interest. Although it is worth mentioning that the accepted industry definition of commissioning is often limited to HVAC regardless of the true definition. Second, the test buildings were recommissioned to the original system setpoints but drastic changes to the original design were

not made. This second limitation was unfortunate, since the determination of major system flaws is one of the most useful aspects of recommissioning. This limitation was imposed on the research for two reasons:

1. It was assumed that the original design was still adequate for maintaining the space requirements. It was later verified that the space conditions did not change excessively within any of the test locations (over the approximately 2 years considered here) and that these VAV systems all allowed for suitable variation in the load (i.e. the systems were over-designed to compensate for the variations).
2. Building operators were generally unwilling to implement major changes to systems that had been functioning “adequately” for a number of years. This was primarily due to economic considerations. Thus, the research focused on fixing calibration errors. It should also be noted that these facilities were all operating for a number of years, thus, no major design changes were required.

The results of this research are valid despite the fact that a formal recommissioning procedure was not completed in its entirety (a modified recommissioning procedure was completed, which is discussed in Section 4.0). The possible benefits of completing this additional work would not be sufficient to justify the large time and cost requirements.

1.2 Variable Air Volume Design and its Role within HVAC

VAV systems are capable of maintaining several different zones with adequate outdoor air, ventilation, cooling, or heating and are versatile enough to complete these operations independently of each other by using separate air terminals. Each terminal is equipped with an airflow sensor, which typically differential pressure and is calibrated for accuracy to monitor the airflow into each zone. The terminals can also be equipped with heating coils for improved zone temperature control, although for the majority of cases VAV systems are used in cooling applications. A secondary heating system, like baseboard heaters, is added if required. A basic VAV system is shown schematically in Figure 1.

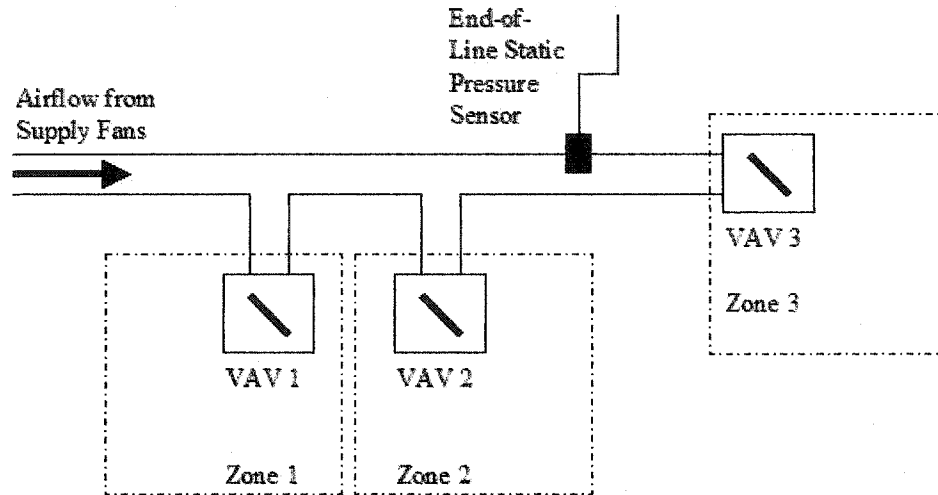


Figure 1: A simplified schematic of a VAV system, in this case with three zones serviced by three VAV airflow terminals and one supply duct, note the EOL sensor location.

Supply air is provided into one central air duct and the supply fan speed (and thus flow rate) is controlled using DDC and the End-of-Line (EOL) static pressure transducer. The end-of-line transducer, as the name implies, is located upstream of the last VAV terminal on the longest duct run, or where the pressure losses are the greatest. The supply fans will then increase or decrease in speed to provide the last VAV terminal (designated VAV 3 in Figure 1) with adequate static pressure, or airflow, while the other VAV terminals are allowed to modulate open and closed as they respond to the loads of each individual zone. The minimum damper position is a function of the ventilation requirements for the space, such as the minimum allowable amount of outdoor airflow; VAV terminals are seldom designed to fully close. The damper position then changes to control the inflow of air, which is usually cooler than room air. Thus, the VAV operating point is often controlled by cooling needs, which are stipulated by zone thermostats.

VAV systems provide several distinct advantages over other HVAC systems. The capital costs of VAV systems are generally quite low, relative to other systems, since only one central duct is required and the installation time is reduced. In addition, since the supply fan power requirements are directly dependent on the VAV damper positions (through the static losses that occur as terminals are opened and closed) the supply fan is able to immediately reduce flow if less ventilation is required. Thus, the system automatically consumes only as much fan power as required for the zone conditions at a particular time, minimizing the operational costs. Finally,

improved zone control is one of the largest benefits of a VAV system. Different temperature and ventilation conditions can be maintained in each zone using the same HVAC system.

1.3 Direct Digital Control Systems Overview

The functions of a DDC will vary with the manufacturer, but they are all used to monitor building conditions and control the mechanical aspects of the HVAC system to ensure adequate conditions are maintained. The majority of DDC systems have several primary control loops running at all times, for instance a feedback loop is used to adjust the supply fan speed based on the EOL static pressure signal (as previously discussed). Other control loops are used to monitor the air temperature in each zone, assign an airflow setpoint, and then adjust the damper (between the minimum and maximum setpoints) to maintain an adequate zone temperature. DDC systems also typically have alarm codes for system errors. For instance, if a terminal has exceeded the maximum airflow setpoint or if a zone temperature has become too high a DDC alarm code is initiated. All DDC systems also have the ability to provide data “trends” that indicate the setpoints and measured response of the system, for each air terminal and for the central Air Handling Unit (AHU). It is important to note that the standard definition of a data “trend” implies that a group of data has been analyzed and that the results suggest some sort of pattern; however, there is a secondary HVAC definition where a DDC system is said to produce “trend” data. This output is simply the HVAC system variables monitored with the DDC system, over time. For the purposes of this research, data trends will refer to the output of DDC systems and not to recognizable patterns found in data after post processing. Each DDC also allows calibration factors to be applied to the instrumentation used to monitor the HVAC system; for instance, individual calibration factors are input into the DDC to convert the differential pressure signal from each VAV terminal into an airflow signal. The use of DDC data trends was of pivotal importance to the completion of this research. Clearly, the reliability of these data trends is dependent on the accuracy of the DDC systems instrumentation (pressure transducers and thermostats for the most part). Thus, the calibration and adjustment of the DDC calibration factors was a central requirement of the field research. There were also instances when the control system loops were modified; however, the majority of the commissioning improvements were made to the DDC system.

2.0 Statement of Objectives

There is a need within the building sciences (and the HVAC community) for quantitative experimental research that concerns the recommissioning of VAV systems equipped with DDC. Specifically, there is a lack of research dealing with the following topics:

- 1) Determination of the most significant portion of the recommissioning process for VAV systems with DDC using field research. The factors that most significantly affect recommissioning longevity can be hypothesized (such as terminal calibrations within the DDC System) but they have never been determined on the basis of longevity.
- 2) Estimate the longevity of recommissioning VAV systems with DDC. This will be a significant finding because no past research has focused on this topic for these systems.
- 3) An understanding into how VAV airflow sensor accuracy is related to system performance, from a recommissioning standpoint. This topic focuses on VAV airflow response in relation to different upstream flow conditions, and the identification of the “worst” upstream conditions, from a recommissioning standpoint.

Both field research and laboratory experiments were required to answer these questions. Field research was undertaken to determine the true effects of recommissioning on existing facilities that have been operational for several years. The primary focus of the field research was the evaluation of what factors were responsible for system longevity, based on the evaluation of energy efficiency, economic benefits, thermal comfort, and IAQ. Secondary objectives included the documentation of the recommissioning process and the development of analysis tools for these types of system. The field research forms the salient portion of this thesis.

It was hypothesized that VAV terminal airflow accuracy was the most significant factor considered when recommissioning these types of systems (this was a hypothesis for the 1st objective). Laboratory experiments were undertaken to determine the effects of upstream conditions on VAV airflow sensor accuracy and response. This included a list of the “worst” upstream duct configurations (which were identified during the field research) in terms of VAV flow sensor amplification loss.

3.0 Literature Review and Theory

VAV systems with DDC have been widely used within the HVAC design community, thus a reasonable amount of previous research has been completed. Past work related to this topic has focused in two areas: the commissioning process and the benefits of VAV systems that includes DDC, or the performance indicators of recommissioning. The first topic outlines the recommissioning procedure and describes the benefits of using VAV systems with DDC over conventional HVAC designs. The second topic deals with indicators that can be used to quantify the benefits of recommissioning VAV systems with DDC, such as: energy and economic efficiency, IAQ, comfort improvements, and DDC accuracy. Unfortunately, there was no past work that has identified the longevity of recommissioning VAV systems with DDC. Likewise, while the response of VAV terminals have been considered (to some degree) there was a shortage of research, especially in relation to VAV response during recommissioning; this lack of research prompted the laboratory experiments. Fluid mechanics was used to estimate the expected response of VAV airflow sensors in relation to different upstream conditions, including past experimental work.

3.1 The Commissioning Process

One of the most common difficulties experienced with the commissioning process is the quantification of improvements made in system performance; this is because commissioning is not a well-defined static process. Although the goals of building recommissioning are generally the same at each facility, the process used to achieve these goals and the reasons why commissioning is undertaken are typically very different. Commissioning agents are forced to modify their approach based on the type of system, the owner's requirements, and the original design intent. There are five stages to the commissioning process: pre-design, design, construction, initial occupancy, and the post-acceptance phase. The benefits of the commissioning procedure are usually related to one of the following categories: economic savings, energy consumption, IAQ, thermal comfort, or DDC accuracy. The following section deals with the recommissioning procedure and some requirements for the process.

Several sources have dealt with recommissioning. Elovitz (1992) provides an excellent summary of the typical HVAC commissioning process, including the development of a commissioning plan, who the commissioning agents are and what role they should play. He argues that building commissioning is important and will increase in importance as systems continue to become more complicated. He specifically mentions the use of VAV systems and comments on the complexity

of VAV with DDC, which he refers to as automation systems, in comparison to older HVAC systems. He states, "The more complex and the more pioneering the system concepts become, the greater the need for the type of testing and analysis that is now called commissioning." Following this argument, it only stands to reason that building systems will continue to become more complex as building technology changes and improves.

Designers, contractors, and building operators generally recognize that recommissioning HVAC systems is worthwhile, although debate continues over the cost-to-benefit ratio, especially in facilities that have been operating for a long time (greater than 15 years). Building operators do not often recognize the cost effectiveness of the full recommissioning process, including verification of the original design intent. Due to budget constraints on older facilities, operators can be hesitant to embrace the recommissioning process since it often competes directly for budget dollars with tangible visible improvement to the building. However, this attitude seems to be diminishing due to continually increasing energy prices and a general societal movement toward more energy efficient homes and buildings. The recommissioning process is becoming increasingly popular because of the improvements that result in energy efficiency, comfort, and IAQ. Ellis (1996) describes a project she completed where a museum/archival facility was recommissioned to deal with a variety of mechanical and control systems problems. The facility incorporated both constant volume and VAV components with a DDC system. When focusing on the VAV components, Ellis determined problems that ranged from installation errors to controller problems to faults in the original design. She goes on to describe the process taken to solve the various problems, although she had difficulties convincing the contractors to implement the changes. Ellis concludes by stating, "...involving a commissioning agent throughout the design and construction process...instead of just for post-construction troubleshooting would have benefited all parties involved in the project." This highlights the importance of following a well-established commissioning procedure, which includes ensuring that the correct personnel are present at the early stages.

3.2 The Benefits of VAV systems with DDC

VAV systems with DDC are common because they have the potential to provide greater energy savings and improved individual control, on a zone-by-zone basis, than conventional systems. ASHRAE (1995) states that, "Variable Air Volume (VAV) systems are popular because they save large amounts of heating, cooling, and fan energy in comparison with other HVAC systems." Numerous papers have been written about the benefits associated with DDC HVAC systems and

some are specific to VAV. Walker (1984) pointed out that “[much] has been written about direct digital control technology and theory, and many arguments are cited to support its superiority over more conventional systems.” More recent work has also identified the benefits of VAV systems. Cappellin (1997) stated that “When variable-air-volume (VAV) systems work right, they provide excellent temperature and humidity control...[and] satisfy ASHRAE Standard 62...” Cappellin (1997) further outlines how VAV systems can frequently malfunction and makes a sound argument for a “comprehensive commissioning process”, which he recommended should remain an integral part of the design, installation, and operation processes. For the purposes of this research, VAV systems with DDC are generally treated as the best alternative for HVAC systems that are intended to minimize energy costs and maximize individual zone control. However, it is important to acknowledge that most sources that claim VAV systems are superior often refer to the importance of the commissioning process. Thus, the consensus seems to be that although VAV systems are an excellent option, they may behave quite poorly if commissioning is neglected or done improperly.

3.3 Energy and Economic Indicators

The primary goal for the majority of recommissioning projects is to reduce the energy consumption of the structure and thus provide an economic return that will justify some, if not all, of the capital cost. ASHRAE (1995) states “One intent of commissioning is to fully recover the capital investment over the life of the system through management, efficiency, and user satisfaction.” Further research into the economic benefits of commissioning was later completed by Piette et al. (1996) who completed a detailed study on the improved energy efficiency of 16 buildings as a direct result of the commissioning process. Piette et al. (1996) concluded that “[on] average, commissioning was marginally cost-effective on energy savings alone... [and that using] national average [energy] prices, the median payback time is about 3 years.” These results agreed with the preliminary findings of Kjellman et al. (1996) who completed a similar project that focused on quantifying exactly what the energy savings were after commissioning commercial buildings in Southern California. The preliminary results indicated a percentage energy savings that varied between 2.4% and 27%, which corresponded to a payback period of between 1 and 4.3 years (based on the cost of commissioning). Kjellman et al. (1996) also stated, “Recommissioning must be done at periodic intervals to maintain energy savings and operational efficiency” and that “Sensor calibration was generally not done as routine maintenance.” Thus, the TAB procedure was identified as an essential component of the commissioning process and energy savings are generally recognized as one of the most significant justifications for the

commissioning process. It was also shown that the typical payback period is less than 5 years when considering only the economic gains based on the energy savings from building commissioning.

3.4 Health and Wellness Indicators (IAQ)

The improvement of IAQ is another central goal of the recommissioning process, which for the purposes of this research refers almost exclusively to the Outdoor Air Fraction (O/A) provided to each zone. As expected, a great deal of previous work has been completed on the IAQ associated with VAV systems, and the majority of work seems to be quite recent. The reason for this recent work may have been to address speculation that VAV systems could not conform to ASHRAE Standard 62-1999² (previously Standard 62-1989) and could not provide an adequate amount of outdoor air in each zone. This controversy was recognized by Mumma et al. (1994) who stated “The building engineering community has devoted great effort to minimizing the energy costs associated with the operation of building mechanical systems. The result has been the widespread use of VAV Systems...VAV systems as typically designed today conserve considerable energy over many other systems used in the past but fail to meet even the most liberal interpretation of ASHRAE Standard 62-1989.” Mumma et al. (1994) later went on to present a new concept for achieving adequate amounts of outdoor air within each zone while preserving the low energy consumption associated with VAV systems. Bearg (1999) later wrote a similar paper that stressed the importance of IAQ in a VAV equipped facility, which he described as a key “performance evaluation”: here, it is referred to as a performance indicator.

The measurement of O/A can be accomplished in many ways, through both direct and indirect measurements. Direct measurements, such as pitot tubes or hot wire anemometry are generally more accurate and yet more expensive to implement within a DDC system. Thus, indirect measurements such as the concentration or enthalpy balancing techniques are generally used. Bearg (1999) presented a technique that included multipoint continuous monitoring to identify adequate ventilation rates using CO₂ monitoring in each zone. However, it is more common in industry to simply assume that adequate mixing takes place, thus the O/A in each zone is identical, or quite close to the O/A in the supply duct. The difficulty associated with measuring the O/A in each zone is a major criticism of VAV systems and was addressed by Krarti et al. (2000) during the course of ASHRAE RP 980, who specifically dealt with the measurement of

² This ASHRAE standard specifies the minimum outdoor air ventilation rates for various structures and zones, usually referring to the expected occupancy and their activity level.

outside air intake rates in VAV systems using the CO₂ concentration method. Krarti et al. (2000) concluded that due to "...the current CO₂ sensor limitations, this technique [CO₂ monitoring to determine O/A ventilation rates] only works accurately when a single sensor is used to measure outdoor air, return air, and mixed air CO₂ concentrations...". Krarti et al. (2000) further concluded over the course of RP 980 that "...VAV systems present additional complexities compared to CAV systems..." and that "...fixed minimum outside air damper position and volumetric fan tracking are inadequate control strategies to maintain minimum outside air rates in VAV systems." The field research considered in this thesis did originally make use of tracer gas injection and a CO₂ monitoring technique that was similar to the one used by Krarti et al. (2000) during RP 980. However, problems were soon encountered with the CO₂ measurements and the technique was ultimately abandoned (discussed further in Section 4.3.4).

Experimental work, using SF₆ tracer gas, completed by Maki et al. (1997) provided an excellent outline for quantifying VAV system performance in terms of both outdoor air delivery and thermal comfort under normal operating conditions. Maki et al. (1997) make reference to a number of papers completed on VAV performance that considered the system to be constant volume; however, in their research only the normal operation of VAV systems was considered. They concluded that despite several deficiencies, including the fact that, "design intent, commissioning, and recommissioning after modifications were not documented or communicated during building trades...[that the VAV system worked quite well in providing] sufficient outside air to the zone..." During the course of this research the minimum outdoor air percentage for each zone was determined from the original design intent. Tracer gas was then used to experimentally determine the O/A in the supply air stream using the recommendations of Krarti et al. (2000) along with the adequate mixing assumption. The results of this thesis indicated that all of the systems provided adequate IAQ both before and after recommissioning. Therefore, the results of the field tests (which are discussed in Section 5.3) are contrary to the arguments of Mumma et al. (1994) and agree with the results produced by Maki et al. (1997): VAV systems can maintain an adequate O/A.

The determination of DDC accuracy is the last factor that influences IAQ; if the DDC can provide the exact building conditions with a high degree of accuracy, then the building operators or maintenance staff are better equipped to ensure adequate IAQ. The determination of DDC accuracy is not commonly considered as a recommissioning performance indicator although it is always completed during the TAB analysis. The improved accuracy of the DDC system is

essential for fault detection and diagnosis of HVAC systems, a point made by Han et al. (1999): "...both the accuracy of the system model and the quickness in response time...are critical to the performance of the [Fault Detection and Diagnosis] system." The improved accuracy of the DDC system is also an important performance indicator for quantifying the benefits of the TAB procedure, which was a primary consideration.

3.5 Comfort Indicators

Another important justification for building commissioning, or recommissioning, is the improvement of individual zone comfort, which is usually linked to zone control. This is especially true in VAV systems with DDC where the comfort level is to be improved (or at least kept constant) despite the reduced energy usage. There are several variables that affect the comfort level within a space, including: temperature, humidity, or air movement (such as drafts or uneven zone distribution), which make it a subjective term to quantify. For the purposes of this research, only the improvement of thermal comfort was considered. Thermal control is easier to quantify and can be determined by examining the zone temperature control of the VAV systems before and after commissioning. The importance of thermal comfort in HVAC systems has been well outlined in the past by Fanger (1972), who stated, "Creating thermal comfort ... is a primary purpose of the heating and air conditioning industry..." and later provided a detailed analysis that could be used to determine the variables affecting thermal comfort. Previous work completed by Busch (1992) as well as de Dear et al. (1991) also indicates that, despite regional and climate conditions, different cultures have a similar idea of what is a comfortable temperature. Thus, the subjective aspects associated with the improvement of comfort are largely eliminated when considering only thermal comfort. The importance of thermal comfort within HVAC systems cannot be understated; LaBauve et al. (2002) completed a brief study on the effects of temperature and worker productivity from constant air volume and VAV systems and stated "Comfort (specifically thermal comfort) in an office setting is a critical element of a productive working environment". LaBauve et al. (2002) also pointed out that worker productivity is a major economic concern within the vast majority of corporations and cites past research that indicates, "...environmental-related inefficiency can cost companies up to 20% of their annual budget." For the purposes of this research, the primary factors used to determine the improvement in thermal comfort were the accuracy of the zone temperature, the temperature variability in the zone and the systems' ability to control air temperature.

3.6 Airflow Measurement within HVAC Systems

Airflow measurement is very important within a VAV system and during the recommissioning process, thus a brief discussion of common airflow measurement techniques is provided here. A VAV system with DDC could potentially incorporate a variety of airflow sensors. Although sensors often vary in design, they can generally be placed in one of two categories: direct and indirect measurement. One direct measurement technique includes the averaging pitot tube array, which is the most common sensor used within VAV systems. Other direct measurement techniques include electronic thermal anemometry, rotating vane and propeller anemometers, swinging vane anemometers and vortex shedding meters. Common indirect techniques used in VAV systems include an enthalpy or concentration balance, either of which can be used to estimate the O/A from measurements made within the supply, return and mixed air ducts.

The averaging pitot tube array is the most common airflow measurement technique used within VAV systems. The instrument involves a flow sensor that measures the pressure difference between the total and static pressures³ within a duct and converts this to a single reading that is typically an amplified pressure signal. Placing the static pressure port in the wake region provides additional amplification of the pressure differential; which is a very common VAV airflow sensor design. Schroeder et al. (2000) completed an excellent evaluation of the typical airflow measurement errors encountered with several common direct and indirect airflow sensors, and stated that "...averaging the velocity pressure readings across the duct before calculating the velocity...introduces some errors in the measurement. This is especially true when a non-uniform velocity profile exists in the duct..." The behavior of VAV airflow sensors in relation to upstream conditions, thus the local velocity profile, is an essential consideration within this research. Schroeder et al. (2000) state that the accuracy associated with a typical pitot tube is between 1%-5%, and that an averaging pitot tube array is slightly higher. They also state than an averaging pitot tube array has limited accuracy after the air speed drops below 3.0 m/s. It will be shown that these results are consistent with the experimental results completed as part of the laboratory research, specifically concerning the accuracy of VAV averaging flow arrays in response to varying upstream duct conditions (dealt with in Section 7.0).

3.7 VAV Flow Sensors Theory

VAV airflow sensors are simple in design and installation; as such, they are a very common and cost effective way to monitor airflow rates. The sensors utilize a differential pressure signal

³ Note, this is not the true duct static pressure but it is better (for the sake of clarity) to refer to it this way.

(ΔP_{VAV}) to estimate the airflow rate. It is important to note that there are a variety of VAV airflow sensor designs; however, the basic operation of each sensor remains quite similar. There are two critical design concerns within any VAV airflow sensor (note that a sensor is shown in Figure 2):

- 1) The diameter, number, and spacing of the stagnation pressure ports (or “total” pressure ports). These ports face in the direction of the airflow and are meant to provide an average signal, regardless of upstream duct geometries that would affect the velocity profile, and thus the response of the sensor. In particular, the diameter of the pressure ports must be small enough to ensure that there is negligible velocity within the sensor (i.e. the average pressure between the ports is recorded).
- 2) The static pressure port location is suitably located. Manufacturers take steps to make sure that the static port is located within the wake region by adjusting the flow sensor geometry (i.e. cylinders, square cylinders etc.) or even adding flaps to ensure separation takes place. The goal is to ensure that the static pressure signal remains negative, providing an amplified differential signal that allows for a less sensitive (and cheaper) pressure transducer.



Figure 2: Internals of a typical VAV terminal where the flow sensor (blue) is located prior to a circular damper. The total (P_T) and static (P_S) pressure signals are recorded through the red and green tubes that stretch between the center of the flow sensor and the outside of the duct. The following fluid mechanics analysis indicated that if the total pressure (P_T) were recorded along the outside of the duct (i.e. the red tube circled the duct and the arms attached to it from outside the duct) then this would minimize a possible error term. Unfortunately, the current configuration is quite common due to its easy assembly and inexpensive manner.

3.7.1 The Diameter, Number, and Spacing of the Total Pressure Ports

VAV airflow sensor design must be compensated for flow through the total pressure ports.

Unfortunately, there will always be some degree of flow within these types of sensors, simply due to the velocity profiles that are encountered in real world applications. Air is forced into one port at high velocity (if the diameters were incorrectly sized), flow goes through the sensor, and exits through another port. This lowers the amplification of the airflow sensor, thus it is necessary to determine a minimum diameter ratio (d/D : diameter of the total pressure ports versus the diameter of the header tube) to eliminate internal flow⁴. A simple model was used with one sensor arm and two ports, as well as a more realistic case with three pressure ports.

3.7.1.1 Simplified Case: 2 Total Pressure Ports

Consider the following simple example of a VAV airflow sensor (as shown in Figure 3) where only two velocity pressure ports are present, located at points 1 and 2. In this case, the total pressure signal is measured at the extreme right hand side of the figure, and is simply designated as P_T . Note that when hydrostatic forces are neglected that $P_T = P_{2,i}$, where $P_{2,i}$ is simply the interior pressure at 2, since there is no flow from 2 to 3.

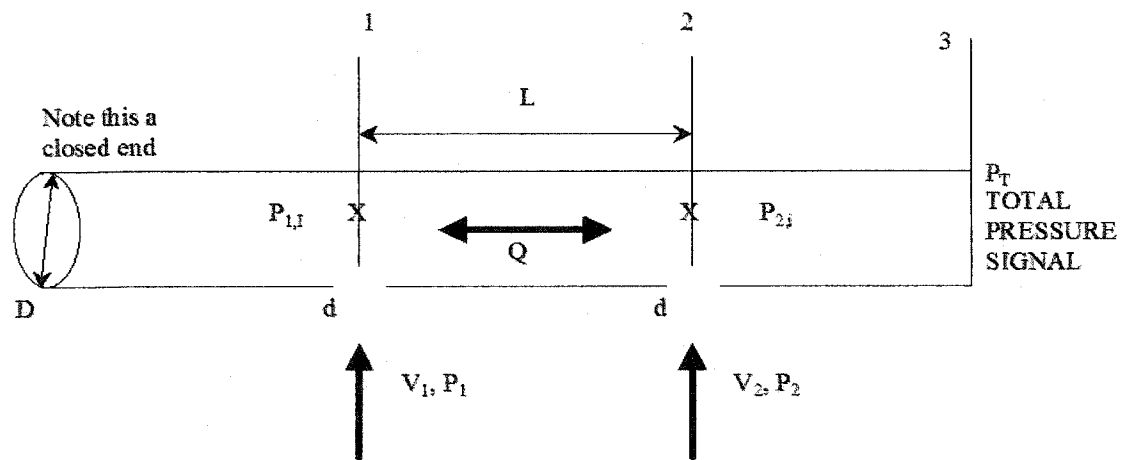


Figure 3: Simple representation of a typical VAV airflow sensor with two total pressure ports. This diagram will be used in the following calculations to estimate the minimum diameter ratio (d/D) required for negligible backflow effects on the total pressure signal. Backflow is represented by Q , which can occur out either port depending on the magnitudes of V_1 and V_2 .

The minimum allowable diameter ratio of the pressure ports to the main tube (d/D) can be determined from the classical Bernoulli Equation for pipe flow along with the orifice and

⁴ Note, in the strictest sense there will always be some internal flow within the sensor. However, with the correct port sizing the magnitude of the flow inside the sensor will become negligible.

conservation of mass equations. Consider the physical system of Figure 3, where V_1 does not necessarily have to equal V_2 and it is more beneficial (for the purposes of this model) if both V_1 and V_2 are left as variables. This will make it possible to describe different velocity profiles, which correspond to different upstream conditions, with the same model. To complete this analysis the goal is to model the VAV total pressure signal as a function of the following variables, [1], which are discussed as they are introduced into the analysis.

$$P_T = P_{2,i} = f(V_1, V_2, d, D, K, L, f, \rho) \quad [1]$$

The first step is to use the basic mass conservation equation, which leads to the conservation of flow rate equation since density is assumed constant throughout the system.

$$\frac{\partial m}{\partial t} = 0 \text{ so that } \dot{m}_1 = \dot{m}_2 \quad [2]$$

$$\rho V_1 A_1 = \rho V_2 A_2 \quad [3]$$

Since the air density (ρ) and area (A) are identical, the velocity through each total pressure port is in equal and opposite direction. Thus, the backflow will occur out the port with the lower velocity. It is then possible to predict the backflow as a function of the diameter ratio (d/D), either as a pressure ratio or a velocity ratio. This is accomplished by considering the Bernoulli equation to model the resistance (or the pressure drop) between $P_{1,i}$ and $P_{2,i}$. Note, in [4] that V_3 refers to the flow within the sensor between points 1 and 2.

$$\frac{P_{1,i}}{\rho} + gz_1 = \frac{P_{2,i}}{\rho} + gz_2 + f \frac{L}{D_3} \frac{1}{2} (V_3)^2 \quad [4]$$

It is possible to re-arrange the terms to achieve the following simple relation. The Q term refers to the flow rate within the sensor between locations 1 and 2 and the A_D term refers to the cross sectional area of the sensor header.

$$\frac{1}{\rho} (P_{1,i} - P_{2,i}) = (gz_2 - gz_1) + f \frac{L}{D} \frac{1}{2} \left(\frac{Q}{A_D} \right)^2 \quad [5]$$

The inclusion of the hydrostatic term ($gz_2 - gz_1$) can be neglected since air is the fluid in this case. VAV airflow sensors will typically incorporate some elevation change between ports, which leads to [6]. It is also important to note that the flow within the sensor will likely be laminar (based on the very small sensor tube diameter: D) so it will be necessary to modify the friction factor (f) later in this analysis.

$$(P_{1,i} - P_{2,i}) = f \frac{\rho L}{2 D} \left(\frac{Q}{A_D} \right)^2 \quad [6]$$

The pressure losses as flow enters the sensor (from P_1 to $P_{1,i}$ and from P_2 to $P_{2,i}$) can be adequately represented by the following equations with identical loss coefficients (K). Using this approach, the flow through ports 1 and 2 are shown to be:

$$Q_1 = A_1 \left[\frac{2(P_1 - P_{1,i})}{\rho K} \right]^{1/2} \quad [7]$$

$$Q_2 = A_2 \left[\frac{2(P_{2,i} - P_2)}{\rho K} \right]^{1/2} \quad [8]$$

Where the loss coefficients (K), areas ($A_1 = A_2 = A_d$, the cross sectional area of the port), and air density (ρ) are equal it can be shown that the following relationship holds:

$$(P_1 - P_{1,i}) = \frac{\rho}{2} K V_1^2 = \left(\frac{Q_1}{A_d} \right)^2 \frac{\rho}{2} K \quad [9]$$

$$(P_{2,i} - P_2) = \frac{\rho}{2} K V_2^2 = \left(\frac{Q_2}{A_d} \right)^2 \frac{\rho}{2} K \quad [10]$$

It is also interesting to note that the pressure within the header is exactly equal to the pressure outside the header, between points 1 and 2 (as shown below).

$$(P_1 + P_2) = (P_{1,i} + P_{2,i}) = \Delta P \quad [11]$$

This relationship can easily be shown by equating the Q terms from [7] and [8]. Recall from [3] that within this model the flow rates must be equal to obey conservation of mass. It is easier to understand what is occurring in the physical model by considering the following resistance analogy, summarized in Figure 4.

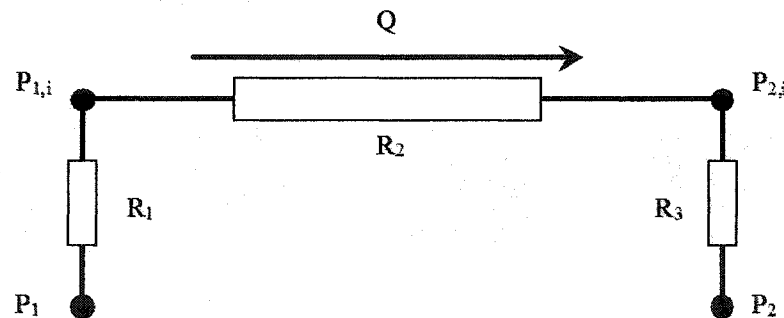


Figure 4: Resistance circuit analogy of the model being considered, note that the values for R_1 , R_2 and R_3 are provided in the following equations, and that $P_{2,i}$ is the variable of interest ($P_{2,i} = P_T$).

Ohm's law is a common analogy used to deal with fluid dynamics. In this case, the pressure loss can be modeled as a resistance loss (R) through a circuit; likewise, the flow rate is modeled as a current (I). It is then possible to make use of the following equation to describe the system:

$$Q = \frac{\Delta P}{\Sigma R} \quad [12]$$

The resistances are then determined from the pressure losses between each of the points considered in the circuit. For instance, the resistance terms R_1 and R_3 can be described using the orifice pressure losses from [9] and [10]. Likewise, the R_2 resistance term is determined from the Bernoulli pipe friction equation, [6]. Thus, all resistance terms necessary to describe this system are provided below.

$$R_1 = \frac{\rho}{2} K \left(\frac{1}{A_d} \right)^2 Q \quad [13]$$

$$R_2 = \frac{\rho}{2} K \left(\frac{1}{A_d} \right)^2 Q \quad [14]$$

$$R_3 = f \frac{\rho L}{2 D} \left(\frac{1}{A_D} \right)^2 Q \quad [15]$$

Notice that the designations for flow rates (i.e. Q_1 versus Q_2) have been all replaced with a generic Q term, since conservation of mass states this must be the case, this has been restated below for clarity.

$$Q = V_3 A_3 = V_2 A_2 = V_1 A_1 = V A_D \quad [16]$$

Thus, using the resistance terms provided in Equations [13], [14] and [15] as well as the circuit equations provided in [12], the following analysis was completed.

$$\Delta P = (P_1 - P_2) = \left[\frac{\rho}{2} K \left(\frac{1}{A_d} \right)^2 Q + \frac{\rho}{2} K \left(\frac{1}{A_d} \right)^2 Q + f \frac{\rho L}{2 D} \left(\frac{1}{A_D} \right)^2 Q \right] Q \quad [17]$$

$$(P_1 - P_2) = \rho \left[\left(\frac{K}{A_d^2} \right) + f \frac{1 L}{2 D} \left(\frac{1}{A_D} \right)^2 \right] Q^2 \quad [18]$$

It is also useful to recall that in all cases the flow rate can be determined from the orifice equations, [7] and [8], which is provided again below for clarity with generic terms simplified through mass conservation.

$$Q^2 = A_d^2 \left[\frac{2(P_{2,i} - P_2)}{K\rho} \right] \quad [19]$$

It is also necessary to recall that the flow within the sensor will be laminar. Thus, it is possible to describe the friction factor (f) within the flow sensor using the Reynold Number (Re_D), as shown, using sensor diameter (D), density (ρ), internal flow (Q) and dynamic viscosity (μ).

$$f = f_{LAMINAR} = \frac{64}{Re_D} = 64 \left(\frac{\pi \mu D}{4 \rho Q} \right) = \frac{16 \pi \mu D}{\rho Q} \quad [20]$$

By substituting the Q^2 term from [19] and the f term from [20] into [18] it is possible to obtain the following, after a little algebra:

$$(P_1 - P_2) = \left[\frac{2K}{A_d^2} + \frac{64}{Re_D} \left(\frac{L}{D} \right) \frac{1}{A_D^2} \right] (A_d)^2 \frac{2(P_{2,i} - P_2)}{K\rho} \quad [21]$$

$$P_{2,i} = P_2 + \frac{P_1 - P_2}{\left[2 + \frac{64}{Re_D} \left(\frac{L}{D} \right) \frac{1}{K} \left(\frac{A_d}{A_D} \right)^2 \right]} \quad [22]$$

$$P_T = P_{2,i} = P_2 + \frac{P_1 - P_2}{\left[2 + \left(\frac{d}{D} \right)^4 \frac{64 \mu L}{[2 \rho K (P_T - P_2)]^{1/2}} \right]} \quad [23]$$

In order to achieve the relationship in [23] it is necessary to relate the velocity (V) terms to the pressure in this system (P). This is accomplished with the Bernoulli equation, where hydrostatic force and pipe friction are neglected to show that:

$$P \approx \frac{1}{2} \rho V^2 \quad [24]$$

With this simplification it is possible to further reduce the physical model of the system in terms of the relative velocities (V_1 and V_2), as follows with one additional P_T term:

$$P_T = \frac{1}{2} \rho V_2^2 + \frac{\frac{1}{2} \rho [(V_1)^2 - (V_2)^2]}{\left[2 + \left(\frac{d}{D} \right)^4 \frac{64 \mu L}{[2 \rho K (P_T - \frac{1}{2} \rho V_2^2)]^{1/2}} \right]} \quad [25]$$

This equation describes the total pressure signal (P_T) that is output from the VAV flow sensor as a function of the relative velocities (V_1 and V_2) at each of the total pressure ports. It is clear from [25] that the equation is slightly more dependent on the total pressure port that is closer to the sampling point; this is a common characteristic of all averaging flow sensors, including VAV sensors. This equation would need to be solved iteratively because it is not possible to separate the P_T term from the denominator. It is also interesting that the diameter ratio figures so prominently in the sensor signal, consider the (d/D) term located in the denominator of [25].

Fortunately (d/D) goes to zero then [25] becomes an expression for the velocity at location 2 (V_2) plus one half the difference between velocities 1 and 2 (V_1 and V_2), as shown below.

$$P_T = \frac{1}{2} \rho V_2^2 + \frac{1}{4} \rho [(V_1)^2 - (V_2)^2] \quad [26]$$

$$P_T = \frac{1}{2} \rho \left[V_2^2 + \frac{(V_1)^2 - (V_2)^2}{2} \right] \quad [27]$$

This is the most likely scenario for a VAV sensor, the effects of which can be seen from an order-of-magnitude analysis. The total pressure diameter (d) typically varies between 0.1 and 0.5 of the sensor diameter (D), thus the 2nd term in the denominator of [25] will be multiplied by a factor of 0.0001 to 0.0625. This verifies that the relationship provided in [27] is the most likely solution to this system. The validity of this analysis is dependent on the local velocity profile and what, in a typical HVAC setting, would constitute a major difference between the velocity experienced at two total pressure ports. Using the equation provided above (and a subsequent equation to describe the effects of the static amplification) it was possible to develop a theoretical model of VAV flow sensor response in relation to varying velocity profiles, discussed in Section 3.7.3.

3.7.1.2 Three Total Pressure Port Case

The previous analysis was a suitable starting point but a survey of local VAV airflow sensor designs indicates that the majority of models have at least three total pressure ports (per arm) facing into the flow. Therefore, it was beneficial to model the case presented in Figure 5.

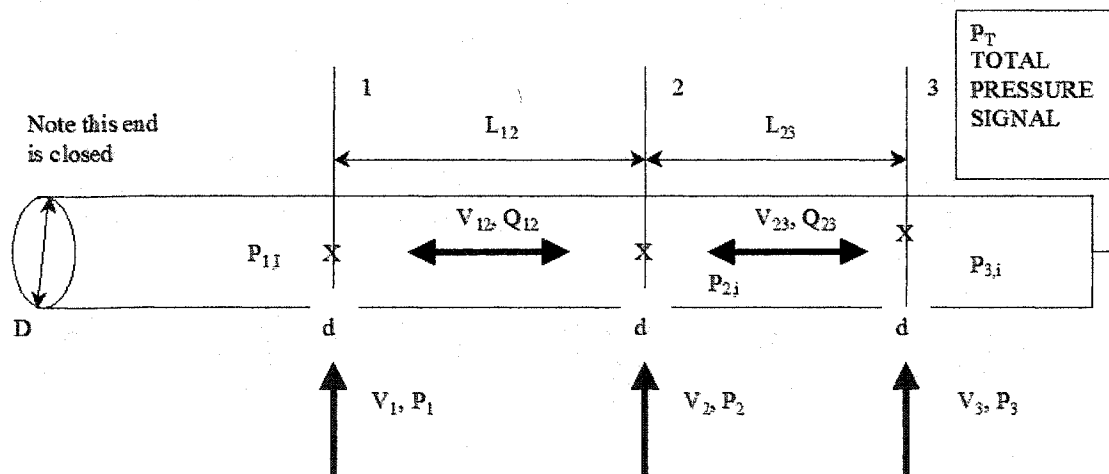


Figure 5: More realistic representation of a typical VAV airflow sensor with three forward facing velocity pressure ports, this diagram will be used in the following calculations to estimate the backflow through the sensor.

Using a similar resistance analysis (note, the steps are available in Appendix A, Section 1) it was determined that the total pressure signal (P_T) to the VAV airflow sensor is represented by the following relationship, [28].

$$P_T = P_{3,i} = P_2 - \frac{\rho}{2} \left(\frac{V_2}{K} \right)^2 + \frac{\rho}{2} \left(\frac{V_3}{K} \right)^2 - \frac{\rho}{2} \left[V_2 \frac{\pi}{4} d^2 + \frac{\frac{16\pi\mu D}{\rho Q_{12}} \frac{L_{12}}{D} (V_{12})^2 + \left(\frac{V_1}{K} \right)^2}{\frac{1}{Q_{12}} \frac{16\pi\mu D}{\rho Q_{12}} \frac{L_{12}}{D} (V_{12})^2 + \frac{1}{Q_1} \left(\frac{V_1}{K} \right)^2} \right] \times \dots$$

$$\left[\frac{1}{Q_{23}} \frac{16\pi\mu D}{\rho Q_{23}} \frac{L_{23}}{D} (V_{23})^2 + \frac{1}{Q_3} \left(\frac{V_3}{K} \right)^2 \right] \quad [28]$$

It was possible to simplify this relationship by removing the Q terms (recall that $Q = VA$) and by completing an order of magnitude analysis as follows. Where $d < D$ it is clear that $d^2 \ll D^2$. Thus, it was possible to neglect all d^2 terms in the numerators and all D^2 terms located in the denominators, which results in [29].

$$P_T = P_{3,i} = P_2 - \frac{\rho}{2K^2} \left[\left(\frac{V_3}{V_1} \right) (V_1)^2 + (V_2)^2 - (V_3)^2 \right] - \frac{\rho}{2} \left(\frac{16\pi\mu D}{\rho Q_{12}} \right) \frac{L_{12}}{D} \left(\frac{V_3}{V_1} \right) V_{12}^2 \quad [29]$$

For the 2nd term and the last term on the RHS to approach zero then V_3/V_1 must become small, which is likely if the air in the duct is within the laminar flow regime. If the airflow within the duct is turbulent, which is far more likely within HVAC systems, then the ratio of V_3/V_1 goes to one. Thus, in the turbulent case the equation will once again require an iterative solution, similar to the 2 Hole case considered in the previous section. Note that in this system the ratio of V_3/V_1 refers to the ratio of velocities that are closest to the sampling point and farthest away.

The previous analysis identified problems that could affect the accuracy of the total pressure signal (P_T) within a VAV flow sensor and indicated how these variables could be minimized. For instance, ensuring that the diameter of the total pressure ports (d) is much smaller than the diameter of the header (D) was found to be quite important. It is also evident that the majority of the amplification (and thus the possibility for a flow error) occurs through the static pressure signal, which is discussed in the subsequent section. The results of the 2 Hole case were used to model the typical VAV airflow sensor response to ensure the laboratory results were valid (Section 3.7.3).

3.7.2 Static Pressure Port Location: Pressure Coefficient Dependence

The second key feature of VAV airflow sensor operation is the deliberate placement of the static pressure port within the wake region, downstream of the sensor. Thus, the VAV sensor does not measure the true static pressure when determining the pressure differential but a negative static pressure that results in an amplified signal. The velocity reported by the VAV terminal (V_{VAV}) is a function of ΔP , where ΔP is equal to the difference between the total and static pressure at the sensor, which is evident from [30].

$$V_{VAV} = A_{DUCT} \left(\frac{2\Delta P}{\rho} \right)^{1/2} = A_{DUCT} \left(\frac{2(P_T - P_S)}{\rho} \right)^{1/2} \quad [30]$$

The differential pressure term, ΔP , will be larger (or amplified) because the static pressure sensor is located within the wake region (so that static pressure signal, P_S , is negative). The amount the static pressure sensor will be reduced is a function of the velocity profile (which is influenced by upstream duct geometry). The exact amplification expected is a function of flow rate; however, it will be shown that the position of the static pressure port generally accounts for a theoretical amplification of 40% to 100%.

3.7.2.1 Cylindrical Model

In order to determine the relationship behind the positioning of the static pressure port it is necessary to first consider the theoretical behavior of airflow around an object, the physics behind external flows around bodies. This is a well-studied branch of classical fluid dynamics and is very relevant for the aeronautical industry and wind engineering. The determination of airflow around common shapes, such as: spheres, flat plates, and cylinders all have classical solutions to help verify models.

Unfortunately, the classical solutions to these types of problems only offer approximations of the true airflow behavior, and in some cases, the true behavior is quite different from what is predicted. Despite this, the theoretical models were explored to determine the expected response of the system. For instance, consider Figure 6, which depicts 2D potential flow (with velocity U_∞) around a common blunt body, a circular cylinder.

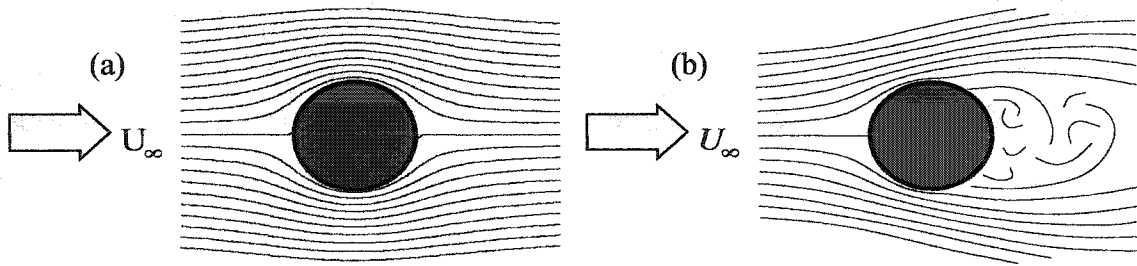


Figure 6: Simple representation of fluid flow past identical blunt bodies where (a) represents flow predicted by solving classical Stokes flow equations, (b) represents the same body and what the real flow behavior would likely be – Recreated based on Figures from Frank White (1999) where the Reynolds number based on diameter (Re_D) is $=10^5$ in both Figures.

Figure 6 (a) represents the theoretical, and impossible (at least within a HVAC setting), case of inviscid potential flow with no boundary layer. The second case indicates the true behavior as fluid flows past the object. Understanding the classical theory will help to explain the true VAV behavior and the determination of a theoretical solution will highlight the experimental results. In order to determine pressure along the back of a flow sensor it is first necessary to make some approximations; the most significant dealing with geometry. In the following analysis the flow sensor will be approximated at a cylinder within the flow, thus it will be possible to determine the approximate wake region and pressure along the rear of the sensor surface using Laplace's equation (for the inviscid, theoretical, case).

Laplace's equation (in Cartesian coordinates) is a starting point for this analysis and is provided in [31] and [32]. This method will utilize some simple vector calculus using functions for the velocity potential (ϕ) and the Laplacian operator (∇^2).

$$\nabla^2 \phi = \nabla \cdot (\nabla \phi) = 0 \quad [31]$$

$$\frac{\partial^2 \phi}{\partial x^2} + \frac{\partial^2 \phi}{\partial y^2} + \frac{\partial^2 \phi}{\partial z^2} = 0 \quad [32]$$

It is then possible to consider the Laplace equation with the combined flow method to model the theoretical airflow around a cylinder immersed in a flow, such as the simple case in Figure 7.

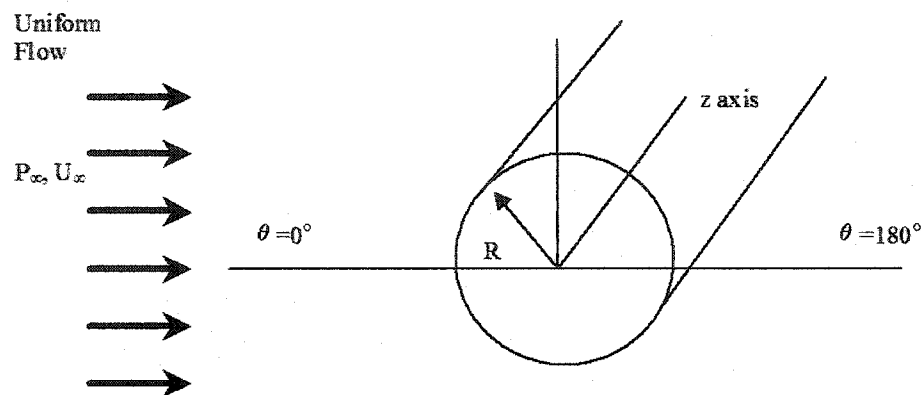


Figure 7: Simple representation of fluid flow past a cylinder with coordinate axis. This simple case will be analyzed using the classical inviscid fluids approach using Laplace's Equation, note this theoretical case is only a first step.

The combined flow method makes use of the fact that the Laplace equation is linear, thus any combination of solutions to the Laplace equation will also become a valid solution. The cylindrical flow problem can be solved using the combined flow method and the following two velocity potentials.

$$\text{2D Dipole:} \quad \phi = m \frac{\cos \theta}{R} \quad [33]$$

$$\text{Uniform Flow:} \quad \phi = U_\infty R \cos \theta \quad [34]$$

Using the combined flow method, the velocity potentials for a 2D dipole and uniform flow profile (both in polar coordinates) were summed to provide the velocity potential for inviscid flow past a cylinder, as shown in [35].

$$\phi = U_\infty R \cos \theta + m \frac{\cos \theta}{R} \quad [35]$$

In this simple model the velocity of the airflow far upstream of the object is designated as (U_∞), the θ term refers to an angle located at the center of the cylinder where the behavior from 0° to 180° will be identical to the behavior at 180° to 360° from symmetry (the top and bottom of the cylinder). It is then necessary to solve for the constant, m , within the previous equation using boundary conditions and the following velocity components (for polar coordinates):

$$V = (V_R, V_\theta, V_z) = \nabla\phi = \left(\frac{\partial\phi}{\partial r}, \frac{1}{r} \frac{\partial\phi}{\partial\theta}, \frac{\partial\phi}{\partial z} \right) \quad [36]$$

The radial velocity component can be determined by placing the velocity potential from [35] into [36]. The radial velocity component (V_R) must go to zero, therefore, it is possible to solve for the constant (m) in the following manner.

$$V_R = U_\infty \cos\theta - m \frac{\cos\theta}{R^2} \quad [37]$$

$$m = U_\infty R^2 \quad [38]$$

The pressure distribution is determined by considering the circumferential velocity component (V_θ) from Equation [36] in a similar manner.

$$V_\theta = -U_\infty \sin\theta - m \frac{\sin\theta}{R^2} \quad [39]$$

After combining the results of the boundary condition analysis, it is possible to determine the relationship for velocity as a function of the angular position (θ).

$$V_\theta = -U_\infty \sin\theta - m \frac{\sin\theta}{R^2} = -U_\infty \sin\theta - (U_\infty R^2) \frac{\sin\theta}{R^2} = -2U_\infty \sin\theta \quad [40]$$

$$V_\theta^2 = 4(U_\infty \sin\theta)^2 \quad [41]$$

It was also necessary to recall an essential equation: the pressure coefficient C_p defined below. This coefficient is commonly used to describe pressure and velocity effects around blunt bodies immersed in flow.

$$C_p = \frac{\text{Static Pressure}}{\text{Dynamic Pressure}} = \frac{P_s}{\frac{1}{2}\rho U_\infty^2} \quad [42]$$

The pressure coefficient, a dimensionless ratio of the static pressure to the dynamic force, is used with the help of the simplified Bernoulli equation to determine the surface pressure along the cylinder ($P_{SURFACE}$).

$$P_{SURFACE} = H - \frac{1}{2}\rho V_\theta^2 = H - \frac{\rho 4(U_\infty \sin\theta)^2}{2} \quad [43]$$

Substituting the results of this relation into the definition of the pressure coefficient allowed for the following analysis. Note that several steps are included for additional clarity:

$$C_p = \frac{P_s}{\frac{1}{2}\rho U_\infty^2} = \frac{(P - P_\infty)}{\frac{1}{2}\rho U_\infty^2}$$

$$C_p = \frac{1}{\frac{1}{2}\rho U_\infty^2} \left[H - \frac{4\rho U_\infty^2 \sin^2\theta}{2} - \frac{1}{2}\rho U_\infty^2 \right]$$

$$C_p = 1 - 4(\sin \theta)^2 \quad [44]$$

This is the theoretical, inviscid, solution to the surface pressure around a cylinder but it clearly does not account for the majority of real world situations, HVAC included: the theoretical flow pattern was also provided in Figure 6 (a). The solution is often represented graphically, as shown in Figure 8.

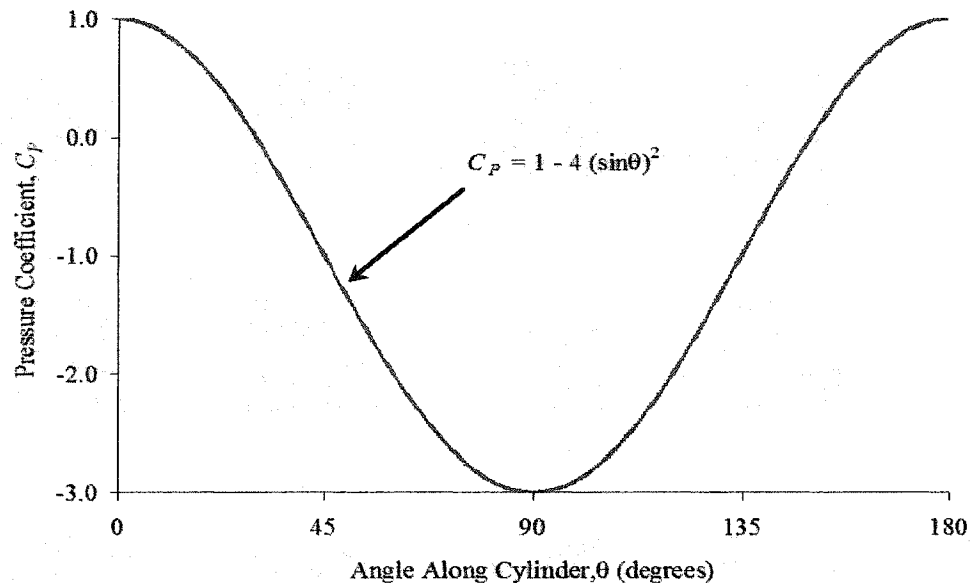


Figure 8: Theoretical representation of surface pressure using Laplace's equation, using the combined flow method, and Bernoulli's equations to simplify the equations. This is the classical solution but it does not model the true flow around an actual cylinder very well, particularly after 90°, which is the area of interest.

Figure 8 represents the classical solution to represent inviscid flow around an immersed cylinder. Note that the pressure coefficient is solely a function of the angular position around the cylinder, thus in this model there is no representation of the wake region. The inviscid flow theory solution is a useful starting point but it does not adequately represent true surface pressure. Unfortunately, aside from various computer models that utilize a Computational Fluid Dynamics (CFD) approach, of varying accuracy and relevance, there is no universal calculation to predict fluid flow effects over immersed bodies; the vast majority of real data on this subject is experimental. Fortunately, this classical problem has been the topic of a great deal of past experimental research. The experimentally determined pressure coefficient for both laminar and turbulent flow are represented graphically in Figure 9.

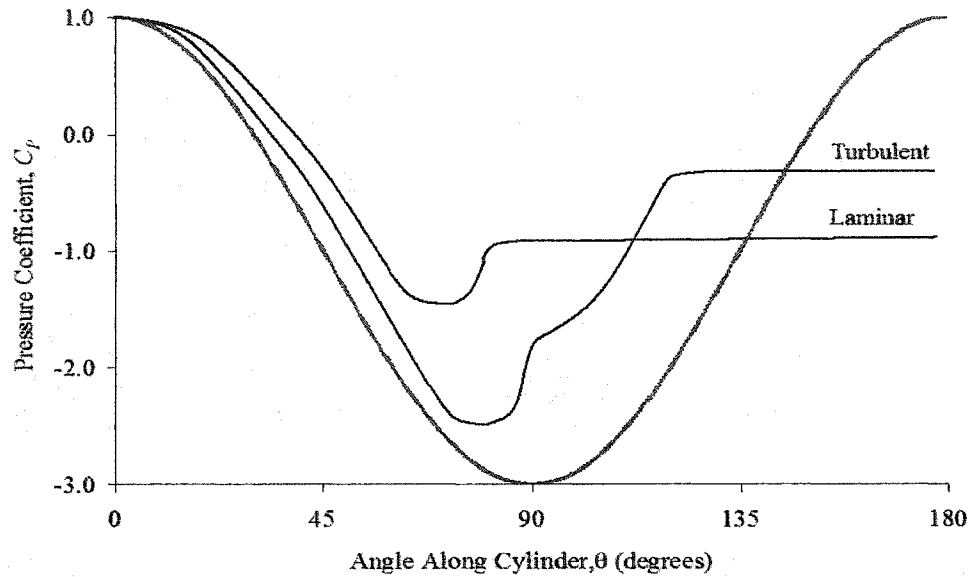


Figure 9: Theoretical and experimental representation of surface pressure around a cylinder immersed in the flow. Note that the theoretical line (for the Inviscid Response) is identical to the relationship previously derived while the experimental curves (Laminar and Turbulent) are recreated based on Figures from Frank White (1999).

Figure 9 is only a recreation of the true experimental data (and cannot be considered exact by any means); however, it is clear that the real experiments concerning flow over cylinders never recover all of the pressure, which was erroneously predicted by the inviscid, theoretical, case. The separation point where the wake region is first formed is also of particular interest, the laminar and turbulent cases are illustrated in Figure 10.

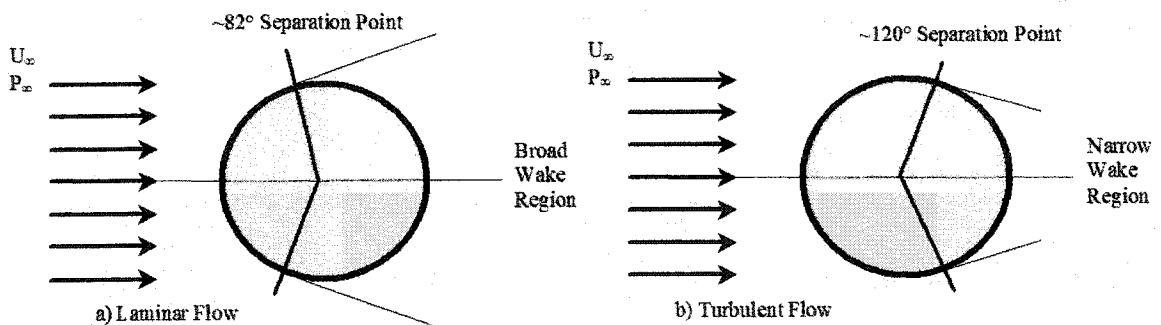


Figure 10: Experimental representation of the separation points around a cylinder immersed in the flow for the Laminar a) and Turbulent cases b), Recreated based on Figures from Frank White (1999).

The separation points can also be inferred from Figure 9, which is simply the largest angle prior to the pressure coefficient becoming a straight line, or uniform with θ , (Figure 9 also indicates

$\sim 82^\circ$ and $\sim 120^\circ$). Note that the wake region of the turbulent case is smaller than the wake region of the laminar flow case. Thus, the turbulent surface pressure is higher. For $C_p = -0.5$ it can be shown that the amplification of the flow signal from the VAV sensor is $\sim 22\%$. The justification for this is provided in the following steps that have been presented together for clarity.

$$\begin{aligned}
 Q_{VAV} &= A_{DUCT} \left(\frac{2\Delta P}{\rho} \right)^{1/2} = \frac{\pi D_{DUCT}^2}{4} \left(\frac{2}{\rho} \right)^{1/2} (P_{TOTAL} - P_{STATIC})^{1/2} \\
 Q_{VAV} &= \frac{\pi D_{DUCT}^2}{4} \left(\frac{2}{\rho} \right)^{1/2} \left[\frac{1}{2} \rho V^2 + P_\infty - \left(C_p \frac{1}{2} \rho V^2 + P_\infty \right) \right]^{1/2} \\
 Q_{VAV} &= \frac{\pi D_{DUCT}^2}{4} \left(\frac{2}{\rho} \right)^{1/2} \left(\frac{1}{2} \rho V^2 \right)^{1/2} (1 - C_p)^{1/2} = \frac{\pi D_{DUCT}^2}{4} V (1 - C_p)^{1/2} \quad [45]
 \end{aligned}$$

Therefore, the volume flow rate (Q_{VAV}) indicated by the VAV sensor is proportional to the square root of the C_p value, if the C_p value is negative. A positive C_p value would result in a reduction of the VAV sensor signal to zero (complete pressure recovery). Using common HVAC conditions, a simple comparison of the true airflow in the duct to the airflow indicated by a VAV sensor is presented in Figure 11.

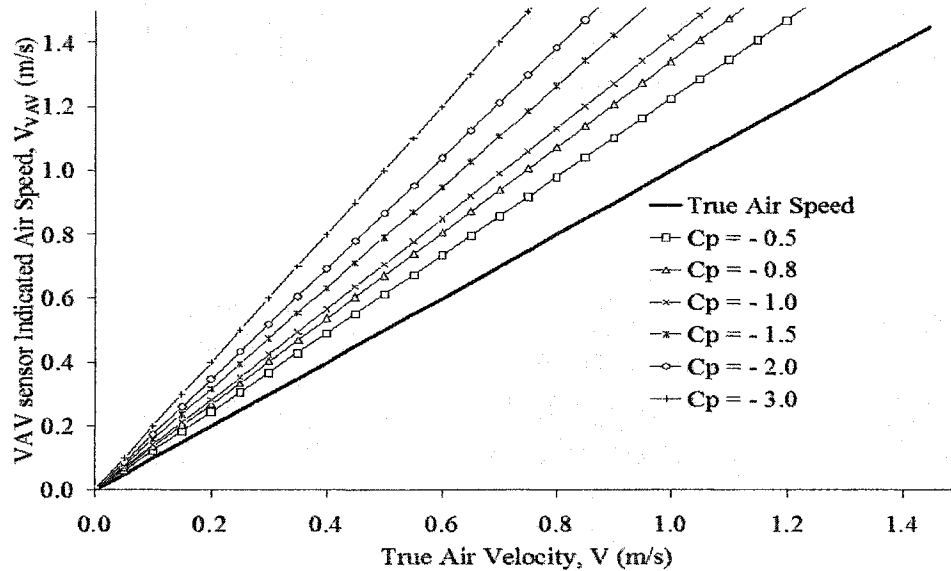


Figure 11: Simple comparison of the true airflow rate signal versus the signal indicated by a VAV sensor that utilizes a static pressure port located in the wake region. This case assumes a standard air density of 1.2 kg/m^3 and various turbulent pressure coefficients (C_p) that provide varying amplification.

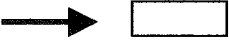

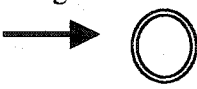

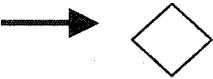
Thus, the effects of differential pressure amplification can be quite significant. Unfortunately, since C_p is also dependent on the velocity profile this will clearly add an element of error to VAV

sensor, although this can usually be minimized by calibrating the sensor to improve accuracy of the VAV terminal over its airflow range.

3.7.2.2 Review of other Common Shapes

Up until this point the VAV airflow sensor has been exclusively modeled as a cylinder immersed in the flow; however, there may be a number of other valid geometries. Common examples include square cross section cylinders and bullet shaped cross sections, which both may be more appropriate. Recent experimental work completed by Gu and Sun (1999) indicates the C_p of a circular cylinder varied between -0.3 and -1.3, other experimental pressure coefficients for non-cylindrical shapes that are common in VAV sensors (such as square and diamond cylinders) are summarized in Table 1. A VAV airflow sensor will often not incorporate a perfectly square or round cylinder; however, the C_p values presented in Table 1 range between -0.3 and -1.7 for shapes that are similar to the VAV flow sensor geometries considered within the laboratory experiments: C. Norberg (1993), W. C. L Shih et al. (1993), I. Taylor et al. (1999).

Table 1: Summary of Other Likely Cylindrical Pressure Coefficients (C_p) for VAV Sensors*

Type of Cylindrical Cross Section		C_p Values
Rectangular, with side ratios that vary from:		
3.0 to 1.0		-1.42 to -1.59
1.0 to 3.0		-1.62 to -0.93
Rough Circular, with surface roughness that varies from:		
$k/D = \text{smooth}$		-1.0 to -0.4
$k/D = 0.0016$		-0.7 to -1.0
$k/D = 0.0062$		-1.0
Square and Diamond, with varying orientations:		
$\theta = 0$		-1.7
$\theta = 45^\circ$		-1.3

*These C_p values are largely based on experimental data; all C_p values are in reference to the surface on the opposite side of the flow (thus they are all considered at 180°), which mimics the placement of the static pressure port on a VAV airflow sensor.

3.7.3 Summary of VAV Flow Sensor Response to Velocity Profiles

VAV flow sensor response has been shown to depend on both the total pressure signal (P_T) and static pressure signal (P_S). Therefore, it was possible to predict VAV flow sensor response to varying upstream conditions. Recall [30], restated below for clarity.

$$V_{VAV} = \left(\frac{2\Delta P}{\rho} \right)^{1/2} = \left(\frac{2(P_T - P_S)}{\rho} \right)^{1/2} \quad [30]$$

It has been shown that a VAV airflow sensor with (2 total pressure ports) will provide an averaged signal that can be described with [27], while P_S can be described with [42].

$$P_T = \frac{1}{2} \rho \left[V_2^2 + \frac{(V_1)^2 - (V_2)^2}{2} \right] \quad [27]$$

$$C_p = \frac{\text{Static Pressure}}{\text{Dynamic Pressure}} = \frac{P_S}{\frac{1}{2} \rho U_\infty^2} \quad [42]$$

By substituting [27] and [42] into [30] it is possible to estimate the VAV signal with the velocity at each port (V_1 , V_2), the centerline duct velocity (U_C) and the pressure coefficient (C_p). The velocity response of the VAV flow sensor (V_{VAV}) is given by [46].

$$V_{VAV} = \left[V_1^2 + \frac{(V_1)^2 - (V_2)^2}{2} - C_p (U_C)^2 \right]^{1/2} \quad [46]$$

Using this model for the expected VAV flow response it was shown that the velocity signal provided by the VAV airflow sensor (V_{VAV}) would always be higher than the true velocity (V_T), with a common turbulent velocity profile. During the course of the laboratory results an amplification coefficient was later defined (C), which was used to describe the majority of the laboratory results.

$$C = \frac{Q_{VAV}}{Q_{TRUE}} = \frac{V_{VAV}}{V_T} \quad [47]$$

where:

C	=	flow amplification coefficient
Q_{VAV}	=	the VAV sensors indicated airflow rate (m ³ /s)
Q_{TRUE}	=	the "true" airflow rate from a standard measurement (m ³ /s)
V_V	=	the VAV sensors indicated velocity (m/s)
V_T	=	the "true" airflow velocity (m/s)

Using the model from [46], the expected amplification coefficient (C) for VAV sizes and conditions similar to the laboratory tests varied weakly with the true velocity (V_T), and strongly

with the C_p (as previously predicted). The predicted results (from the 2 port model) for a typical 8" VAV terminal are provided below in Figure 12, for a range of flowrates and C_p values. The sample calculations are provided in Appendix A, Section 2.

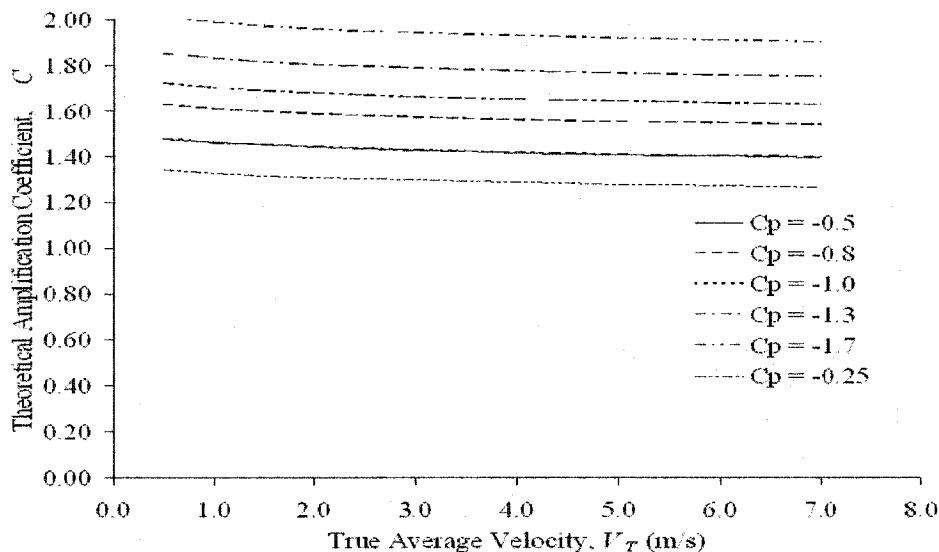


Figure 12: Theoretical prediction of sensor amplification for a typical 8" VAV airflow sensor using a range of likely pressure coefficients (C_p) and true velocities (V_T). Note that the signal is strongly influenced by C_p and remains relatively constant in relation to the true velocity.

The value of this model was to verify that the laboratory results were reasonable for a common turbulent velocity profile (in this case a typical logarithmic profile was used). The analysis did not concentrate on the design of averaging flow sensor but a number of useful facts were determined. Averaging flow sensors are reasonably accurate in terms of combining the total pressure signal together from several ports due to the laminar conditions that are produced within the sensor. As a side note, several VAV airflow sensors also incorporate "cupped" total pressure ports to lower the effects of yaw angle on the total pressure signal, which is one of the reasons that the static pressure port was found to be more significant to the amplification of the flow signal (as well as to the propagation of signal errors). The position of the "static" port is the primary complication for VAV averaging flow sensors, the response of which was determined with laboratory experiments.

4.0 Field Research Methodology

Experimental field-testing was used to estimate the longevity of recommissioning VAV systems with DDC at three facilities within Edmonton and surrounding area. The field tests required the completion of a modified recommissioning procedure with sufficient instrumentation to monitor the system performance prior to (BC), immediately after (AC) and several months after the recommissioning process had been completed (AAC). The test locations, data collection techniques, instrumentation, recommissioning procedure, and possible sources of error associated with the field experiments are discussed in the following section. One of the chief goals of the field-testing was to verify the hypothesis that VAV airflow sensor accuracy was the most significant factor during recommissioning. A series of laboratory experiments were also completed, where focus was placed on airflow sensor accuracy and the response of VAV terminals in relation to varying upstream conditions and static pressures, which are the dominant factors related to VAV sensor amplification. Flow visualization experiments were completed to determine airflow behavior within the VAV terminals tested, in relation to varying damper positions for the “worst” upstream conditions.

4.1 Field Test Locations

Three suitable locations were identified within Edmonton and the surrounding area: The Cross Cancer Institute, Timms Center for the Arts and the Yellowhead Regional Library. A brief systems description for each facility is provided. The HVAC systems at the three test locations were dissimilar in operation, maintenance practices, and technical approach (for instance, return fan tracking, building static pressure control, mixed air plenum pressure control or exhaust fan modulation). Both built-up and packaged Air Handling Units (AHU) were considered. Each facility had a minimum supply ventilation flow rate of 9,439 L/s (20,000 CFM) with at least 17 supply air (or more) VAV terminals to be controlled using a DDC system. In addition, each of the field locations had been operating for at least two years without any formal commissioning or recommissioning process.

4.1.1 The Cross Cancer Institute

The Cross Cancer Institute is a major comprehensive cancer treatment center located in Edmonton, Alberta. This facility provides cancer care programs for the northern half of the province as well as portions of British Columbia and Saskatchewan. Since the HVAC system at the Cross Cancer Institute is far larger than the requirements of this study, only the newest portion of the HVAC system was evaluated. The newest Air Processing Unit (APU) was added to the

facility in November of 1997 and is designated APU9; APU9 is the sole HVAC system for the 4th and 5th floors, including a special care unit located on the 5th floor. The Cross Cancer Institute is equipped with digital box control with exhaust boxes matching flows to supply boxes to maintain zone flow control and building pressurization. The central air system typically operates at 28,316 L/s (60,000 CFM). A total of 51 supply VAV terminals and 20 exhaust, or return, VAV terminals were considered at this facility. The Cross Cancer Institute has a built-up indoor air handler with a Seimens controls system and had the most stringent building requirements due to its function as a medical facility.

4.1.2 The Timms Center for the Arts

The Timms Center for the Arts is a large institutional building located on the University of Alberta campus (in Edmonton) and is used to house the drama/acting departments. The Timms Center was the first facility tested and includes 51 VAV terminals in the backstage/theater sections. The building relies on a Johnson Controls MetaSYS DDC control system to operate the terminal VAV system, as well as a campus control system for the packaged custom indoor AHU. There are three main air handlers within the facility, which service two theaters, a wood working shop, assembly areas, and a large amount of prop storage and practice space. Only the backstage section was considered within this research because it is physically isolated from the remainder of the facility and is serviced solely by the main air handler (designated AHU 1). AHU 1 is a packaged handler that has a capacity of 19,822 L/s (42,000 CFM) of the total 38,700 L/s (82,000 CFM) for the facility. The Timms Center is the second largest facility considered and was the facility where the longest duration of field-testing was completed.

4.1.3 The Yellowhead Regional Library

The Yellowhead Regional Library is the third and smallest facility considered. The building was constructed in 1971 to provide support for local libraries and school systems throughout central and northern Alberta. The facility is an institutional building located in Spruce Grove, Alberta approximately 45 minutes west of Edmonton. A series of renovations were performed throughout the years but no recommissioning or changes to the HVAC system have been made in the last 4 years. The system is designed to operate with a bare minimum of adjustment since no full time maintenance/control staffs are present on site. This facility utilizes a single built-up air handler (designated AC- 1) to supply air to 17 VAV terminals, which are maintained by an Invensys MicroNet MN-FLO3T digital box controllers and an Invensys control system. AC-1 is designed to maintain a 15% minimum O/A by ensuring the return fan vane damper is open 15% more than

the supply fan vane damper at all times. This is the only facility to utilize direct fan tracking, which is an inexpensive method that has been criticized in the literature for poor IAQ without recommissioning⁵.

4.2 Data Collection Techniques

The field research was extremely dependent on the use of DDC data trends. External data loggers and Data Acquisition Systems (DAS) were used to measure environmental and system information that was not otherwise recorded. Trended data from each DDC was an integral part of the project and accounted for the majority of data collection in the field.

4.2.1 Summary of Data Collected

Trending included all relevant control system and external data required to quantify the benefits of building recommissioning and was completed for a minimum 2-week period at each facility. However, this period was usually exceeded; the trending period was sometimes increased to 2 months to provide more data. A summary of important dates is provided in Table 2.

Table 2: Important Dates for Data Collection at each of the Field Testing Locations

	Cross Cancer Institute	Timms Center for the Arts	Yellowhead Regional Library
Start Date	10/30/2001	12/01/2000	08/01/2002
BC Start Date	November 28, 2001 at 12 PM	February 21, 2001 at 12 PM	September 5, 2002 at 9 AM
BC End Date	January 28, 2002 at 2 PM	March 28, 2001 at 7:48 AM	September 25, 2002 at 8:40 AM
AC Start Date	April 12, 2002 at 12:45 PM	October 5, 2001 at 9 AM	December 10, 2002 at 8:40 AM
AC End Date	June 11, 2002 at 00:15 AM	November 2, 2001 at 9 AM	February 10, 2003 at 9 AM
AAC Start Date	Not Available	August 25, 2003 at 12 AM	October 1, 2003 at 12 AM
AAC End Date	Not Available	September 25, 2003 at 8 AM	November 15, 2003 at 12 AM

The DDC systems were set to record data in continuous ten-minute loops for each of the 8 trends considered. Ten-minute time intervals were chosen to provide a suitable amount of detail within the trended data; however, it later became apparent that longer time intervals could have been utilized to generate similar results with less extraneous data.

⁵ It has been criticized because a small error in fan tracking could have very large consequences to the amount of indoor air provided to the facility.

4.2.2 Explanation of DDC Data Trends

A variety of measurements were made over the course of field-testing but the vast majority of data were collected through the existing DDC systems at each of the facilities. This was, of course, the intent of the field research; however, this also created some complications due to differing instrumentation, software, equipment, and design of each DDC system. The DDC trends included variables for each VAV terminal as well as the central AHU at each facility. A summary of important test variables that were collected is summarized in Table 3.

Table 3: Summary of the test variables considered for each of the field tests

VAV Terminal and Zone Variables	AHU Variables	Building Variables
Airflow Rate and Setpoint*	Return, Supply, Outdoor and Mixed air temperatures, Flow Rates and Setpoints	DDC system mode (i.e. normal operation, conservation mode, heating mode etc.)*
Damper Positions	EOL Static Pressure and Setpoint*	Building Pressurization*
Minimum Setpoint*	Supply and Return Fan Power and Speeds*	Energy use of major system components
Maximum Setpoint*	Damper Positions and Setpoints	
Temperature and Setpoint*	Relative Humidity and Setpoint	

*These parameters were particularly important to the data analysis

4.2.3 “Tunable” DDC Parameters for Recommissioning

The nature of DDC systems allows for calibration, or “tunable” parameters that can be used to increase system accuracy with recommissioning. For instance, it was hypothesized that the calibration of VAV airflow sensors was found to be the most significant way to improve system efficiency. The DDC sensor parameters were designed to account for non-ideal duct configurations, variations in static pressure and flow rate at each box location and variability in the sensitivity of the flow sensors that would otherwise decrease the accuracy associated with each VAV terminal. Other significant DDC tunable parameters include the recalibration of pressure transducers (such as system static pressure, building pressurization, supply fan pressure etc.) and temperature sensors. By contrast, mechanical improvements included things like damper misalignment; especially in VAV terminals, which account for significant airflow errors and wasted supply static pressure. During the course of the field-testing over 80% of the

improvements made to the existing HVAC systems were through tunable parameters, the remainder were mechanical improvements.

4.3 Project Equipment

Field-testing was completed using external equipment (in addition to each DDC system), which included both common measurement tools, such as pressure transducers and thermocouples, as well as a few custom built instruments and measurement systems. The custom systems include a DAS that was used to monitor system characteristics such as air temperature, building pressurization, duct static pressure, EOL static pressure, and the gas concentrations indicated by the tracer gas injection system (which were used to monitor O/A). Further discussion of common instrumentation, custom equipment, and problems with tracer gas injection are dealt with below.

4.3.1 Common Instrumentation

In order to complete the recommissioning process in each of the facilities a variety of standard measurement equipment was utilized. Measurement error for this equipment was typically quite low: less than or equal to a 2%. A list of common equipment used during the field tests is provided in Table 4.

Table 4: List of common Instruments used within the Field-tests

Instrument	Purpose	Instrument Error and Range
Air Data Multimeter (Shortridge, model ADM-970)	Temperature, Pressure, Air Velocity measurements using both a flow hood and a pitot tube, as necessary	+/- 0.25°C from 0°C to 70°C, otherwise +/- 0.5°C over -55°C to 120°C range +/- 1% from 0 to 20 psi +/- 2.3% (see Section 4.6.1 for this sample calculation)
Multimeter and Amp clamp	Fan Voltage and Power Usage	+/- 5mV, +/- 2% amps
Data logger: SmartReader Plus 4 LPD Pressure	Various Pressure Measurements	+/- 0.05" H ₂ O over (+/-5"H ₂ O)
Data logger: SmartReader Plus 8 Temperature	Various Temperatures Measurements	+/- 0.2°C over the range of 0 to 70°C, otherwise +/- 0.5°C over -35 to 95°C range

4.3.2 Overview of DAS and Tracer Gas Injection

The O/A at all field test locations was experimentally monitored with a tracer gas injection system that was used to introduce a set amount of SF₆ into the supply air stream, using the concentration method⁶. The preferential way to measure the outdoor airflow is to use a hot-wire anemometer grid or a multi-point pitot tube station; however, it is often difficult to use these techniques in the field because they require a long section (greater than at least 10 straight, unobstructed duct diameters) to work effectively. Tracer gas (SF₆) was injected into the supply air stream immediately after the main supply fans ~ 3D downstream, initially in large quantities to reach a measurable return air concentration. The tracer gas was injected immediately following the supply fans to ensure adequate mixing (note that despite these measures the mixing of the tracer gas was still a major concern, and will be discussed further). The space was allowed to reach an equilibrium concentration, which was indicated by the MIRAN gas analyzer. The flow was then restricted to allow a typical supply air concentration of 1 ppm. This value was chosen to provide an acceptable signal while remaining under the recommended safety limits⁷.

The concentration of SF₆ was measured within the return duct, the outside air duct, and the supply duct using a multi-point sampling grid. As expected, the outdoor air concentration of SF₆ remained at zero for all tests. Grids were always placed as far as possible downstream within the ducts to increase mixing time, although the consideration of “adequate” mixing may well have been one of the major problems with the tracer gas technique in this application. The temperatures at each of these locations were also recorded using a self-averaging thermocouple circuit that measured the temperature over a minimum four-point grid at each test location. The DAS then measured all thermocouple temperatures ~ 6000 times over each 10 minute interval and averaged the results to create four final temperature readings for the outdoor, supply, return and mixed air streams. The air stream concentration values, temperatures, number of counts required for the temperature within the loop and the last known calibration gas reading were then recorded. It would have been possible to use the DAS to record much more data, in steps as frequent as 4 minutes. However, due to the slow system response of a typical HVAC system, which can be measured in hours and not minutes, this would only result in a large amount of extraneous data.

⁶ The concentration method (utilizing constant injection of tracer gas) is discussed further in this section.

⁷ Health and Safety acknowledges that SF₆ will be safe in concentrations less than 1000 ppm but during all field tests a self-imposed constraint of 5 ppm was chosen.

4.3.3 The MIRAN Gas Analyzer and Tracer Gas Selection

The MIRAN gas analyzer was used to measure the concentration of tracer gas in the return, supply, and outdoor air streams where the outdoor air concentration should ideally read zero⁸. The MIRAN 1A gas analyzer used in this study is a single-beam infrared spectrometer with three distinct wavelength ranges that span from 2.5 μm to 14.5 μm and an adjustable path length cell that can be set to between 0.75 m to 20.25 m. The MIRAN utilizes a regulated nichrome wire-heating element as an infrared source and a pyroelectric lithium tantalite element as the infrared detector. The MIRAN 1A is also equipped with a reasonably large 5.6 L gas-sampling chamber and a built in vacuum pump (that was replaced with a larger pump, which improved the speed at which the DAS could collect data).

The MIRAN 1A gas analyzer can be used to test for multiple gas samples, based on the corresponding wavelength of the tracer gas molecule absorption; thus, it was necessary to select a suitable tracer gas. Samples of CO_2 , R22 (or Freon 22), R-134a, and SF_6 were all evaluated as possibilities⁹ where the main criteria for tracer gas selection were: public safety, overall suitability for the study, MIRAN sensitivity and cost for continuous operation. All of the tracer gases were found to be safe for use in this application, although the refrigerants R22 and R-134a could not be exposed to open flames or high temperatures since they would react to form hydrochloric and hydrofluoric acids. It was also found that CO_2 was difficult to maintain in an HVAC system based on earlier field tests completed at Northlands Spectrum, testing began at this facility but was never completed, or included within the results. The levels of CO_2 in the atmosphere often fluctuate widely based on local conditions (a value like 2500 ppm would be reasonable); this introduced another complication into the measurement of the airflow data. The use of CO_2 as a tracer gas has received mixed reviews in the literature but it is generally accepted that without a suitable number of people (to generate a background CO_2 reading) the use of CO_2 as a tracer gas is not acceptable. An acceptable CO_2 background concentration was difficult to maintain within the test locations; past research indicates a minimum differential of ~ 350 ppm is required.

The sensitivity of the MIRAN analyzer was determined for each of the remaining tracer gases using a calibration circuit that was completed per the specifications of the manufacturer (Wilkes).

⁸ Note that the outdoor concentration will be zero using SF_6 tracer gas, the outdoor concentration will obviously not be equal to zero using CO_2 .

⁹ Note that these gas samples were identified from a literature review of similar experiments were CO_2 and SF_6 were the most common tracer gas selections.

The calibration circuit was comprised of a small vacuum pump (1/8 hp and ~ 2 CFM), a voltmeter, a pressure-lock sampling syringe, Tygon tubing equipped with a septum and a sample bag for obtaining a pure, laboratory grade, sample of tracer gas. The MIRAN was then calibrated in a heated box that was designed to maintain the temperature at 30°C because instrument temperature sensitivity is quite significant in a long path IR analyzer. The MIRAN was adjusted to find the correct wavelength, path length, range, zero setting, slit width and time response after it was allowed to reach an equilibrium temperature. After identifying the correct wavelength, such that the MIRAN indicated a zero reading in the presence of atmospheric air but provided an output in the presence of the various tracer gases, it was possible to carry out several calibration trials. Each of the tracer gases were calibrated several times to minimize human error when injecting gas samples and to evaluate the repeatability and hysteresis.

Both the R22 and R134a refrigerants could only be monitored on the lowest MIRAN range (0.25A) with sensitivities of 700 ppm/Volt and 208 ppm/Volt, respectively. The lower sensitivity also meant that a larger amount of tracer gas was needed, which was worse in terms of both occupant safety and cost. The approximate cost¹⁰ per lb of tracer gas was ~ \$4.03/lb for R22, ~\$5.98 for R-134a and ~\$16.32/lb for SF₆. The amount of tracer gas required to operate the DAS for 1 week with a typical 4720 L/s (10,000 CFM) supply airflow and a desired output voltage of only 0.25 V would have cost ~\$3,219/week for R22, ~\$9,005/week for R-134a and only ~\$158/week for SF₆ injection. SF₆ was chosen as the best tracer gas for use within this research project, it is a cost effective choice with minimal human impact. It was also determined that SF₆ provided the best response with approximately 1.0 V output from a 1.0 ppm sample on the highest range setting (1A range), which also provides the least amount of fluctuation. A schematic of the tracer gas injection and measurement system is provided in Figure 13.

¹⁰ Prices from PRAXAIR as of July 2002.

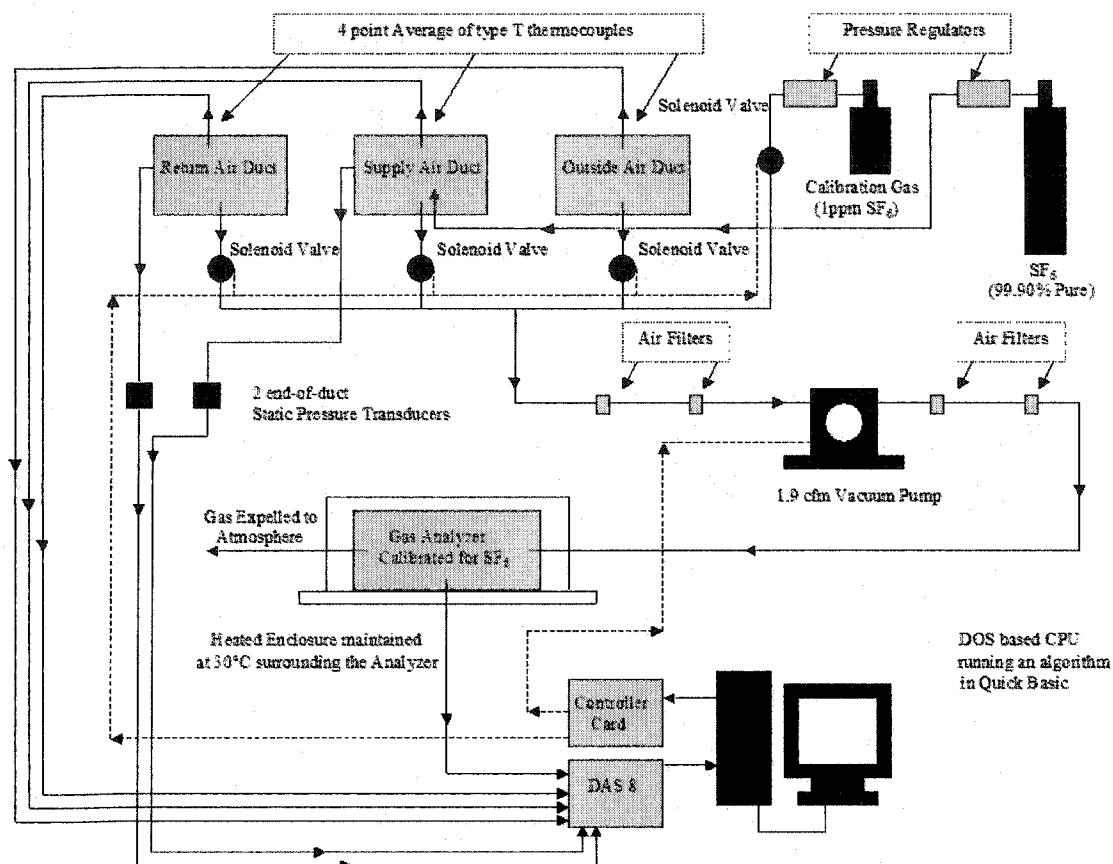


Figure 13: A schematic of the typical tracer gas injection system setup, this exact configuration was used at the Yellowhead Regional Library. The supply air concentration was measured upstream of the gas injection point within the supply duct. The tracer gas concentration was then adjusted until the return and supply concentrations reached relative equilibrium.

The MIRAN gas analyzer is expected to drift by 0.006 absorbance units per 8 hours or a maximum of 0.018 V/day from both the manufacturers stated accuracy and from the laboratory calibrations. For this reason, the DAS was set to read a calibrated gas sample of 1 ppm SF₆ with a balance of atmospheric air to maintain a record of drift over time. The DAS was only allowed to operate for three days (or less) so the use of a calibrated gas sample may have been redundant since the maximum possible drift over three days accounts for an error of only 0.054 Volts or 2.25% of a typical 2 ppm full scale reading. Typically the analyzer was only operational for 12 hours, however the calibrated gas sample was still used to ensure system reliability over the trend period. The tracer gas injection system was useful for taking “point” measurements for short periods, which typically lasted 12 hours in duration.

4.3.4 General Problems with the Tracer Gas Method

Despite the successful installation of the MIRAN, it was determined that continuous tracer gas trend data was not reliable, which is why tracer gas measurements were limited to 12 hours. This was due to environmental fluctuations and adequate mixing concerns. Originally a CO₂ injection system and a secondary gas analyzer were used to monitor system operation (not the MIRAN that was used later to monitor SF₆); however, environmental fluctuations and the difficulty experienced creating a suitable differential concentration of CO₂ in the facilities made this approach generally unsuccessful. The second gas injection system involved the use of a much more complicated gas analyzer (the MIRAN) to monitor SF₆ injection. The MIRAN gas analyzer was reliable if left undisturbed but concerns were raised about the equipment being moved while the research team was not present. Precise calibrations and long setup times were also required, which significantly reduces the benefits of this type of measurement. Tracer gas injection was found to be insufficient for continuous use during field-testing. The literature seems to indicate mixed results using tracer gas injection. For instance, earlier work completed by Fisk et al. (1992) stated that "...we conclude that the tracer gas decay and setup procedures, with data analyses based on age distribution theory, are impractical or inappropriate for many large complex buildings..." and later went on to estimate the measurement error in the neighborhood of 10%. Clearly this amount of experimental error is unacceptable, thus the constant injection (and not the decay method) was used. Unfortunately, there is still a large amount of uncertainty associated with the constant injection, or even measured injection, method because the results are highly dependant on the mixing of the tracer gas within the system. More recent studies by Fisk et al. (1999) utilized SF₆ tracer gas to measure the airflow within two commercial buildings and concluded that the overall uncertainty was approximately +/-7% of the flow rate. This high uncertainty was due to insufficient mixing; despite the fact that Fisk et al. (1999) added a secondary mixing fan within the supply air duct. Despite the well-documented problems with the tracer gas method there are also several instances in the literature that identify tracer gas (and the use of SF₆ in particular) as an essential research tool. The results of the field tests agree with the conclusions of Fisk et al. (1999) regarding insufficient mixing and find the tracer gas injection method generally unacceptable for continuous field-testing. Fortunately, the determination of DDC system accuracy in conjunction with point tracer gas measurements made it possible to complete the relevant IAQ calculations without continuous testing.

4.4 Recommissioning Procedure at Each Facility

The recommissioning procedure is important when interpreting the results of the field tests due to the varying requirements and definitions of building recommissioning, and is described below. Despite fundamental system differences, there were several steps of the recommissioning process that remained constant at each location. For instance, the process always began with a thorough inspection of the mechanical blueprints, systems maintenance logs, a number of building/system inspections and meetings with the existing maintenance/control system staff. This was completed to determine the original design intent, such as: the reasons for existing set point calibrations, preferred system operation speeds, minimum outdoor air requirements, building pressurization settings and existing sensor/instrumentation choices. The recommissioning process then included an air balancing verification and recalibration procedure that was performed on each of the VAV terminals within the facility. Indicated airflow rates were verified with standard measurements made with pitot-tube (or airfoil) traverses and adjusted. Pitot tube traverses were completed using the equal-areas method where a minimum of 2 traverse planes and 16 points were considered to ensure accuracy. Data analysis was completed as the recommissioning process was being completed. Further discussion of the analysis used during recommissioning is available in Section 5.2. Fortunately, the recommissioning process identified few unique problems within the original HVAC system designs; thus, the procedure for all of the test buildings was relatively uniform. The majority of problems identified in the test buildings were related to individual system components such as the mechanical systems (i.e. VAV dampers, heating or cooling valves) or problems with the DDC systems. Common problems with DDC systems included unattainable system set points and inadequate calibrations completed on system devices, especially with regards to the airflow calibrations made for each VAV terminal.

4.4.1 The Timms Center for the Arts

The Timms Center for the Arts was the first building tested; variables were monitored by a DAS that was verified with onsite calibrations of the equipment and the DDC trends. The DDC system was installed with commercial controllers located on a common bus-network; however, no common control modules were available. Therefore, a control module and a secondary PC were temporarily installed to allow trend logging of the terminals. The AHU 1 system and the other mechanical room equipment at the Timms Center were monitored through the Remote Control Monitoring System (RCMS) for the University of Alberta. The DAS, AHU 1 computer system, and the computer that monitored the VAV terminals were set to record data in continuous loops every 10 minutes.

4.4.2 The Cross Cancer Institute

The Cross Cancer Institute was the second major facility and the largest system considered within the field tests. The DDC measurement capabilities at this location were quite extensive and were used to make detailed trends of the system operation after on site calibrations were performed to ensure the accuracy of the readings. No external DAS was required at this facility; however, a number of instruments (pressure transducers and data loggers mainly) were left to trend the operation of the system. The Cross Cancer Institute was unique because it already possessed a robust DDC system that was capable of measuring the time trends for all of the test variables; thus, emphasis was placed on ensuring the DDC system was accurate.

4.4.3 The Yellowhead Regional Library

The Yellowhead Regional Library was the final test building considered and the smallest. This facility required both a DAS and a secondary PC to trend the DDC system, similar to the setup required at the Timms Center.

4.5 Recommissioning Data Analysis

Data analysis was completed to compare the actual system operation with the original design intent at each facility during recommissioning, focusing on the identification of system faults from the trended data. Both established recommissioning practices and new techniques were used to interpret the results and to gauge the performance indicators of the recommissioning process. For example, consider Figure 14. In this case, the calibration equations from the AC and AAC trends have very good agreement, indicating a negligible drift since recommissioning was completed (note these were 2 point calibrations due to DDC system limitations). In addition, it is evident that the calibration of the airflow sensor and DDC system parameters (the tunable parameters) significantly improved the DDC response for this terminal unit. Ideally the indicated and actual flow rates would be identical, thus the closer the calibration equation comes to approaching a 45° line (or the line of perfect agreement) the more accurate the flow sensor signal.

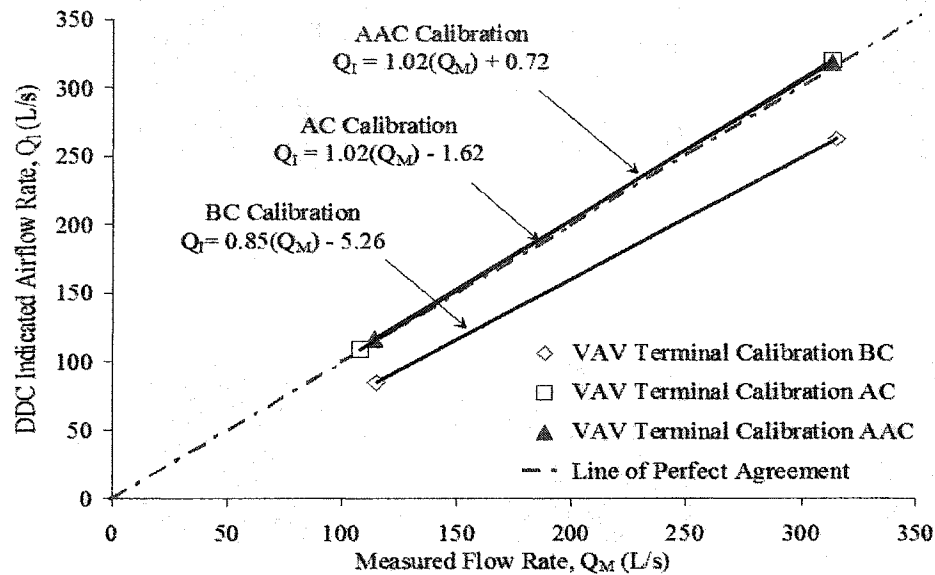


Figure 14: An example of the VAV terminal airflow calibration equations from the BC, AC and the AAC trends (VAV Terminal #1 from the Timms Center); notice that the terminal was originally (BC) providing more flow than the DDC was indicating. However, this was greatly improved with recommissioning (the calibration is much closer to the line of perfect agreement); also notice that the AC and AAC equations have excellent agreement. Thus, this terminal unit had a negligible deviation in flow accuracy between the AC and AAC trends (which were 8 months apart in this case).

Data collected during recommissioning was also used to identify mechanical faults or defective equipment. For instance, another technique used during recommissioning was to plot the relationship between the airflow error (in this case the difference between the DDC indicated flow rate and the desired system set point) for each VAV terminal unit versus the set point flow rate. The benefit of knowing this relationship is that it became easy to identify potential problems with the dampers in each VAV terminal unit, which is otherwise difficult to find. A typical plot is provided in Figure 15 for a VAV box that was found to have a significant damper misalignment.

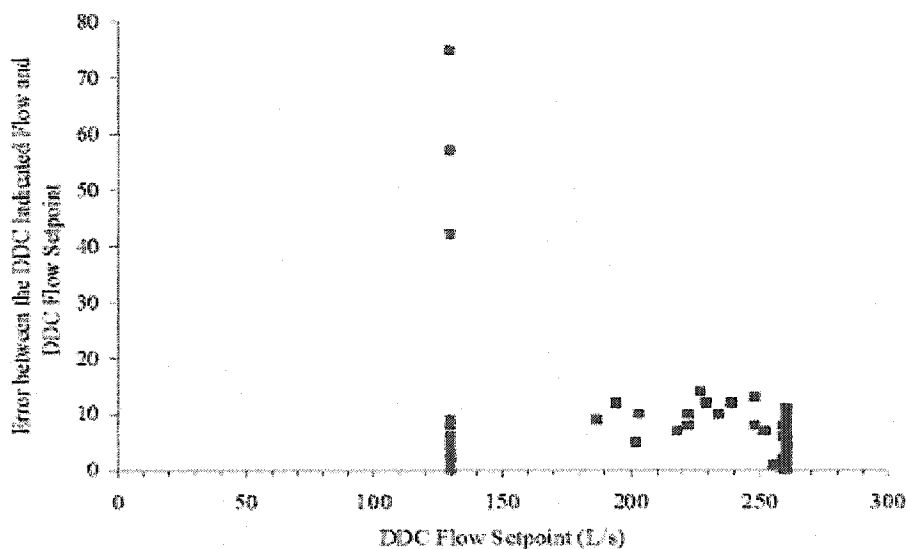


Figure 15: A typical plot of the error in flow rate (Indicated - Set point) versus the flow set point, from the Yellowhead Regional Library BC series, VAV Box #9. Note the error is highest at the maximum and minimum flow set points (260 L/s and 130 L/ on x-axis), indicating that the box experiences its greatest errors when trying to maintain either the fully opened or the fully closed position.

The indication of excessive error “peaks” at the minimum and maximum flow set points indicated a misaligned damper, where a single peak at either the minimum or maximum indicates that the damper simply has a problem in the either the fully closed or fully open position, perhaps indicating a blockage or broken actuator. The terminal presented in Figure 15 had a damper that was misaligned, so that when the controller tried to maintain a fully open position the box was slightly obstructed, likewise, when the box tried to fully close it remained slightly open. Note that in this case the error was as high as ~95%. Ideally, the flow error would be constant and as low as possible, evenly distributed between the maximum and minimum flow set points. For instance, consider Figure 16, which indicates a similar analysis for a terminal that had better damper alignment.

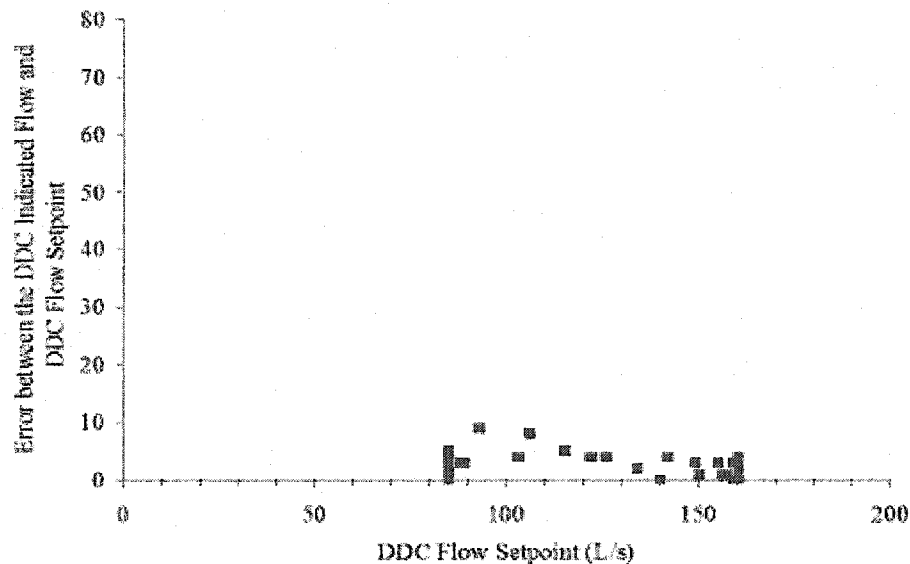


Figure 16: A plot of the Error in flow rate (Indicated - Set point) versus the flow set point, from the Yellowhead Regional Library BC series, VAV Box #11. Note that in this particular case, the error is relatively constant (below 10%) between the maximum and minimum flow setpoints; therefore, the damper was aligned correctly.

This technique was particularly useful during the field-testing, since it is difficult and costly to open the ductwork and examine the damper position of the VAV terminal in an existing facility. Although the actuators and mechanical action are routinely checked during the commissioning process, an internal misalignment would otherwise be quite difficult to identify. These types of operational checks were responsible for catching the majority of the mechanical errors.

4.6 Sources of Error

Sources of error associated with the data collected during field-testing and laboratory experiments were minimized in a variety of ways. DDC systems were checked to ensure the correct variables were being trended through out the recommissioning process, thus the only sources of error commonly encountered during field-testing were measurement and equipment uncertainty. Project equipment was checked regularly and often compared to known standards; for example, pressure transducers were calibrated with a low-pressure measurement system in conjunction with a needle mounted micro-manometer apparatus. Pitot tubes and airflow measurement devices were checked using a standard wind tunnel (with a flat velocity profile) to verify the accuracy and repeatability of the system equipment. The following section addresses the instrumentation and human error associated with this thesis.

4.6.1 Instrumentation Error

The reduction of error involved with the measurement of airflow rate was obviously a major concern within the field testing; unfortunately, relatively little previous work has been published on the topics of airflow measurement and VAV control error, which was also pointed out by Krarti et al. (1999) during the course of ASHRAE RP 980¹¹. Recall that the propagation of standard uncertainty analysis can simply be expressed by the following two equations. Consider a variable (y) that can be expressed by some function, where x_A , x_B , x_N are independent variables and M is a constant, such that:

$$y = f(x_A, x_B, M, x_N) \quad [48]$$

Note that the Taylor method used here assumes that the uncertainty associated with each variable is independent and occurs with equal probability; that is that the uncertainties associated with each variable are random and uncorrelated. If that is true, the errors are considered independent and to find the most probable uncertainty the errors are added in quadrature as indicated in [49].

$$\varepsilon_y^2 = \left(\frac{dy}{dx_A} \varepsilon_A \right)^2 + \left(\frac{dy}{dx_B} \varepsilon_B \right)^2 + 0 + \left(\frac{dy}{dx_N} \varepsilon_N \right)^2 \quad [49]$$

Thus, when determining the uncertainty associated with the airflow measurement (ε_Q), recall that the airflow rate (Q) is simply determined from [50] and [51]. Recall that the velocity (V) is measured with a pitot tube, and is simply an ideal reduction of the Bernoulli Equation where, incidentally, the Bernoulli Equations are a reduction of the Navier-Stokes Equations along a streamline within the flow. Cross sectional area (A) is determined from the diameter of the duct.

$$Q = AV \quad [50]$$

$$V = \sqrt{\frac{2\Delta P}{\rho}} \quad [51]$$

Note that the pressure differential (or velocity pressure, P_V) is simply the difference between the total pressure (P_T) and static pressure (P_S) in the duct as shown below in Equation [52].

$$\Delta P = P_V = P_T - P_S \quad [52]$$

Likewise, the air density (neglecting the effects of humidity) can simply be described using the ideal gas law, where $Ru = 8315$ J/kmol K and the molecular weight (M_{air}) is 28.966 kg/kmol assuming a simplified 79.05% N₂ and 20.95% O₂ mixture.

¹¹ M. Krarti, C. C. Schroeder, E. Jeanette, and M. J. Brandemuehl (2000), "Experimental Analysis of Measurements and Control Techniques of Outside Air Intake Rates in VAV Systems" ASHRAE Transactions 2000 (2), pp. 39 – 52.

$$\rho = \frac{m}{V} = \frac{P}{RT} = \frac{P_{atm}}{\left(\frac{Ru}{M_{air}}\right)T_{duct}} \quad [53]$$

However, an additional error component must be considered because the effects of humidity were ignored. The true air density (accounting for humidity) is represented by [54], where P_b is the corrected barometric pressure; P_{PO} is the partial pressure of water and T_o is the air temperature¹²:

$$\rho_{TRUE} = \frac{1000(P_b - 0.378P_{po})}{R(T_o + 273.15)} \quad [54]$$

An error analysis was completed by Krarti et al. (1999) in RP 980, who used both the accepted ASHRAE standards and experimental data from a number of typical US cities to conclude that the typical error associated with neglecting humidity range from 0.48% to 0.63%¹³. For the purpose of the field testing it was assumed that using the Ideal Gas Law provided in [53], and thus neglecting the effects of humidity, will introduce a maximum error of ~1.0% with respect to the air density term (with a factor of safety to account for the worst case conditions). By applying the Taylor approach, recall [48] and [49] to [50] and [51] it can be shown that the uncertainty associated with a typical airflow measurement (ε_Q) is related to the uncertainty of the area, pressure differential and air density, as shown with the following partial derivatives:

$$(\varepsilon_Q)^2 = \left(\frac{dQ}{dA} \varepsilon_A\right)^2 + \left(\frac{dQ}{d\Delta P} \varepsilon_{\Delta P}\right)^2 + \left(\frac{dQ}{d\rho} \varepsilon_\rho\right)^2 \quad [55]$$

A pitot tube was typically used in both the laboratory and field tests to determine airflow rate. Note that within the field test locations an AirData Multimeter was utilized that had a manufacturer's calibrated accuracy that was better than a typical pitot tube (due to a very accurate pressure transducer, recall Table 4). The maximum uncertainty of the pressure transducers used during field-testing was < 2%. Likewise, it was found from experimental measurements that the diameter of spiral circular ductwork varies by less than 1% from the mean value; note a 6" duct was found to be only +/- 0.04" but a larger 2% uncertainty was used to estimate the worst case conditions. Thus, the uncertainty associated with the area will be 4% (or twice the uncertainty of the diameter), as shown in [56]:

$$\frac{\varepsilon_A}{A} = \frac{2\varepsilon_d}{d} \quad [56]$$

¹² ANSI/ASHRAE Standard 41.2, "Standard Methods for Laboratory Airflow Measurement", ASHRAE, 1987

¹³ Moncef Krarti, Michael J. Brandemuehl, Chris Schroeder and Erik Jeannette, RP 980 Final Report: Techniques for Measuring and Controlling Outside Air Intake Rates in Variable Air Volume Systems, ASHRAE, Final Report JCEM TR/99/03, 1999, Appendix B, pg 74-76.

By considering the terms in Equation [55] it can be shown with Equations [50] and [51] that the following partial derivatives can be substituted into the error analysis:

$$\frac{dQ}{dA} = \sqrt{\frac{2\Delta P}{\rho}} \quad [57]$$

$$\frac{dQ}{d\Delta P} = A \sqrt{\frac{2}{\rho}} \left(\frac{1}{2\sqrt{\Delta P}} \right) \quad [58]$$

$$\frac{dQ}{d\rho} = \frac{-A}{2} \sqrt{2\Delta P} (\rho^{-3/2}) \quad [59]$$

Therefore, by simply substituting [57], [58] and [59] back into [55] with the uncertainties of 1%, 2% and 2% for the density (ε_{ρ}/ρ), diameter (ε_D/D) and pressure ($\varepsilon_{\Delta P}/\Delta P$) components, respectively, it can be shown that the uncertainty associated with the flow rate measurement (ε_Q/Q) is 2.3%. An error of 2% was considered reasonable for all other instrumentation, recall from Table 4 that the typical instrumentation error is substantially less than 2%. After the consideration of calibration and data acquisition uncertainty, these values varied (and remained close to 2%) with respect to flow rate. The results of this uncertainty analysis were expected and followed the calculations completed by Krarti et al. (1999); thus, the experimental measurement error is considered acceptably low.

4.6.2 Human Error associated with a Pitot Tube Traverse

Human error is a potentially significant factor in any experimental work. The majority of measurements minimized human error by using automated measurement systems, such as a DAS or the trend functions of DDC systems. However, there was a significant portion of the research where human error sources could not be eliminated: the pitot tube traverse. The pitot tube traverse is an extremely common measurement technique, largely due to its simplicity. However, correctly traversing a circular duct using the ASHRAE recommended equal-areas method requires a degree of experience and control. Throughout the recommissioning process as many as 7 people were responsible for completing pitot tube traverses. For this reason, a laboratory experiment was carried out to statistically determine the human error that could be expected. Individuals were asked to complete both single point and full duct traverses (full refers to the equal-areas method) in a controlled apparatus with an “ideal” and “poor” location. The “poor” location was characterized by transitions or other non-straight ductwork placed immediately upstream of the traverse plane.

4.6.2.1 Experimental Setu

This experiment was primarily a statistical study that focused on determining the typical human error when making both centerline and equal area pitot tube traverses. A population of 30 people from the Mechanical Engineering Department at the University of Alberta was asked to complete both centerline and full traverses at two test locations. The first location was immediately after $\sim 30D$ of straight circular ducting and was designated as the “ideal” case; the second location was immediately following both a 90° elbow and a 10” to 8” concentric reducer, and was designated as the “poor” case. The “poor” location included secondary flow regions and a sharply skewed velocity profile. The experimental setup is outlined in Figure 17.

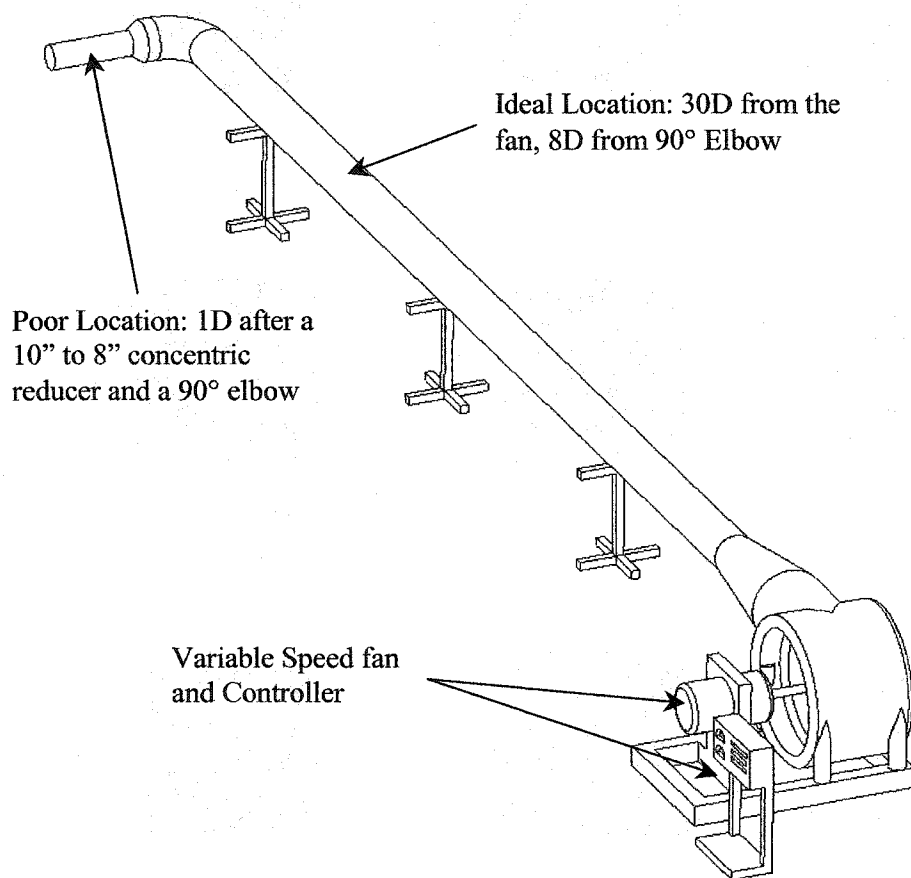


Figure 17: Experimental setup for the pitot tube laboratory study. Pitot tube traverses were completed at both the “ideal” and “poor” test locations; measurements were made with the Shortridge instrument pack and included both an Equal-Areas (24 point) traverse and a centerline velocity measurement.

The Shortridge instrument pack was used take all measurements during this experiment and the readings were compared to a standard VAV airflow sensor that was calibrated with a full pitot tube traverse (using a stationary pitot tube holder and precise measurements). The Shortridge

was calibrated in a wind tunnel. Each of the 30 subjects was instructed to take velocity measurements with the Shortridge: first, the subjects measured a centerline velocity in the ideal duct location and recorded the value. Second, the subjects did a 3-plane pitot tube traverse in the ideal duct location using the Equal-Areas method to record a 24-point traverse of the duct, which is outlined by ASHRAE and shown in Figure 18. This procedure was repeated in the “poor” test location.

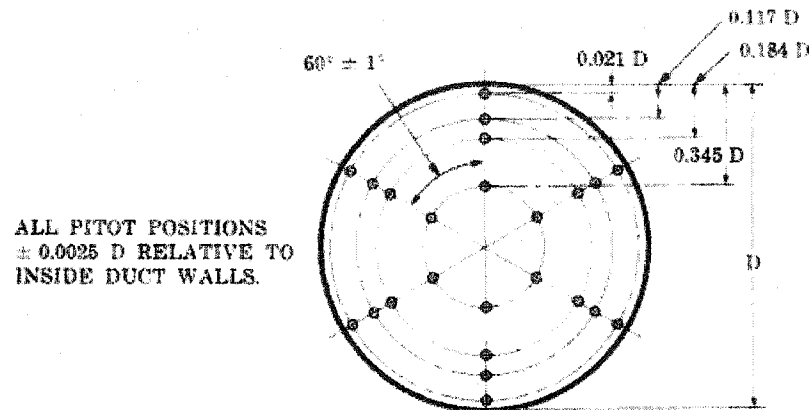


Figure 18: The equal area method for a pitot tube traverse that is recommended by ASHRAE for round ducts. Although this is (arguably) the best way to make a standard field measurement, a full traverse is seldom completed due to the significant amount of time required to setup and make this type of measurement accurately.¹⁴

4.6.2.2 Theory

It was expected that the variance in pitot tube measurements would follow a roughly normal distribution; that is the indicated airflow rates would form a symmetrical bell shaped curve around the mean value, μ , with some standard deviation, σ . The true definition of a normal distribution specifies that any velocity value must be possible, however, this requirement is often waived to improve the practicality of the method. A typical recommissioning procedure involves a large number of measurements, thus it is also common for a contractor to save time by completing only a centerline velocity measurement prior to a VAV terminal. During the course of the field-testing only pitot tube traverses were completed to improve accuracy; however, centerline velocity measurements were included because they are such a common occurrence. The centerline velocity (U_C) is typically the maximum velocity in the duct; thus, a recommissioning agent often determines the average velocity in the duct (V_T) from the centerline readings using [60].

¹⁴ ANSI/ASHRAE Standard 41.2-1987 (1987), “Standard Methods for Laboratory Airflow Measurement”, ANSI/ASHRAE Standard.

$$\frac{V_T}{U_C} = (1 + 1.33\sqrt{f})^{-1} \quad [60]$$

The friction factor (f) was based on the Moody Diagram since the Re_D was determined to be 2×10^5 , thus the true velocity is given by [61] at the “ideal” and “poor” test locations.

$$\text{Ideal: } V_T \cong 0.84(U_C) \quad \text{Poor: } V_T \cong 0.83(U_C) \quad [61]$$

It is important to note that the coefficient provided above will change with the flow rate and is only valid for these laboratory experiments. The study highlights the variance in both a full traverse and a single centerline measurement since both are commonly used in the HVAC industry. The centerline velocity measurements provide a valuable check of the traverse data.

4.6.2.3 Results

The results of 30 trials were evaluated statistically and it was concluded that the data were best represented by a normal distribution (note, ranking was evaluated using a Chi-Square comparison). A summary of the airflow rates (Q) is provided in Table 5.

Table 5: Summary of Results for Human Error associated with a Pitot Tube Traverse

	Ideal Location		Poor Location		True Airflow Rate
	Traverse	Centerline	Traverse	Centerline	
	Q (m ³ /s)	Q (m ³ /s)	Q (m ³ /s)	Q (m ³ /s)	Q _{TRUE} (m ³ /s)
μ	0.615	0.626	0.644	0.678	0.612
σ	0.019	0.020	0.026	0.021	0.005
Minimum Value	0.568	0.584	0.585	0.609	0.600
Maximum Value	0.651	0.662	0.681	0.709	0.620
$\mu + \sigma$	0.635	0.646	0.669	0.699	0.617
$\mu - \sigma$	0.596	0.606	0.618	0.658	0.606
% in region	69	67	63	76	70
$\mu + 2\sigma$	0.654	0.666	0.695	0.719	0.623
$\mu - 2\sigma$	0.576	0.586	0.593	0.637	0.601
% in region	97	95	97	97	95
$\mu + 3\sigma$	0.674	0.686	0.721	0.740	0.628
$\mu - 3\sigma$	0.557	0.567	0.567	0.617	0.595
% in region	100	100	100	99	100

It was expected (and verified with the results in Table 5) that the air velocity from the traverses was higher than the true velocity, simply due to the nature pitot traverses. The full traverse requires several points to be measured quite close to the duct walls, where intuitively an

individual will tend to measure more points near the center of the duct (where the velocity is much higher). Thus, it was expected that the average velocity in each of the traverses would be over estimated. When comparing centerline velocities at the good location, the traverse indicated $0.615 \text{ m}^3/\text{s}$ while the centerline value was, on average, $0.626 \text{ m}^3/\text{s}$. The values for the poor location were $0.644 \text{ m}^3/\text{s}$ and $0.678 \text{ m}^3/\text{s}$, respectively. The transverse values were lower than the centerline flow rates by factors of 0.98 and 0.95 for the ideal and poor locations, respectively; this is quite different from the theoretically predicted coefficient of 0.84. The % change in the average flow rates (ϵ), [62], are summarized in Table 6.

$$\epsilon(\%) = \frac{|Q_{TRUE} - Q|}{Q_{TRUE}} \quad [62]$$

Table 6: Summary of % Changes*

		Ideal Location		Poor Location	
		ϵ , Traverse	ϵ , Centerline	ϵ , Traverse	ϵ , Centerline
Average	(%)	0.55	2.33	5.24	10.86

*The true flow rates (Q_{TRUE}) are the values presented in Table 5, and the difference between the average velocities for each of the trials is presented above.

The data for each of the four test were well represented by a normal distribution. The results for the “ideal” traverse location are presented in Figure 19. The human error associated with a pitot tube traverse is, as expected, dependent on the departure from ideal symmetrical flow at the traverse location (it varied from 0.6% to 5.2% when “ideal” and “poor”).

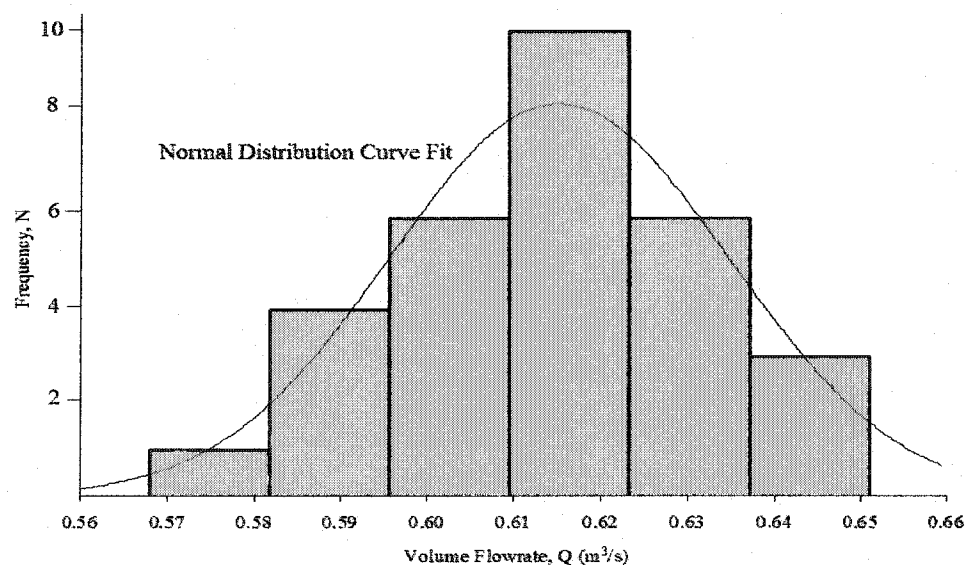


Figure 19: Normal Distribution fit for the “ideal” location, full traverse.

5.0 Discussion of Field Results

As expected, the experimental results indicate that building recommissioning is beneficial in terms of system performance, DDC system accuracy, and energy efficiency as well as variables that are harder to quantify, such as thermal comfort. The field test results were also used to estimate the frequency at which commissioning should be completed on an existing VAV system with DDC (the longevity of the recommissioning process). Longevity was evaluated by considering DDC accuracy, IAQ, energy savings and thermal comfort at each facility before and after recommissioning was completed and after tracking the deviation in performance; these results are summarized below. Unfortunately, it was determined that a longer period (2 years was the maximum considered here) would be required to gauge the true longevity. It was also verified that the improvement of individual VAV zone control is the most significant benefit of recommissioning, and resulted in greater IAQ, thermal comfort, DDC system accuracy, and energy efficiency. The change in DDC system accuracy for every VAV terminal considered during the field tests were created. These charts are of the same form as Figure 14, and indicate the DDC system calibrations during each of the data trends (BC, AC and AAC). These results are crucial to the following analysis. The laboratory experiments evaluated the significance of various upstream conditions on VAV sensor accuracy and identified the “worst” conditions, from a recommissioning standpoint.

5.1 DDC System Errors

A small number of significant control system errors were identified during the field tests. These errors are often due to the complexity of the DDC systems and occur at the design level. These errors are not detected with regular maintenance and can waste a significant amount of energy. Fortunately, control system errors are quite rare as DDC systems are generally well designed.

1. EOL static pressure measurements are typically used to control the supply fan speed; however, at the Cross Cancer Institute the EOL pressure was also used within a secondary feedback loop to control static pressure dampers. A control logic error in the system forced the supply fan to run at the static high-pressure limit of the plenum at all times. Both the 4th and 5th floors were equipped with modulating static dampers; presumably in the belief that this would facilitate better control. However, while the dampers were programmed to limit duct static pressure to 250 Pa, the supply fan was programmed to maintain 250 Pa with no reference between the control loops. Thus, a conflict ensued between the separate control loops that caused the dampers to close while simultaneously ramping the fans to the high limit, resulting in a large energy inefficiency.

The solution to this problem was quite simple, the dampers were disabled restoring fan control and constant static pressure was thus maintained in all supply ducts (+/- 40 Pa from one duct to the next). This DDC system error was continually wasting ~200 Pa of supply fan static pressure; further discussion of these energy savings is completed in Section 5.4.3.

2. The central heating coil in the AHU of the Yellowhead Regional Library was originally stuck open and although the supply air temperature often exceeded the maximum allowable system setpoint, the DDC system indicated no system alarms. Due to this fundamental DDC control error the HVAC system was allowed to operate in this manner for a great deal of time (the supply air was effectively being fully heated, even in cooling mode). Thus, the heat was not only wasted but the air was then reconditioned and cooled, resulting in excessive energy losses and compromised thermal comfort.

This is not an exclusive list of all the control system problems identified within the field tests but these are a couple of the more significant examples. These major errors were found at two of the three field test locations and either of the problems could be used to partially (if not fully) justify the expense of a recommissioning procedure.

5.2 Improved DDC System Accuracy

The improvement of control system accuracy in a VAV system equipped with DDC is the single most important benefit of the recommissioning process; likewise, the DDC accuracy analysis is an essential tool used to evaluate the effectiveness of recommissioning. DDC system accuracy can dramatically affect the energy savings associated with VAV systems as well as the comfort and IAQ within each zone. Note that for the purposes of this discussion that the term accuracy refers to the difference between the indicated flow rate (monitored by the DDC system) and the true flow rate (based on direct measurements) while the term precision refers to the scatter associated with the indicated flow rates. The accuracy analysis described in this section is limited in that it cannot adequately account for the time response of the system (this is discussed further in Section 5.2.4). However, a similar approach could be followed by a dedicated recommissioning agent who wished to quantify the benefits of their work, or by a building owner to indicate which terminals were contributing to excessive system errors or energy inefficiencies.

5.2.1 Methodology for DDC Accuracy Analysis

The methodology used to complete the DDC accuracy analysis is presented below for added clarity. The benefit of this simple analysis is that DDC system trend data is not needed. The relationship between the measured and indicated airflow rates was determined using a linear calibration equation and compared to the ideal case; where the ideal case is simply $Q_I = Q_M$, or that the indicated flow rate equals the measured flow rate over the entire VAV range. The improvement in DDC system accuracy for a single VAV terminal can then be determined at any point by subtracting the absolute value of the ideal case and the BC calibration equation from the absolute difference between the ideal case and the AC calibration equation, shown in Figure 20.

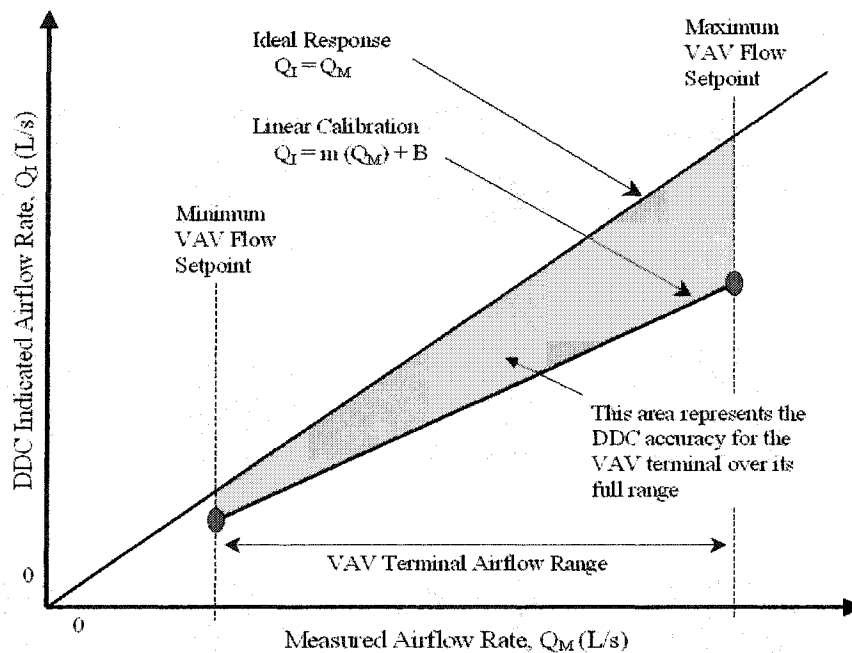


Figure 20: A simple representation of the DDC error region associated with a linear VAV terminal calibration. The linear calibration equation is determined by airflow measurements taken at the minimum and maximum VAV flow setpoints; the area between the linear calibration and the ideal case is related to DDC error. After recommissioning, the points become closer to the ideal case and the error region decreases in size.

5.2.2 Sample Calculations for the Yellowhead Regional Library

The calculations for the Yellowhead Regional Library are provided below. Identical analyses were completed for each of the test locations (included in Appendix B, Section 1), however, in the interest of clarity and brevity only the Yellowhead Regional Library calculations are directly discussed here. The calibration equations for each VAV terminal were determined (for each data trend, BC, AC and AAC) by comparing the airflow indicated by the DDC system to the experimentally measured airflow rates, as shown in Table 7.

Table 7: Recommissioning Airflow Measurements at the Yellowhead Library*

VAV	BC Trend				AC Trend				AAC Trend			
	M1 (L/s)	M2 (L/s)	I1 (L/s)	I2 (L/s)	M1 (L/s)	M2 (L/s)	I1 (L/s)	I2 (L/s)	M1 (L/s)	M2 (L/s)	I1 (L/s)	I2 (L/s)
1	153	344	148	289	147	284	147	295	209	286	205	289
2	95	344	80	289	88	174	83	179	85	173	83	179
3	69	151	60	110	78	132	59	113	80	120	63	111
4	118	312	116	231	125	218	120	232	142	222	123	235
5	108	174	70	141	94	151	72	143	92	150	72	143
6	87	161	83	160	87	160	84	161	84	156	82	160
7	166	222	111	220	114	211	113	221	104	222	111	227
8	214	248	143	250	129	248	140	245	108	290	143	270
9	71	149	134	256	126	274	134	269	142	249	132	255
10	341	687	293	582	306	571	300	585	253	566	308	573
11	106	197	84	162	86	165	87	161	76	160	88	161
12	234	394	236	400	234	394	236	400	245	410	235	410
13	155	293	132	257	136	258	132	260	130	252	131	258
14	234	394	236	400	234	394	236	400	228	388	238	392
15	166	303	115	227	128	230	120	234	109	214	118	222
16	180	298	175	300	185	309	180	308	173	308	180	302
17	172	198	108	210	153	210	105	212	126	222	108	205

*Note: the “M” terms refer to the direct airflow measurements and the “I” terms refer to the airflow indicated by the DDC system for each of the three trends (BC, AC and AAC). DDC systems only make allowances for linear calibration factors; so only two values were needed for each terminal, one at the minimum flow setpoint and one at the maximum (labeled 1 and 2).

The terminal calibrations were determined using linear equations to predict the relationship between the true and DDC indicated flow rates using the form in [63].

$$Q_M = \frac{(Q_I - B)}{m} \quad [63]$$

Laboratory testing later verified that this relationship is better represented with a second order polynomial. However, all of the DDC systems considered during the field tests only allowed for a linear calibration equation, which is a common weakness of older DDC systems. The slope and y – intercept (designated m and B in [63], respectively) should ideally be 1.0 and 0.0 if a perfect calibration were completed; however, it is often impossible to achieve a perfect VAV terminal calibration even with a detailed recommissioning procedure. The values for the calibration equations at the Yellowhead Regional Library are provided in Table 8.

Table 8: Linear Calibration Equations for the Yellowhead Regional Library*

VAV	MIN	MAX	BC Trend		AC Trend		AAC Trend	
	(L/s)	(L/s)	m	B	m	B	m	B
1	200	290	0.74	35.05	1.08	-11.80	1.09	-23.00
2	80	180	0.84	0.26	1.12	-15.23	1.10	-10.26
3	60	110	0.61	17.93	1.00	-19.00	1.20	-33.00
4	116	233	0.59	46.05	1.20	-30.54	1.40	-75.80
5	70	142	1.08	-46.18	1.25	-45.09	1.22	-40.62
6	80	160	1.03	-6.63	1.05	-7.77	1.08	-9.13
7	110	280	1.95	-212.11	1.11	-13.93	0.98	8.76
8	140	280	3.15	-530.47	0.88	26.18	0.70	67.97
9	130	260	1.55	24.43	0.91	19.07	1.15	-31.23
10	295	590	0.84	8.18	1.08	-29.09	0.85	93.80
11	85	160	0.85	-5.93	0.94	6.44	0.87	21.95
12	230	400	1.03	-3.85	1.03	-3.85	1.06	-25.16
13	130	260	0.91	-8.40	1.05	-10.69	1.04	-4.33
14	235	400	1.03	-3.85	1.03	-3.85	0.96	18.55
15	115	230	0.82	-20.71	1.12	-23.06	0.99	10.04
16	175	300	1.06	-15.68	1.03	-10.97	0.90	23.66
17	105	210	3.92	-566.77	1.88	-182.21	1.02	-20.25

*Note: Linear equations are of the form $Q_I = m(Q_M) - B$ where Q_I refers to the DDC indicated airflow rates and Q_M refers to the true airflow rates from direct measurement. Note that the slopes are typically closer to 1.0 after recommissioning (in the AC and AAC Trends) to signify an improvement was made. The "MIN and MAX" columns refer to the setpoints used by the DDC to control that space and specify the range of the VAV terminals operation.

The DDC airflow error (ε_{FLOW}) was determined as a percentage of the true flow rate at the midpoint of the VAV operational range using [64].

$$\varepsilon_{FLOW} = \frac{(Q_I - Q_M)}{Q_M} \quad [64]$$

The choice of where along the range to evaluate DDC error is significant; for instance, it will later be shown that the error at the minimum flow setpoint has a large effect on energy consumption when the HVAC system is in heating mode. For the purpose of this analysis, the midpoint of the VAV terminal range was chosen, halfway between the maximum and minimum setpoints. The results for the Yellowhead Regional Library are summarized in Table 9 where a negative error (ε_{FLOW}) indicates excessive ventilation and a positive error indicates under ventilation within a zone.

Table 9: Flow Error at the midpoint of the VAV range for the Yellowhead Library*

VAV	VAV Midpoint (L/s)	BC Trend		AC Trend		AAC Trend	
		Q _M (L/s)	ϵ_{FLOW} (%)	Q _M (L/s)	ϵ_{FLOW} (%)	Q _M (L/s)	ϵ_{FLOW} (%)
1	245.0	284.4	-13.9%	237.7	3.1%	245.6	-0.3%
2	130.0	154.5	-15.9%	130.1	-0.1%	127.8	1.7%
3	85.0	110.0	-22.7%	104.0	-18.3%	98.3	-13.6%
4	174.5	216.6	-19.5%	170.2	2.5%	178.7	-2.4%
5	106.0	141.4	-25.1%	121.3	-12.6%	119.7	-11.5%
6	120.0	122.3	-1.9%	121.1	-0.9%	119.0	0.8%
7	195.0	209.1	-6.8%	187.6	3.9%	189.4	2.9%
8	210.0	235.2	-10.7%	208.3	0.8%	203.8	3.0%
9	195.0	109.7	77.7%	192.8	1.1%	196.8	-0.9%
10	442.5	519.9	-14.9%	438.5	0.9%	411.8	7.4%
11	122.5	150.6	-18.7%	123.9	-1.1%	115.7	5.9%
12	315.0	311.0	1.3%	311.0	1.3%	320.3	-1.7%
13	195.0	224.5	-13.2%	196.0	-0.5%	191.4	1.8%
14	317.5	313.5	1.3%	313.5	1.3%	310.6	2.2%
15	172.5	236.3	-27.0%	174.9	-1.4%	164.0	5.2%
16	237.5	239.0	-0.6%	240.7	-1.3%	236.6	0.4%
17	157.5	184.6	-14.7%	180.9	-13.0%	174.6	-9.8%

*Note: Flow error refers to [64] where the VAV midpoint is used as the Q_i and the true flow rate, or Q_M value, is then used to determine the flow error. The VAV midpoint is simply the value halfway between the minimum and maximum VAV airflow setpoints; thus, flow error could also be labeled as the DDC system error associated with a particular VAV terminal calibration.

This analysis was useful because it could be used to approximate the improvements made to DDC accuracy at each stage of the recommissioning process. For instance, consider the results for VAV terminal #1 in Table 9. Prior to recommissioning, the terminal was providing 284.4 L/s while indicating 245.0 L/s; this resulted in apparent over ventilation of the zone by 39.4 L/s or 13.9%. Immediately after recommissioning (AC) the calibration was improved so that the DDC was now accurate within ~ 8 L/s (or 3.1%). This analysis was useful for indicating the percentage improvement at each terminal, without the use of DDC trend data. This technique can also be used to indicate the recommissioning longevity by considering the improvements made from the BC to AC trend versus the BC to AAC trend, as shown in Table 10.

Table 10: Improvement for the Yellowhead Regional Library*

VAV	Improvement from BC to AC (%)	Improvement from BC to AAC (%)
1	10.8	13.6
2	15.8	14.2
3	4.5	9.2
4	17.0	17.1
5	12.5	13.6
6	1.0	1.1
7	2.9	3.8
8	9.9	7.7
9	76.6	76.8
10	14.0	7.5
11	17.6	12.8
12	0.0	-0.4
13	12.6	11.3
14	0.0	-1.0
15	25.6	21.8
16	-0.7	0.3
17	1.7	4.9

*Note: The improvement refers to the absolute difference between the BC flow error (ϵ_{FLOW}) and the AC and AAC flow errors. By comparing these values for each terminal, it is possible to gauge the deviation of the recommissioning process over time. In this case, the deviation occurred over an 8-month period at the Yellowhead Regional Library. A positive value indicates that the accuracy is better than it was originally. In addition, recall that the experimental error associated with these values is 2.3%.

It was expected that the values in Table 10 were similar since the space requirements at this small facility did not change significantly; note that the deviation between the percentage improvements are never greater than 7% and are on average only 2% (between the BC to AC and the BC to AAC trends). This indicates very good recommissioning longevity over 8 months.

5.2.3 Results of DDC Accuracy Analysis

The DDC system accuracy results (evaluated at the midpoint of the VAV terminal range) for all of the field test locations are summarized in Table 11. These results are still dependent on the midpoint assumption and do not use the DDC trend data.

Table 11: Summary of DDC Accuracy Analysis Improvements for all VAV Terminals

		Yellowhead Regional Library (17 VAV Terminals)		
		BC to AC Trend	BC to AAC Trend	Difference
Average	(%)	13.0	12.6	0.4
Maximum	(%)	76.6	76.8	
Minimum	(%)	-0.7	-1.0	

		Cross Cancer Institute (51 VAV Terminals)		
		BC to AC Trend	BC to AAC Trend	Difference
Average	(%)	3.8	1.9	1.9
Maximum	(%)	19.3	16.7	
Minimum	(%)	-4.6	-4.4	

		Timms Center for the Arts (51 VAV Terminals)		
		BC to AC Trend	BC to AAC Trend	Difference
Average	(%)	9.0	10.4	-1.4
Maximum	(%)	38.8	29.5	
Minimum	(%)	-1.7	-1.5	

*Note: This is a summary of the same analysis that has been presented throughout the section; the results for the first block are directly from Table 10. The “Difference” column is a merely a measure of longevity: in this case a positive difference means that the DDC systems accuracy has been reduced with time while a negative value means the system accuracy has improved. Recall that the experimental error associated with these values is of the scale of 2%.

The results of the DDC accuracy analysis from the Timms Center for the Arts are very consistent with the conclusions from the Yellowhead Regional Library. The Timms Center improved significantly in terms of the average DDC system accuracy, by 9.0% and 10.4% during the BC to AC and BC to AAC trends, respectively. By comparison, the improvements made at the Cross Cancer Institute were far more modest at 3.8% and 1.9 % during the BC to AC and BC to AAC trends, respectively. This was primarily due to poor upstream duct conditions, which were quite common at the Cross Cancer test location; the effects of poor upstream conditions prior to VAV flow sensors is discussed further on in Section 7.0.

The “worst” VAV terminals, represented by the “Minimum Improvement” rows in Table 11, were quite similar for all three-test locations. At each test location, there were a small number of VAV terminals that were less accurate after the recommissioning process. Although typically the decrease in accuracy was well within the ~ 2% uncertainty associated with the measurements there were also 3 instances, out of the 119 VAV terminals considered during the field tests, where terminal accuracy was simply reduced (greater than 2%). All three of these cases were at the Cross Cancer Institute and can be attributed to human error on the part of the recommissioning team in combination with extremely poor duct geometry. Poor upstream geometry made it

difficult to take an accurate measure of flow rate using a pitot tube traverse or a flow hood. For instance, Terminal #17 at the Yellowhead Regional Library test location (recall Table 9) was originally inaccurate by 14.7%; after recommissioning, the error was found to be 13% (AC) and 9.8% (AAC). In this instance recommissioning provided only a marginal improvement to the DDC system accuracy, and yet the calibration procedure was applied consistently at other terminals in this facility and was responsible for a far greater improvement. The primary reason for this discrepancy is non-ideal upstream duct geometry, which was present at the Yellowhead Regional Library prior to a number of terminals, including VAV terminal #17. With the exception of a few terminals, the results indicate that the recommissioning procedure substantially improved DDC system accuracy.

It will be shown, with subsequent laboratory experiments (which are presented in Section 7.0), that the true VAV calibration curve is better represented by a second order polynomial in cases with non-ideal upstream duct conditions. The laboratory experiments show that the shape of the polynomial will vary but only the ideal case (which was simulated with 40D of straight ducting) provides a linear calibration equation. For instance, consider Figure 21; the linear calibration clearly does not represent the true response of the VAV terminal well, thus, recommissioning will provide only a limited improvement.

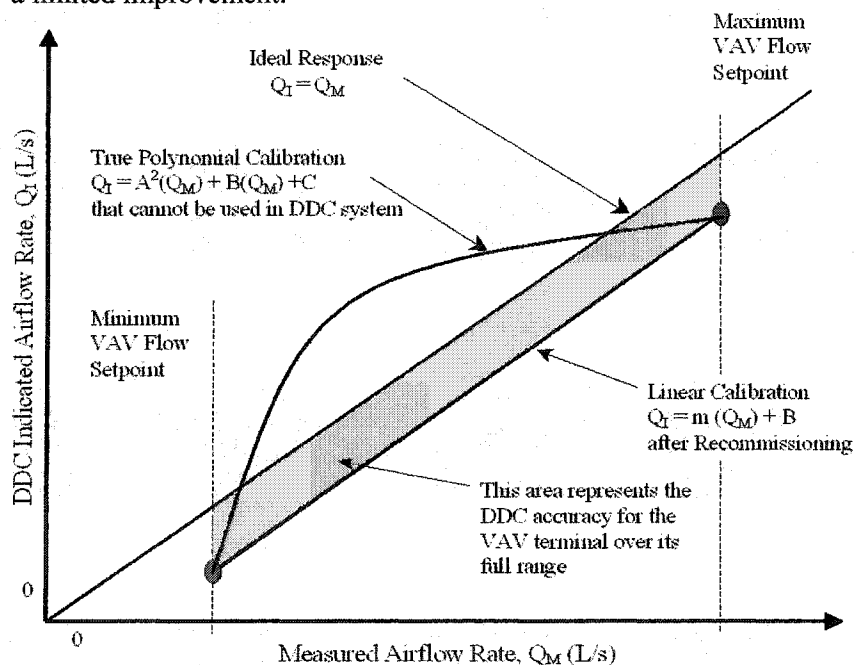


Figure 21: A simple representation of the DDC error region associated with a linear VAV terminal calibration when compared to the true VAV response. The polynomial becomes more pronounced with non-ideal duct conditions that affect the terminal flow accuracy. This relationship was inferred from the laboratory tests.

It is partially because of the linear limitation on DDC system calibrations that certain VAV terminals at all three facilities showed only marginal improvement, or in the case of the Cross Cancer Institute a reduction in accuracy. Recommissioning did improve the DDC system accuracy for the vast majority of VAV terminals but the local duct conditions sometimes limited the improvement.

5.2.4 Limitations and Benefits of the Analysis

Unfortunately, the previous analysis cannot completely describe the benefits of recommissioning because it is unable to account for the time varying flow rates required in each zone. Recall Figure 21; although the calibration analysis indicates the improvement in airflow accuracy over the entire range of the terminal it is impossible to estimate (without the use of trend data) where the VAV terminal is operating within that range. VAV terminals often do not vary through the entire range of available flow rates in a day, varying slightly in response to the temperature requirements of the space. VAV terminals will operate at the maximum flow setpoint when cooling is required and at the minimum flow setpoint when in heating mode. The airflow accuracy will increase or decrease in relation to the appropriate calibration equations but it is impossible to determine the true improvement in this manner. In the subsequent analysis, the DDC system data trends were used to account for the time variation and provide a quantitative measure of system improvement. However, building operators and recommissioning agents commonly need to work without the benefit of a full DDC system data trend; in which case the previous analysis would be invaluable. Despite the limitations, the previous analysis was also useful for determining which terminals were the most inaccurate, which terminals had the largest influence on the system accuracy (a function of the flow rate at that terminal), and which terminals were improved during the recommissioning procedure.

5.2.5 Methodology for DDC Accuracy Analysis (with Trend Data)

It was determined that the best way to monitor DDC system accuracy was to use the system trend data. This technique is very similar to the analysis that was described within the previous sections; however, the key difference is that the actual airflow rates (collected during the DDC data trends) were utilized instead of assuming the VAV terminal operates at its midpoint. This provided an excellent estimate of the true variations, since the trend period was often quite long (a minimum of 2 weeks to 2 months in duration). With a large trend period, this analysis defines

the absolute improvement of system accuracy due to the recommissioning process; it was assumed that a minimum 2-week trend period provided enough data.

The linear calibration equations for each VAV terminal, recall [63] were used to determine the true airflow rate at each VAV terminal, which corresponds to the measured flow rate (Q_M). The DDC indicated flow rate (Q_I), the true flow rate, (Q_M) and the VAV terminals setpoint flow rate (Q_S) were then used to generate the true DDC system terminal accuracy using [65], [66] and the trend data.

$$\Delta Q = (Q_M - Q_I) \quad [65]$$

$$dQ = VolumeFlowRate(\%) = \left[\frac{Q_S + \Delta Q}{Q_S} \right] \quad [66]$$

The time dependent airflow error (dQ) was determined for each VAV terminal, which in turn was used to indicate the time dependent DDC system accuracy; the results were summed and averaged for each trend period to indicate the total system performance. Thus, if the dQ is closer to 100% after the recommissioning process then this indicates that the system performance has improved. A value greater than 100% means the DDC is indicating over ventilation of the space and conversely, a value less than 100% indicates the DDC believes the space is under ventilated.

5.2.6 Results of DDC Accuracy Analysis (with Trend Data)

It is expected that the accuracy of existing control system sensors will be improved during the course of recommissioning, which is verified from the simple results that were achieved without the benefit of trend data. The results for each of the field test locations (with trend data) are summarized in Table 12. The results of this analysis should agree with the previous DDC accuracy estimations (without trend data); however, the values provided in this section will vary because this analysis uses the correct system operation. The results in the previous section are also slightly skewed because the accuracy of each VAV terminal was simply averaged together. In this section, the results include the relative importance (or weighting) of the VAV airflow rates. For instance, if the DDC system accuracy is improved substantially on several of the very large VAV terminals it is expected that the system response should improve. The previous analysis did not account for the weighted airflow rate of each terminal and could not represent this. Therefore, although 3 VAV terminals decreased in accuracy at the Cross Cancer Institute the improvement to the system was actually very dramatic because all three of these terminals were quite small in terms of the airflow they provided.

Table 12: Results of DDC Accuracy (with trend data) to gauge IAQ*

	Trend Period	Q_I	Q_M	Q_S	ΔQ	dQ
		(L/s)	(L/s)	(L/s)	(L/s)	(%)
Cross Cancer Institute 51 VAV Terminals	BC	9,622	11,497	11,080	1,875	117.7%
	AC	10,596	10,652	11,697	56	100.5%
Timms Center for the Arts 51 VAV Terminals	BC	6,159	6,728	6,016	568	109.5%
	AC	6,539	6,543	6,442	3	100.1%
	AAC	5,961	5,887	6,316	-73	98.9%
Yellowhead Regional Library 17 VAV Terminals	BC	3,602	3,936	3,647	334	109.2%
	AC	3,371	3,298	3,390	-60	97.8%
	AAC	3,425	3,316	3,802	-105	97.3%

*Note: This table includes the average trend data from each of the three test locations in conjunction with the DDC accuracy analysis; a dQ value of 100% indicates that the DDC system is perfectly accurate.

The results of this analysis indicate that the DDC systems at all three of the test locations were originally inaccurate by ~10%; and in each case the HVAC system was providing significantly more ventilation than the DDC system indicated. Prior to recommissioning, test locations 1, 2, and 3 were indicating an over ventilation of 17.7% (1875 L/s), 9.5% (568 L/s) and 9.2% (334 L/s), respectively, when compared to the actual flow rates. After the recommissioning process, the actual airflow closely matched the indicated airflow of the DDC. For instance, locations 1 and 2 indicated an over-ventilation of only 0.5% (56 L/s) and 0.1% (3 L/s) when compared to the DDC system, which is accurate beyond the 2% error associated with the airflow measurements. The Yellowhead Regional Library test location was under-ventilating the space by 2.2% (60 L/s) when compared to the DDC system, although this is still a large improvement in system accuracy. From an IAQ perspective it is beneficial to have more O/A (and thus more ventilation); however, from a system performance perspective it is much more beneficial to be able to accurately monitor the airflow provided to each zone. Indeed, if any of the systems had been providing airflow of 9% or more below the required design set point (for instance, a dQ of 91% or lower) this would pose a significant problem and almost certainly violate IAQ guidelines as well as the original design constraint. For example, the DDC system accuracy within the Cross Cancer Institute was quite important (compared to the other locations considered) since the facilities primary role is as an outpatient care facility and serves as a hospital, yet the control system was found to be underestimating the true supply flow rate by almost 20%. Clearly, there

would be extremely serious consequences if the system were providing 20% less airflow than the DDC system was indicating.

The results also seem to indicate that DDC control system performance improvements do not deteriorate significantly over time, although it is important to note that without further monitoring it is impossible to predict exactly when the recommissioning process ceases to be beneficial. Based on the AAC trends completed at the Timms Center and the Yellowhead Regional Library the maximum deviation in DDC system accuracy was found to be only 1.2%, well within the 2% uncertainty. It is expected that the DDC system accuracy will not deviate significantly since the space usage at each facility remained relatively constant. If all of the VAV terminals operated in a completely different portion of their range (due to a dramatic change in the space usage) then the DDC system accuracy may be affected. However, the relative uniformity of these results (from AC to AAC) indicated that DDC system accuracy is not affected with time. Therefore, it can be concluded that the space usage did not change significantly at the test locations and that the trend lengths were long enough to complete this type of analysis, verifying the earlier assumption.

5.3 Variations in IAQ due to Recommissioning (with Trend Data)

The IAQ associated with having a control system manage each individual zone is one of the most beneficial aspects associated with VAV systems that utilize DDC. Unfortunately, the IAQ associated with the majority of systems does not reflect the benefits that VAV systems should offer, a point that is made by Cappellin (1997):

When VAV systems work right, they provide excellent temperature and humidity control...and meet all criteria required for acceptable indoor air quality...(however) the successful performance of VAV systems is often compromised by flawed conception, faulty design, defective installation, poor start-up, inaccurate operation, and inadequate maintenance.¹⁵

A commissioning procedure is an essential tool for improving indoor air quality by ensuring that the VAV systems do indeed "work right." For instance, Piette et al. (1996) stated, "In general, improvements made in indoor air quality [IAQ] and other non-energy benefits may be more

¹⁵ T. E. Cappellin (1997), "VAV Systems - What Makes them Succeed? What Makes the Fail?" ASHRAE Transactions 1997 part 2, pp. 814 -822.

important than the energy-savings benefits from commissioning.”¹⁶ Piette also discussed the benefits that building commissioning may have on worker performance, noting that employee costs are typically greater than the system costs by several orders of magnitude before concluding that commissioning is “...marginally cost-effective on energy savings alone...”¹⁷ Past work by Krarti et al. (2000), Maki et al. (1997) and Bearg (1997) all commented on the importance of maintaining the minimum outdoor ventilation rates in each zone, while acknowledging that this was not always easy within VAV systems. The field tests sought to verify that each system delivered adequate amounts of outdoor air to the facility before and after the recommissioning process. To accomplish this, an adequate mixing assumption was used to determine the O/A within each zone, which was compared to the minimum O/A from the original design intent.

The following section outlines the experimental method and test results for the tracer gas analysis used to verify system O/A. Past experimental work completed by Maki et al. (1997), on a similar field study involving VAV systems; as well as by Krarti et al. (2000) during the course of ASHRAE RP 980, was used to formulate the tracer gas testing for this research. It is possible to use the tracer gas method to directly measure the O/A throughout each trend; however, due to the limitations of the technique, especially when used continuously within field-testing, a modified analysis was utilized. Tracer gas testing was utilized to ensure adequate O/A but not on a continuous basis; point measurements (which typically lasted ~10 hours) were made instead. The results indicated that all three test locations were providing an excessive O/A, which is excellent from an IAQ point-of-view. However, DDC system accuracy was improved in every case and if any of the systems were under ventilating by the same percentage then serious IAQ problems would have resulted.

5.3.1 Tracer Gas Analysis to verify minimum O/A

The determination of O/A was a primary consideration during the field tests. It was determined that the constant injection tracer gas method was the preferred method to complete these measurements based on previous experimental work. Two tracer gases were initially used, CO₂ and SF₆, however it was found that a suitable differential signal could not be maintained with CO₂ so all tracer gas testing was completed with SF₆ (recall the discussion of tracer gas problems in Section 4.3.4). The constant injection method for a tracer gas measurement is briefly outlined

¹⁶ M. A. Piette and B. Nordman (1996), "Costs and Benefits from Utility-Funded Commissioning of Energy-Efficiency Measures in 16 Buildings", ASHRAE Transactions 1996 (1), pp. 482- 491.

¹⁷ Ibid

below for the purposes of clarity; note that this method is identical for any tracer gas. The O/A is determined from [67]. Note that an excellent explanation of the equations leading to [67], from first principles, were completed by Mui et al. (2003)¹⁸ who also completed a study on VAV systems using CO₂ and SF₆ with the constant injection tracer gas method.

$$O/A = \left(\frac{Q_{O/A}}{Q_{S/A}} \right) = \frac{C_{R/A} - C_{S/A}}{C_{R/A} - C_{O/A}} \quad [67]$$

The O/A, which is simply the ratio of the outdoor air volume flow rate ($Q_{O/A}$) over the supply air volume ($Q_{S/A}$) can be determined by measuring the concentration of tracer gas in the supply, return and outdoor air ducts (designated $C_{S/A}$, $C_{R/A}$, and $C_{O/A}$, respectively). When CO₂ tracer gas is used, the outdoor concentration ($C_{O/A}$) is simply the local environmental concentration when SF₆ is used this value is zero, since a negligible concentration of SF₆ exists naturally in the atmosphere. The constant injection method involves the steady release of tracer gas in the supply duct after a suitable equilibrium is established within the facility. The decay concentration method was criticized in the literature in similar field-testing because the initial and final concentrations (as the tracer gas leaks away) are unusable and judgment must be used to choose the useful data range.

It was experimentally verified that the O/A at each test facility always exceeded the minimum allowable values from the original design intent. The minimum O/A at each facility is based on space usage and occupancy¹⁹, the original design intents specified a minimum O/A of 15% at all three of the test locations. Sample experimental results from the Yellowhead Regional Library are provided in Figure 22, which were completed during the BC trend (prior to recommissioning).

¹⁸ H. K. W. Mui, D. W. T. Chan and J. Burnett (2003). "Dynamic evaluation of airflow rates for a variable air volume system serving an open-plan office", Blackwell Munksgaard Publishing, Denmark, Indoor Air 2003; 13: pp. 311-323.

¹⁹ Recall that the minimum O/A is determined from industry standards, such as the ASHRAE 62-1999 guideline but will also vary with the original HVAC design at each of the test facilities

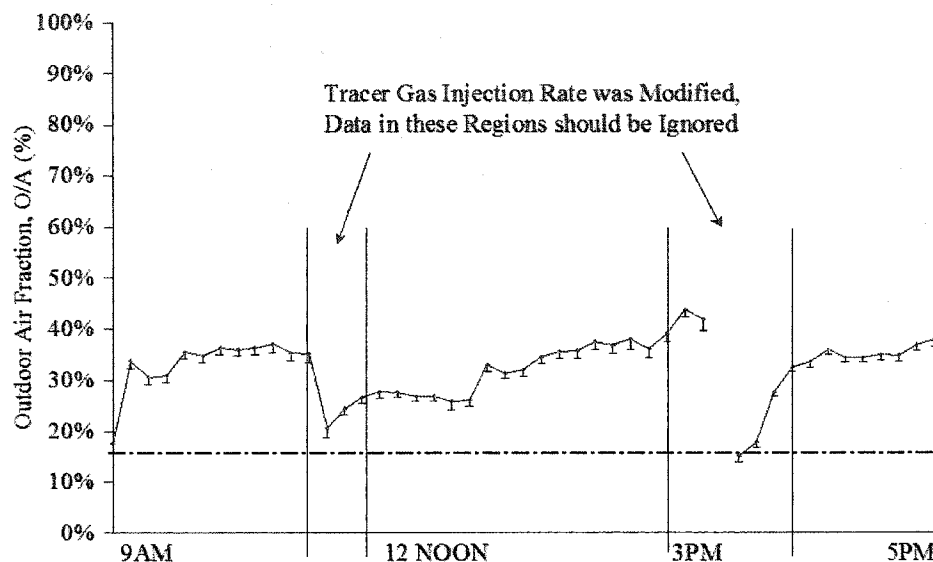


Figure 22: A typical plot of the outdoor air fraction (O/A) determined using the constant tracer gas injection method. This data is from the Yellowhead Regional Library (taken Sept 13, 2002) where the design called for a minimum outdoor air percentage of 15% at all times. Thus, the tracer gas was able to verify that the AHU was ensuring an adequate percentage of outdoor air to the facility (note that O/A does not drop below 15% minimum). The measurements were made over a single day and were later extrapolated over the full trend using the results of the DDC accuracy analysis. The regions located around 11 AM and 3 PM correspond to times when the tracer gas injection rate was manually changed, the data taken after these times (for ~5 points or 50 minutes) should be ignored.

Similar point measurements were made at each of the test locations to verify that the O/A met the minimum values outlined by the original design intent. The measured O/A was then used to determine the volume flow rate of outdoor airflow, as shown in [68].

$$Q_{O/A} = Q_{S/A} (O/A) \quad [68]$$

The same type of calculation was completed on the flow rate from each VAV terminal to determine the outdoor airflow rate into each zone; however, it is important to realize that the zone calculations require an assumption of adequate mixing. This assumption is generally valid at each of the field test locations; a well-designed system will have adequate mixing. It was found that the minimum O/A was exceeded both before and after the recommissioning process for each test location, this concluded the IAQ verification for the field tests.

5.4 Energy Savings due to Recommissioning (with Trend Data)

The efficient energy utilization and, by implication, the economic benefits of VAV systems with DDC have been recognized for some time. The optimization of building and HVAC systems is a

more recent trend that reflects both a growing energy consciousness and a greater sense of economic awareness. Hayter and Judkoff (1999) made the point that “A building that is not properly commissioned will not meet the energy efficiency design goals.”²⁰ when they completed a recent study focused on building optimization. Elovitz (1992) also made the argument that building commissioning is an essential tool, especially when concerning the use of VAV systems. He further went on to say, “One of the most important aspects of building commissioning is verifying sensor calibration.”²¹ Previous work completed by Piette et al. (1996) also concluded that building commissioning is “...marginally cost effective on energy savings alone...” within the 16 building recommissioning projects that were considered within their study. They also made the argument that the “...non-energy benefits, which are difficult to quantify, are greater than the energy benefits.”²²

Despite the clear economic benefits, recommissioning is often ignored after significant renovations or changes to space functions; thus, these systems may not fulfill basic ventilation or comfort requirements and will certainly not operate in an energy efficient manner. One of the chief goals of the field research was to identify the energy savings that result from the recommissioning process and to determine how these cost savings deviate with time. In this section, annual energy savings that resulted from recommissioning will be discussed. The literature indicates the energy benefits of recommissioning VAV systems are between 5% and 30% of the total system energy, Roth et al.²³ (2003). During the course of the field tests it was determined that the supply fan energy savings associated with recommissioning are quite consistent with this estimation; for instance, it was determined the supply fan energy savings were on the scale of 10% by simply improving the EOL static pressure transducer calibrations.

Supply fan energy use was found to be one of the best indicators for the assessment of the energy benefits: although in terms of cost there are several other factors that are more significant. For instance, return fan energy use is also considerable but since return fans often simply track the supply fan speed, or maintain a building pressurization setpoint, the change in energy use can be

²⁰ S. J. Hayter and R. Judkoff (1999), "Optimizing Building and HVAC Systems", ASHRAE Journal, December, 1999, vol. 41, no. 12.

²¹ K. M. Elovitz (1992), "Commissioning Building Mechanical Systems", ASHRAE Transactions 1992 (2), pp. 543 – 552.

²² M. A. Piette and B. Nordman (1996), "Costs and Benefits from Utility-Funded Commissioning of Energy-Efficiency Measures in 16 Buildings", ASHRAE Transactions 1996 (1), pp. 482- 491.

²³ K. W. Roth, D. Westphalen and D. Brodrick (2003), "Saving Energy with Building Commissioning", ASHRAE Journal, November, 2003.

estimated with only the supply fan speed. Other energy considerations may include the wasted energy required to condition incorrect (too large) airflows, which can be estimated with a simple degree-day analysis. Note, although a degree-day analysis was completed (Appendix B, Section 2), and the results are generally consistent with the other energy indicators, this technique will not be included in the discussion due to the many assumptions required to complete the calculations. Other benefits associated with recommissioning may include incidental improvements such as identifying a misaligned damper or an out of calibration pressure transducer, which may also be significant depending on the flow rate or the function associated with the device. The following section focuses on the energy savings associated with: EOL static pressure sensor calibrations and supply fan savings in heating mode (at the minimum flow setpoint where the flow error is typically the highest). A brief discussion of economics is used to estimate the energy costs and payback periods.

5.4.1 Simple Economic Considerations

A number of assumptions were needed to approximate the economic consequences of recommissioning, including estimations of the local cost of energy (electrical power) and the recommissioning cost at each facility. The economic calculations are quite basic; however, the implications for energy savings are readily apparent. Electrical prices in the area have increased steadily over the last 4 years²⁴. The cost of electricity for all of the economic calculations within this research were based on the rate of 0.0745\$/kWh²⁵. It is evident from past energy rates that further increases can be expected within the local area, indicating that the benefits of recommissioning will continue to become more apparent. Conclusions are later discussed in terms of the simple payback period for the recommissioning process, which is determined using [69]. This simple payback period is only accurate for “short” time-periods (say up to 3 years). Interest rates will become more significant over longer time-periods.

$$\text{Payback} \equiv \left[\frac{\text{Commissioning Cost}}{\text{Annual Savings}} \right] \quad [69]$$

The expected capital cost of recommissioning was determined based on the industry practices for the local area²⁶. The estimated recommissioning cost at the Yellowhead regional Library was

²⁴ The cost of electricity has increased by ~ 83% from early 2000 (0.0405\$/kWh to 0.0745\$/kWh).

²⁵ Current rate for commercial facilities in Edmonton, AB (and area) as of January 2002 when the bulk of this research was completed based on an ATCO quote, which is an electricity provider.

²⁶ This is not an absolute standard but it is a good representation of the current cost of building commissioning from Stantec Consulting Ltd., a company that frequently completes similar recommissioning projects in the Edmonton Area.

\$1,000 while the cost at both the Timms Center and the Cross Cancer Institute was estimated to be \$2,500 (CAN\$).

There are a number of assumptions needed to complete the economic analysis; for instance, the energy use for a single trend period is often applied to the savings found from all three trends (BC, AC, and AAC) to account for the varying energy consumption as a function of the environment conditions. The energy savings from each trend would have provided a skewed economic representation: heated air energy savings will obviously be more significant in the winter than the summer. This assumption is valid as long as it is stressed that the economic component is only an indication of economic savings and the real value of the method is comparing the changes between the different trend periods. These calculations also assume that the savings represented during the trend period can be applied over the entire year; which is generally acceptable since long trend periods (of up to 2 months) are used. To determine the energy change as a result of recommissioning (W) one needs to determine the average ratio of the indicated and actual flow rates (Q) raised to the third power, as shown in [70].

$$\sum \frac{1}{n} \left[\frac{W_1}{W_2} \right] = \sum \frac{1}{n} \left[\frac{Q_1}{Q_2} \right]^3 = \text{AverageEnergySavings} \propto \text{EconomicSavings} \quad [70]$$

The method of determining the difference in airflow rate will vary with the variable that is being considered, and will be further discussed as the analysis is completed. Another general assumption built into the economic analysis states that the fans operate at the Best Operating Point (BOP) at all times. Thus, the reduction in fan static pressure, flow rate, and power is located directly along the BOP curve of the respective fan curves. The electrical and mechanical efficiencies were approximated from the manufacturers stated values located in the system design binders.

5.4.2 Methodology for EOL Static Pressure Related Savings

The annual supply fan energy savings were determined, in part, based on the improvement in the EOL static pressure transducer calibrations; improved calibrations lead to a reduced supply fan speed since all buildings were originally over ventilated. The EOL static transducer can dramatically affect both the energy consumption and the economic viability of a VAV system. As the name indicates, the EOL transducer is located at the end of the longest supply duct run where the pressure losses are greatest; pressure losses are also dependent on upstream geometry, transitions, or branches. To estimate fan savings it is necessary to recall the basic fan laws, shown below in [71] to [73], from the ASHRAE Handbook (2000).

$$\frac{Q_1}{Q_2} = \left(\frac{N_1}{N_2}\right) \left(\frac{D_1}{D_2}\right)^3 \quad [71]$$

$$\frac{P_1}{P_2} = \left(\frac{N_1}{N_2}\right)^2 \left(\frac{D_1}{D_2}\right)^2 \left(\frac{\rho_1}{\rho_2}\right) \quad [72]$$

$$\frac{W_1}{W_2} = \left(\frac{N_1}{N_2}\right)^3 \left(\frac{D_1}{D_2}\right)^5 \left(\frac{\rho_1}{\rho_2}\right) \quad [73]$$

By considering [72] and [73], where the diameter ratio (D_1/D_2) and density ratio (ρ_1/ρ_2) equal 1 it is evident that the pressure can be related to the fan power by [74]. Thus, a reduction in EOL static pressure of 10% results in a reduction in fan power of approximately 15%.

$$\frac{W_1}{W_2} = \left(\frac{P_1}{P_2}\right)^{3/2} \quad [74]$$

The theoretical amount of over ventilation (Q_1/Q_2) is provided in [75].

$$\frac{Q_1}{Q_2} = \left(\frac{P_1}{P_2}\right)^{1/2} \quad [75]$$

It is important to note that this over ventilation does not occur at the VAV terminals since terminals are (in theory) pressure independent²⁷. The over ventilation term (Q_1/Q_2) simply refers to the higher supply fan flow rate equivalent to the higher duct static pressure. The difference between the DDC system indicated (P_{IND}) and the actual (P_{ACT}) EOL static pressures were used with the setpoint pressure (P_{STP}) as shown in [76] and [77].

$$P_{IND} - P_{ACT} = \Delta P_{EOL} \quad [76]$$

$$\left(\frac{P_1}{P_2}\right) = \left(\frac{P_{STP} - \Delta P_{EOL}}{P_{STP}}\right) \quad [77]$$

In this manner, a pressure ratio (P_1/P_2) greater than 1.0 (or 100%) indicated that the EOL static pressure is too high and fan energy is being wasted. Conversely, a value less than 1.0 indicated that supply duct static pressure is too low and that the last few VAV terminals may not have provided sufficient airflow.

²⁷ Some sources have questioned the pressure independence of VAV terminals: laboratory experiments completed in Section 7.4 indicate that VAV terminals are not truly pressure independent. Despite this fact, for the purposes of the energy analysis it is beneficial to consider the terminal with no over ventilation, since this would account for an additional energy loss.

5.4.3 Results of EOL Static Pressure Related Energy Savings

The wasted supply fan energy that resulted from over pressuring the supply air ducts was determined for each of the three trend periods (BC, AC and AAC); the analysis verified that the accuracy, and thus the energy efficiency of the HVAC system is very sensitive to the EOL static pressure sensor. The supply fan energy that was originally being wasted due to poor EOL transducer calibration was ~10% at the Yellowhead Regional Library and ~27% at the Timms Center. The Cross Cancer Institute had an improved EOL static sensor design that is further discussed in this section. The results are summarized in Table 13.

Table 13: EOL Static Pressure Sensor Energy Savings*

	Trend Period	Pressure Ratio	Airflow Ratio	Power Ratio	% Wasted Fan Power
		$\left(\frac{P_{STP} - \Delta P_{EOL}}{P_{STP}}\right)$	$\left(\frac{Q_1}{Q_2}\right)$	$\left(\frac{W_1}{W_2}\right)$	$\left(\frac{W_1}{W_2}\right)^{-1.0}$
Cross Cancer Institute 51 VAV Terminals	BC	111.0%	107.2%	105.3%	5.3%
	AC	109.7%	106.4%	104.8%	4.8%
Timms Center for the Arts 51 VAV Terminals	BC	160.0%	136.8%	126.5%	26.5%
	AC	110.0%	106.6%	104.9%	4.9%
	AAC	113.3%	108.7%	106.5%	6.5%
Yellowhead Regional Library 17 VAV Terminals	BC	126.4%	115.3%	110.7%	10.7%
	AC	96.2%	96.5%	97.0%	-3.0%
	AAC	101.8%	101.1%	100.8%	0.8%

*Note: This table includes the DAS and DDC system trend data from each of the three test locations. Note that the wasted fan power refers to the supply fan specifically; however, the return fan will also be affected by faulty EOL transducer calibrations. Energy savings are in terms of %'s to remove any seasonal influence on the energy savings.

The EOL static pressure transducer at the Timms Center was indicating to the DDC system that the static pressure was too low, thus the supply fan speed was higher than necessary. The time series averaged pressure ratio (P_1/P_2) was originally determined to be 160.0% (i.e. the EOL static pressure was 60.0% too high), which corresponded to 26.5% wasted supply fan power during the BC trend. After recommissioning, the supply pressure was still too high with an EOL pressure ratio (P_1/P_2) of 110.0%, which corresponds to a waste of 4.9% of the supply fan power. During the final trend (AAC), after nearly two years, it was determined that 6.5% of the supply fan power was being wasted, which is still a clear improvement. The recommissioning process resulted in a fan power savings of 21.6% (BC to AC), which was reduced to a savings of 20.0% (BC to AAC)

after nearly two years. The annual supply fan cost at the Timms Center was estimated to be \$5,478/year, thus the payback period, calculated from Equation [69], for the BC to AC and the BC to AAC cases was 2.1 or 2.3 years respectively, simply from the improvement of EOL static pressure accuracy.

The EOL static pressure was also too high at the Cross Cancer Institute; the time series averaged pressure ratio (P_1/P_2) was determined to be 111.0% (the EOL static pressure was 11.0% too high originally). This corresponded to 5.3% wasted supply fan power during the BC trend, which is certainly a significant amount of energy to be wasting simply to due to a faulty static pressure transducer. After recommissioning, the EOL static pressure calibration was slightly improved so that 4.8% of the supply fan power was wasted. Thus, recommissioning resulted in a supply fan energy savings of only 0.6% (BC to AC) due to calibration errors; however, the Cross Cancer Institute was also unique because a control system error was identified (recall Section 5.1). Essentially two control loops were fighting each other; the result was that the supply fan was running at full speed while the duct dampers remained fully closed at all times. By eliminating the static pressure dampers from the control algorithm the supply fan static pressure was reduced from an average value of 748.8 Pa to an average value of 567 Pa. This accounted for an additional savings of ~18% of the supply fan power due to recommissioning. The annual supply fan cost at the Cross Cancer Institute was estimated to be \$5,634/year, thus the payback period based on the BC to AC trend was ~ 12 years at this facility, including the recommissioning improvement to the control algorithm.

By comparison, the results gathered at the Yellowhead Regional Library were consistent with the data from the Timms Center for the Arts; the supply duct was originally over pressured resulting in substantial wasted supply fan energy. During the BC trend the true static pressure was, on average, 304 Pa despite the fact that the EOL transducer indicated a pressure of 249 Pa, thus the time series averaged pressure ratio (P_1/P_2) was determined to be 126.4%. The Yellowhead Regional Library was originally wasting 10.7% of the supply fan power, which was improved after recommissioning (to slightly under the desired static pressure). During the final trend (AAC) it was determined that the supply fan was once again providing too much static pressure. Recommissioning resulted in a supply fan savings of 13.6% (BC to AC), which deteriorated to a savings of 9.9% (BC to AAC) after a 8-month period. The annual supply fan cost at the

Yellowhead Regional Library was estimated to be \$588.66/year, thus the payback periods were 9 and 12 years for the BC to AC and BC to AAC cases, respectively²⁸.

The results of the EOL static pressure calibrations were quite consistent; all three systems were originally providing excessive supply duct static pressure that contributed to energy inefficiency. Including the control algorithm error from the Cross Cancer Institute the reduction in supply fan power was between ~10% and ~20% for all cases. It is also important to note that the Cross Cancer Institute utilized a unique control loop where four separate EOL static pressure transducers were referenced (all located at the end of 4 different supply ducts); the lowest transducer signal was then used to control the supply fan speed. The use of these additional sensors greatly reduced the initial error associated with the EOL static pressure transducers at the Cross Cancer Institute. Thus, there is a need to calibrate the EOL static pressure transducer regularly even though the longevity of the EOL transducer calibration appears to be adequate. The results of the field tests indicate that the longevity of the EOL static pressure sensor calibration are such that a recalibration is prudent in intervals of ~ 6 months to 1 year, which will not be difficult since the calibration of the sensors is relatively minor. Variations from the AC to AAC trends are likely because of varying levels of accuracy within the sensor calibrations. The best solution would be to improve the quality of the sensors but (barring this) a series of regularly spaced calibrations will ensure the system does not deviate excessively.

5.4.4 Methodology for Supply Fan Energy Savings at the Minimum Setpoint

The improved accuracy of the DDC system with respect to the individual VAV airflow sensors has already been discussed (recall Section 5.2) but there is also a subsequent improvement in energy efficiency. The scale of these energy savings can be quite large. For instance, approximately 70% of the supply fan power can be wasted while the system is trying to maintain the minimum flow setpoint. However, since the system only operated at the minimum setpoint for a fraction of the year the real annual savings will be significantly lower (which falls in line with the expected values from past research).

Recall that at all three test locations the DDC system was typically indicating less airflow than what was actually being provided. Due to the compensating nature of DDC, the VAV terminals

²⁸ Note this is to cover the entire cost of recommissioning with only the improvements made in the EOL static pressure accuracy.

will not call for more ventilation than the space requires (since the individual VAV dampers are temperature controlled) except when the system is at the minimum airflow setpoint. When the HVAC systems enters heating mode (at the minimum flow setpoint) the DDC will be incapable of compensating for poorly calibrated VAV airflow sensors, resulting in a substantial energy loss. In heating mode each VAV terminal responds to what the DDC systems indicates is the minimum flow set point. However, because of the poor airflow sensor calibration (which was found, to varying degrees, within every VAV terminal considered in the field test), the resulting airflow to the space was always too high. The EOL static pressure drops, the fan speed increases and the power requirements of the supply fan are significant (recall fan power is proportional to the cube of the airflow rate).

$$\frac{W_1}{W_2} = \left(\frac{Q_1}{Q_2} \right)^3 \quad [78]$$

5.4.5 Results of the Supply Fan Energy Savings at the Minimum Setpoint

This section uses the same analysis used within Section 5.2, considered at the minimum airflow setpoint. Thus, using the DDC and the time-series trend data it was possible to determine the supply fan power wasted when the system was at the minimum flow setpoint, which is summarized in Table 14.

Table 14: Energy Savings at the Minimum Airflow Setpoint (during heating mode)*

		Over Ventilation	Wasted Power
	Trend Period	$\left(\frac{Q_1}{Q_2} \right) - 1.0$	$\left(\frac{W_1}{W_2} \right) - 1.0$
Cross Cancer Institute 51 VAV Terminals	BC	20.3%	73.9%
	AC	4.5%	14.0%
	AAC	11.4%	38.0%
Timms Center for the Arts 51 VAV Terminals	BC	18.0%	64.3%
	AC	5.3%	16.6%
	AAC	6.6%	21.0%
Yellowhead Regional Library 17 VAV Terminals	BC	19.4%	70.0%
	AC	7.2%	23.2%
	AAC	1.8%	5.4%

*Note: These supply fan energy savings appear to be quite large; however, there are a few reasons provided below to explain these results.

It is evident from these results that the space usage and building size are dominant factors; for instance, consider how similar the results are from the Cross Cancer Institute and the Timms Center for the Arts. The Yellowhead Library was the only test building that registered an improvement from the AC to AAC trend periods, although the over-ventilation coefficient only improved slightly. The supply fan energy being wasted appears to be quite large (for all these cases); for a couple of reasons:

1. Recall that the VAV airflow sensors provide a parabolic signal but rely on a linear calibration within the DDC system, introducing added DDC system error. It will also be shown that the VAV airflow sensor provides a non-linear amplified signal that contributes a significant amount of flow error near the minimum flow setpoint, thus the effects of recommissioning seem more dramatic.
2. It is also important to remember that these supply fan energy savings will only occur when the entire system is in heating mode, which will only occur during a fraction of the year, even during the winter. The true system savings will be smaller, and in line with the literature.

Despite the high numbers, the results of this analysis are very consistent: all three facilities were originally over-ventilating the space (while in heating mode) by 18.0% to 20.3% of the supply airflow. This corresponds to a significant amount of wasted supply fan power, 64% to 74%, when the HVAC system is operating at the minimum flow setpoints. The improvements, with respect to the initial (BC) conditions, are summarized in Table 15.

Table 15: Improvements at the Minimum Airflow Setpoint (during heating mode)*

	Change in Over Ventilation $\varepsilon \left[\left(\frac{Q_1}{Q_2} \right) - 1.0 \right]$		Change in Wasted Power $\varepsilon \left[\left(\frac{W_1}{W_2} \right) - 1.0 \right]$	
	BC to AC	BC to AAC	BC to AC	BC to AAC
Cross Cancer Institute 51 VAV Terminals	15.8%	8.9%	59.8%	35.9%
Timms Center for the Arts 51 VAV Terminals	12.8%	11.4%	47.7%	43.3%
Yellowhead Regional Library 17 VAV Terminals	12.1%	17.6%	46.8%	64.7%

*These are the improvements made taken with respect to the BC conditions. Note this is the same data that was presented in Table 14. A positive value corresponds to a flow reduction or an energy savings, in all cases an improvement was realized.

5.5 Temperature Variations due to the Recommissioning Process

The improvements made in comfort are an important, albeit difficult to quantify, benefit of the recommissioning process; especially in VAV systems where comfort is meant to be optimized with individual zone control. Unfortunately, comfort remains a rather subjective performance indicator simply because of the number of variables that contribute to individual body comfort (temperature, humidity, air movement, clothing ensemble etc.). Therefore, the results of this study will be limited to improvements made in temperature control accuracy.

5.5.1 Methodology for Determining Zone Temperature Accuracy

It is relatively simple to show that the accuracy of the thermal systems improved after the recommissioning process. Zone temperature is controlled through airflow adjustment, where the central AHU regulates the supply air temperature in either the heating or cooling mode of operation. Zone temperature sensors for each VAV terminal were calibrated using an external instrument pack to measure the actual zone temperature and to compare it to the DDC indicated value. Prior to the recommissioning process, some workers complained of localized areas of poor comfort; i.e. one zone was frequently too hot and stale while another was too drafty and cool. In the case of the Yellowhead Regional Library (which had the greatest number of comfort complaints) the occurrence of poor comfort zones was likely the result of a renovation completed several years ago, in which new walls were constructed and the occupants relocated. Unfortunately, the physical positions of the thermostats were not relocated after the renovation and the result was several thermostats in one zone that controlled VAV terminals in isolated zones. The improvement of the local comfort levels was very important to the occupants of this facility.

In order to quantify the increased system performance, the original calibration errors of the thermostats were compared to the errors subsequent to recommissioning. The absolute difference between the indicated temperature from the DDC (T_{IND}) and the true temperature (T_{ACT}) is determined by [79].

$$T_{ERROR} = |T_{IND} - T_{ACT}| \quad [79]$$

Note that this very simple analysis simply considers the DDC accuracy in monitoring the system zone temperatures; however, the thermal comfort of the zone is still a function of the thermostat settings. Simply put, it does not matter to the individual occupying the space if the zone temperature is indicated as 1°C too high (or 50°C too high) in the DDC system, as long as they can adjust the thermostat to establish a comfortable environment temperature. Thus, the analysis

considered here does not quantify the zone comfort but the thermal accuracy of DDC systems. A brief discussion of thermal comfort is completed in the following section.

5.5.2 Sample Results from the Yellowhead Regional Library

The thermal accuracy results from all three facilities were generally consistent: the thermostats and zone heating/cooling functioned correctly, the DDC system was inaccurate but was improved during recommissioning. The following discussion applies to the Yellowhead Regional Library, which had the greatest number of thermal comfort complaints despite its small size. During the recommissioning process, it was determined that the thermostats seemed to be well calibrated at one end of the building but that the accuracy of calibrations rapidly decreased at the other. The same calibration was applied to every thermostat within the facility. The actual zone temperature was found to be hotter than the indicated temperature in every zone, sometimes by as little as 0.8°C but often in excess of 1°C, and to a maximum of 2.3°C. On average, it was determined that all 17 zones were 1.9°C hotter than the indicated thermostat temperatures, making the adjustment of local temperatures more difficult for the office workers. The local temperatures were also extremely dependant on the outdoor environmental conditions due to a large number of windows and offices spaced along the exterior walls of the facility. For instance, during the BC trend the indicated zone temperatures (in the worst cases) routinely climbed as high as 26°C, thus the actual zone temperatures were in excess of 28°C. Typical results are provided in Figure 23 of a zone that was ~2°C hotter than the DDC indicated.

During the BC trend, several VAV terminal units were witnessed to be operating at the maximum flow set point while trying to cool adjacent zones, while VAV terminals within the adjacent zones were not fully open due to a poorly calibrated thermostat. Obviously, the full DDC monitoring of each zone was not being maintained under these conditions. After the recommissioning process was completed, all thermostat temperatures were calibrated to within 0.1°C. On average, it was determined that the actual temperature in each zone was only 0.05°C higher than the DDC indicated temperatures; which is a significant improvement in terms of system accuracy.

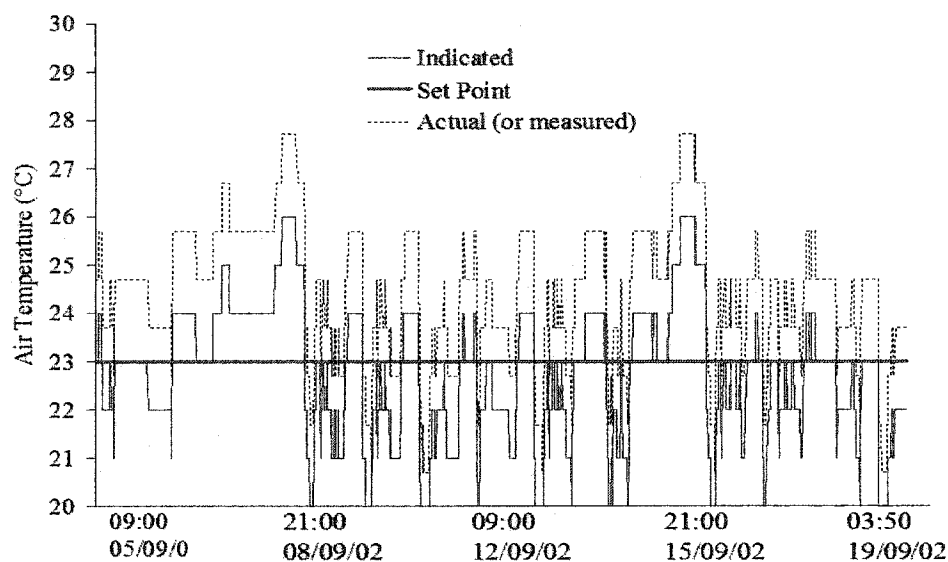


Figure 23: A typical zone temperature plot, this one corresponds to the Yellowhead Regional Library prior to the commissioning process (the BC Trend), for the zone serviced by VAV terminal #1. Note that the true temperature is significantly hotter than the DDC indicated value and rarely meets the zone setpoint.

5.5.3 Discussion of Thermal Comfort

The thermal comfort in this facility (and the other two test locations) was improved during the recommissioning process, although this was done primarily from a DDC accuracy point of view. The recommissioning process identified a number of broken comfort influencing components, a few undersized VAV terminals and several poorly placed thermostats that were not moved after a significant renovation (or simply located poorly to begin with). These mechanical problems were impossible to fix during field-testing largely due to the budgetary constraints of the building operators. The identification of several thermostats that were no longer located within the correct zone (the zones they were supposed to control) was not dealt with during the recommissioning process. During a formal recommissioning process these problems would all be repaired. In this case, the DDC accuracy was improved and a list of recommended thermostat locations was prepared for each of the building operators, who plan to institute the changes in the future when their budgets allow. For the purposes of the field research, the most important conclusion that was formed regarding thermal comfort was that a recommissioning procedure would successfully identify these types of problems.

6.0 Methodology for Laboratory Experiments

A series of laboratory experiments was initiated to quantify the amount of airflow sensor error that could be observed with varying upstream conditions. It was found that VAV airflow sensor response was highly dependant on the duct geometry into each terminal, so that even with a perfect calibration the sensor signal may report wide fluctuations. The laboratory experiments compare the airflow signal of similar VAV flow sensors located after various upstream geometries to a 40 Diameters (D) length of straight duct that represents the “ideal” case. By determining the variation in the VAV signal after different duct geometries, it was possible to predict geometries that would hinder the recommissioning process and result in lower accuracy. The laboratory experiments also provided a table of coefficients that could be used to estimate the reduction in VAV airflow sensor amplification in relation to terminal size, manufacturer and the upstream geometry.

6.1 Laboratory Setup

Laboratory experiments were undertaken to determine the amplification, precision, and general response of VAV airflow sensors. Several non-ideal duct configurations were recreated in a laboratory to resemble the “worst” VAV terminals that were observed within the field tests. Two brands of VAV terminals were utilized in varying sizes and the signal produced by the VAV airflow sensor was compared to the true airflow rate from a custom VAV airflow sensor. As mentioned, two common brands of VAV terminals were also acquired (designated A and B from this point on) since the design of the airflow sensor will clearly change with manufacturer. The equipment needed to complete these experiments is detailed in Table 16.

Table 16: Summary of Equipment needed for the Upstream Laboratory Experiments

Apparatus	Measurement
Chicago Blower Centrifugal Fan, Variable speed drive and Six VAV terminals with airflow sensors from local manufacturers: Two in each of the 6”, 8” and 10” sizes	Thermometers, Standard barometer, Validyne Pressure Transducers of varying ranges (various ranges, 0-1 psi and 0-1” H ₂ O) with a 10 channel demodulator, Custom VAV Airflow Sensor ²⁹ and Two dual channel averaging voltmeters
Lengths of circular duct work (6”, 8” and 10” diameters) and various components (reducers, expanders, elbows, dampers, etc.), Steel stands	Incline manometers of various ranges (0 –250 Pa and 0 –1250 Pa), Pitot tubes of various sizes and Air Data Multimeter (Shortridge, model ADM-970)

²⁹ This custom VAV airflow sensor was designed from ANSI/ASHRAE standard 41.2-1987; it was calibrated with a series of pitot tube traverses. It was very convenient to have a custom VAV airflow sensor available during the laboratory tests.

Several test sections were used prior to the VAV terminals to simulate the effect of “adequate” duct lengths, including 10D, 5D, 3D, 2D, and in some cases 0D. Only the 10D case complies with ASHRAE recommendations for minimum duct lengths downstream of an obstruction (which is 7.5 D). A typical experimental setup would include a combination of elbows (90° and 45°), reducers, expanders, and transitions to test the effect on terminal response. Several different duct configurations were constructed to test the effects of each obstruction (elbow, reducer etc.) individually and in combination. Examples of non-ideal duct geometries that were identified within the field test locations are provided in Figure 24.

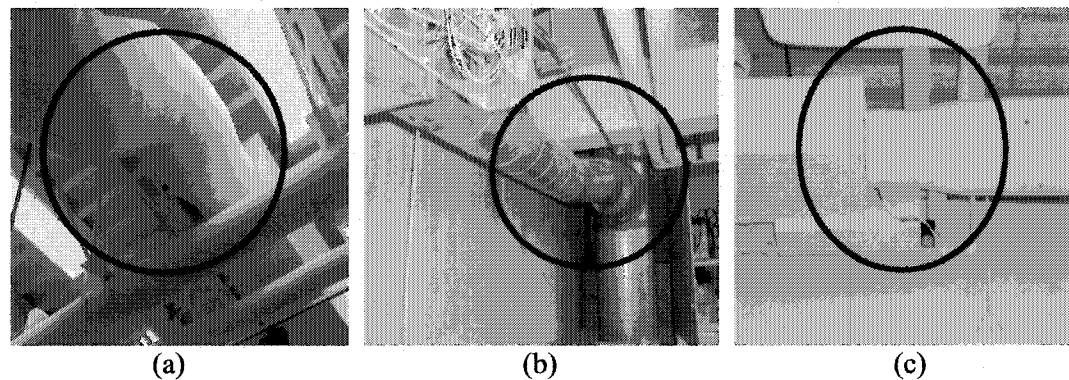


Figure 24: Examples of common non-ideal duct geometry examples from the Timms Center for the Arts: (a) two 45° elbows (an S-shape geometry) are attached to a concentric reducer, immediately prior to the VAV terminal unit, (b) a concentric reducer with less than 1 diameter prior to the VAV Terminal, (c) a T-intersection into a concentric reducer and two 30° bends prior to the VAV Terminal.

The laboratory experiments were setup at the University of Alberta in the air conditioning laboratory within the Mechanical Engineering building. Airflow was monitored by measuring the differential pressure indicated by both the VAV terminal and a known standard, which included orifice plates and custom pitot arrays. The difference between the indicated flow rate from the VAV terminal (Q_{VAV}) and the standard flow rate indicated by the pitot array (Q_{TRUE}) was represented by a dimensionless flow coefficient (C), which can be directly related to the amplification term using the pressure coefficient (C_p). Recall that the relationship between flow rate (Q_{VAV}) and the pressure coefficient (C_p) was provided in [45]. However, it is more convenient to discuss the amplification change in terms of a unique coefficient (C), which was defined in [47]. The laboratory experiments focused on determining the amplification coefficient (C) for a number of known upstream duct geometries. During testing a duct geometry was constructed and the longest test section (10D) was attached before the VAV terminal. A variable

speed fan was then used to provide a steady flow rate that was slightly lower than the manufacturers recommended minimum value, as indicated by the standard flow array. Readings were taken at five different VAV damper positions: fully open, 20° closed, half closed, 20° open and fully closed. Fan speed was increased and the tests were repeated until the fully open flow setting resulted in an airflow rate that was higher than the recommended maximum value. This process was repeated for the 5D, 3D, 2D and the 0D tests sections and for both brands of VAV terminals. Several duct configurations were constructed over the course of these experiments (see Figure 25 for example), including an ideal duct section with at least 40D of straight duct prior to the VAV terminal. This ideal case was used for the experimental baseline.

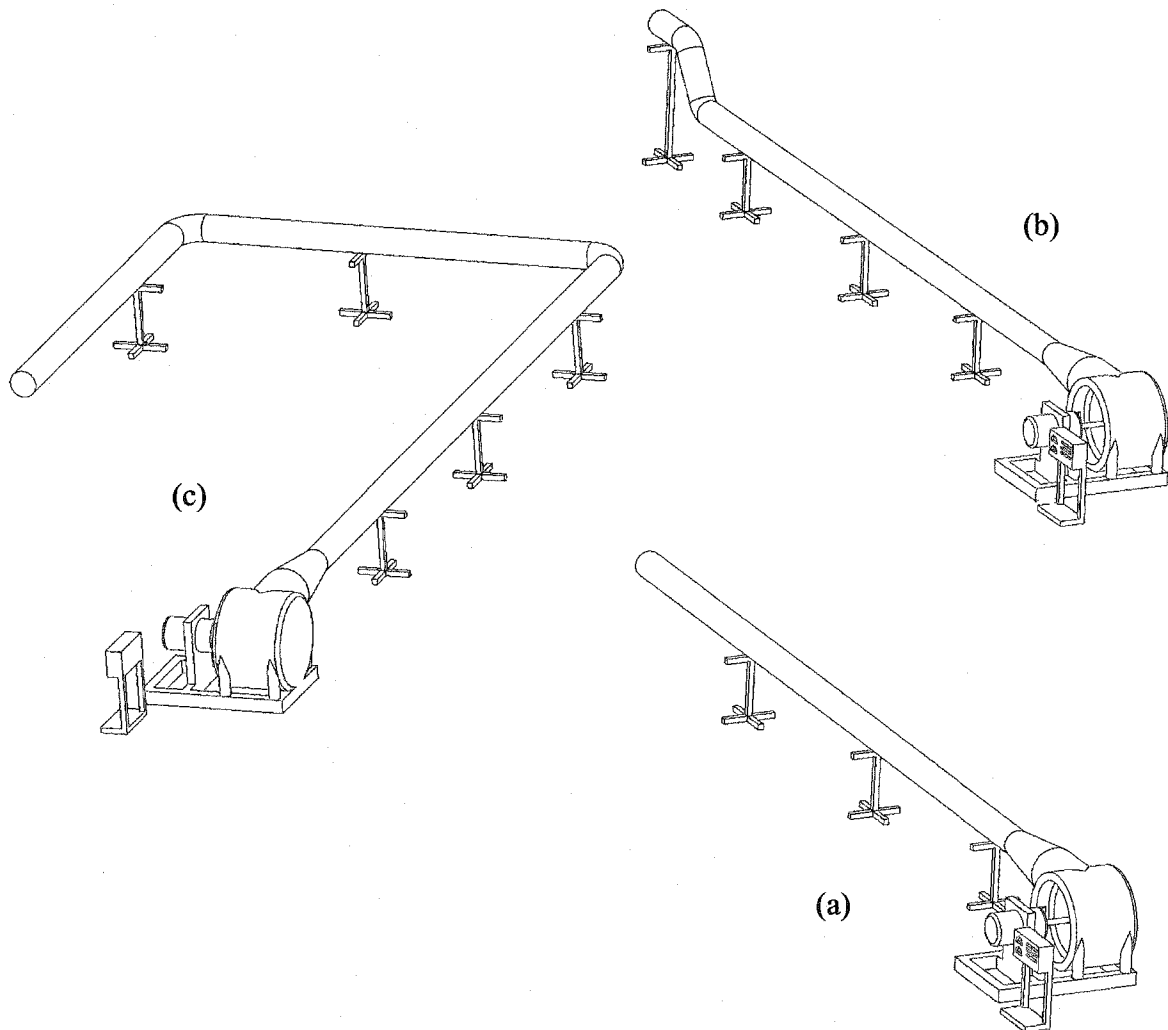


Figure 25: Sample non-ideal duct geometries that were investigated during the laboratory study. Note that in every case the variable speed fan (in red) is located prior to a 40D straight section where the standard airflow rate measurements were made and the VAV terminals were located at the end of the duct (in black): (a) 40D straight case used for baseline (b) S-Shape geometry made of two 45° elbows, commonly used for elevation changes (c) two 90° elbows

6.2 Velocity Profile and Sensor Response

The laboratory experiments were conducted to determine the effects of upstream conditions on the response of VAV terminals; however, it is worth noting that this simply refers to the effects of the velocity profile at the VAV flow sensor. The position of the total pressure ports (which will vary with the manufacturer) is the only change that will be affected by the velocity profile and can be used to predict the signal accuracy. The velocity profile within common HVAC duct configurations is a well-studied topic in the building sciences, thus it can be predicted that certain upstream conditions will produce lower flow accuracy. For instance, the velocity profile following a 90° elbow or concentric reducer is particularly non-uniform and it can be inferred that the accuracy of a VAV airflow sensor immediately after this type of obstruction would be quite low; flow visualization was also used to test this hypothesis.

6.3 Flow Visualization Setup

Flow visualization experiments were used to verify primary assumptions that were made regarding the effects of the velocity profile and the assumed airflow distribution around the VAV sensors. This included the evaluation of different damper positions and flow rates for three types of upstream conditions: straight sections (in excess of 30D), 90° elbows, and concentric reducers. The smoke wire visualization method was used to show the wake region following the VAV flow sensor, as well as the upstream behavior prior to the total pressure ports.

Smoke is a common airflow visualization technique that can be traced back to fluid mechanics work completed in the time of Leonardo da Vinci, J. Diep (2001). The smoke wire technique is a well-documented visualization method where mineral oil (paraffin oil) is allowed to flow down a thin stainless steel wire prior to the region of interest; the oil naturally forms regular spaced beads (due to its viscosity) that will remain on the wire for several seconds: A.J. Smits (2000). The wire is rapidly heated (in this case with a VARIAC transformer) and the oil beads burn away to produce regularly spaced white smoke trails that typically last between 1 and 3 seconds, depending on the air speed in the test section. Due to the relatively short duration of the smoke, a high-speed digital camera was used with “frame grabber” software to extract the useful images. The equipment used to complete the visualization experiments is summarized in Table 17.

Table 17: Summary of Equipment needed for the Flow Visualization Experiments

Apparatus	Measurement
ILG Industries Fan (BCL 1225, centrifugal, backward facing vane), 8" Spiral Ducting, 10" to 8" reducer, 90° elbows	2 Manometers (0 to 25 mm H ₂ O column)
Smoke Wire Sub Assembly: Oil Reservoir, Stainless Steel Wire (0.007" diameter), Light Mineral Oil (Paraffin oil Saybolt viscosity 158 max, kinematic viscosity < 35.5 centistokes at 40°C), Power supply (VARIAC transformer, Output 0 to 140 V, 10A), Tygon tubing, Air Pump	2 Manometers (0 to 750 mm H ₂ O column) Static piezometer ring and Pitot tube

The "worst" upstream components were tested using flow visualization, including both a concentric reducer and a 90°elbow. Air was drawn into the duct (a flow straighter was used to reduce turbulence) and through a transparent test section using a variable speed fan. The three duct configurations tested are provided in Figure 26.

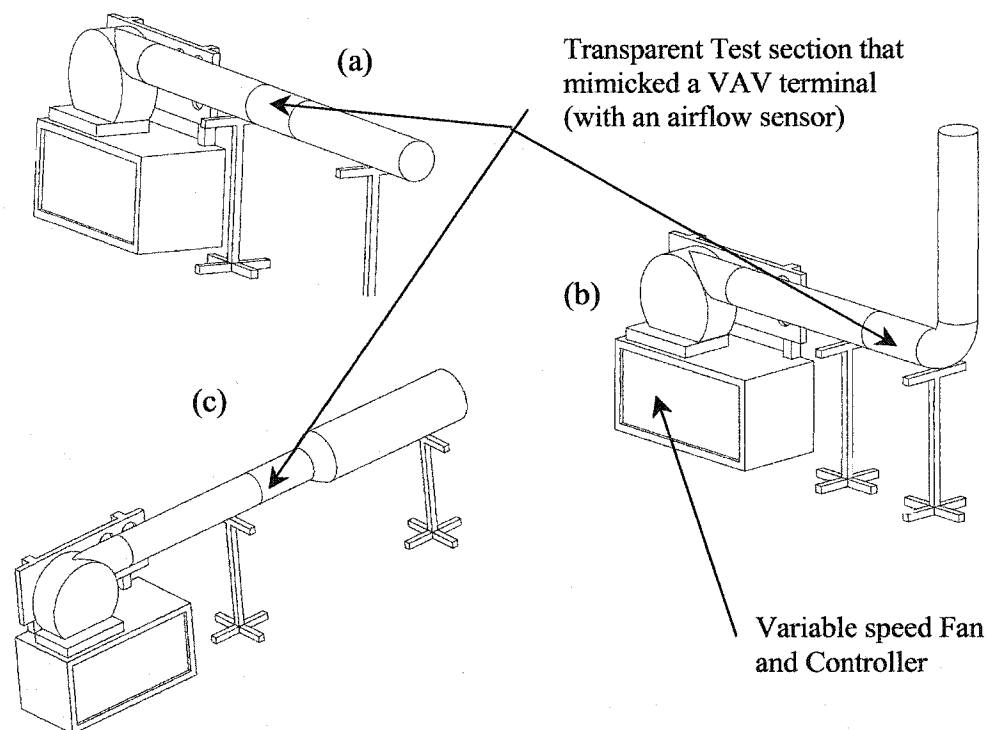


Figure 26: Representation of the three duct geometries that were tested in the flow visualization experiments, including: (a) a straight section for the "ideal case," (b) a concentric reducer, (c) a 90° elbow. In all cases, an 8" duct was used and the VAV flow sensor was located within the test section, with a circular damper that mimicked a true VAV terminal.

Flow was achieved using a centrifugal fan equipped with a mechanical variable speed drive where air was drawn through the test section. The air speed was maintained at 4.5m/s (or

0.15 m³/s), which is at the low end of the usable range for the 8" VAV flow sensors. A low flow rate was preferable for these experiments for two reasons: the smoke wire technique produces better results with lower flow rates and it was hypothesized that VAV flow sensors were prone to errors at low flow rates. It was also assumed that since the C_p value changed only slightly with Re_D that a low flow rate would be acceptable for the visualization experiments ($Re_D \sim 60,000$). Tests were completed on each of the duct geometries (straight, 90° elbow and 10" to 8" concentric reducer) with three different damper positions (fully open or 90°, 30° and half closed or 45°). Static pressure was allowed to vary from 125 Pa (0.5" H₂O) to 500 Pa (2" H₂O column) while the flow rate was kept constant, regardless of damper position.

7.0 Discussion of Laboratory Experiment Results

Field-testing verified that the improvement of DDC calibration coefficients for individual VAV terminals was the most beneficial aspect of recommissioning. Thus, poor upstream geometry can dramatically reduce the effectiveness of the recommissioning procedure. HVAC system designers commonly need to include non-ideal duct geometry prior to VAV terminals (such as reducers, elbows etc.) due to space constraints; however, there is also an industry misconception that the VAV airflow sensors will compensate for poor upstream duct conditions. The laboratory experiments deal with the worst upstream conditions that were observed during the field-testing. The “worst” upstream geometries are ranked and a table of coefficients has been developed that indicates the resulting degradation of signal. The laboratory experiments also show that the upstream effects are as significant after 10D of straight ducting; although it is often assumed that after 10D the effects of non-ideal conditions are lessened. The results indicate that adequate duct length³⁰ does not affect sensor response. The laboratory experiments provide insight into how the accuracy of VAV airflow sensors could be improved during the manufacturing, design, and installation stages prior to the recommissioning process.

7.1 Baseline (C_{40D}) Experiments used to Standardize the Laboratory Results

VAV sensors are designed to provide an amplified flow signal (recall the discussion of C_p from Section 3.7.2); unfortunately, amplification is heavily dependent on upstream conditions and damper movement in the VAV terminal. The baseline results are summarized in Table 18.

Table 18: Baseline (C_{40D}) results for Laboratory test of the VAV Terminals*

	Type “A” VAV Units		Type “B” VAV Units	
	μ of C_{40D}	σ of C_{40D}	μ of C_{40D}	σ of C_{40D}
6"	1.587	0.028	1.719	0.030
8"	1.267	0.028	1.333	0.013
10"	1.233	0.013	1.300	0.019

*Note that the C term is referred to in [47]: These are the average (μ) and standard deviations (σ) of the C values between the minimum and maximum recommended range for each VAV terminal, from the manufacturer. A low standard deviation and a high average C value are desirable.

The amplification provided by the smaller (6") VAV terminals is greater in both cases, where the maximum average amplification coefficient is 1.719. The minimum amplification occurs within

³⁰ “Adequate” duct length refers to the industry-accepted value of 10D prior to a VAV terminal: the results of the laboratory tests indicate that this is hardly “adequate” to compensate for all possible upstream geometries.

the largest VAV terminals at 1.233 and 1.300, for type A and B respectively. Since the 40D is a very long straight section then the benchmark flow rate (Q_{40D}) can be equated to the actual flow rate (Q_{TRUE}), therefore, the benchmark tests also result in the largest pressure coefficients (C_p). Recall that the expected C_p values for various geometries should vary between approximately -1.7 and -0.3 based on past experimental results (recall Section 3.7.2.2). The resulting amplification from the experiments is also consistent with the expected, theoretical, results for the C values. Recall Figure 12, where the C value was predicted to vary between ~ 1.3 and 1.85 for an 8" VAV terminal with a C_p of -0.5 and -1.7 , respectively. The laboratory results clearly agree with these estimates. The lab tests also verify that the amplification coefficient (C) is only weakly dependent on the true air velocity (V_T), which was also predicted theoretically (Section 3.7.3). The static pressure signal is the dominant factor in the determination of signal amplification. In addition, the standard deviations of the flow coefficients in each case are quite low with a maximum standard deviation of 0.03 (or 1.7% of the average) in each of the smallest VAV terminals. Recall that for the laboratory experiments a coefficient (C) was defined that can be related to the pressure coefficient (C_p) behind a VAV airflow sensor, sample results are displayed graphically in Figure 27 for added clarity.

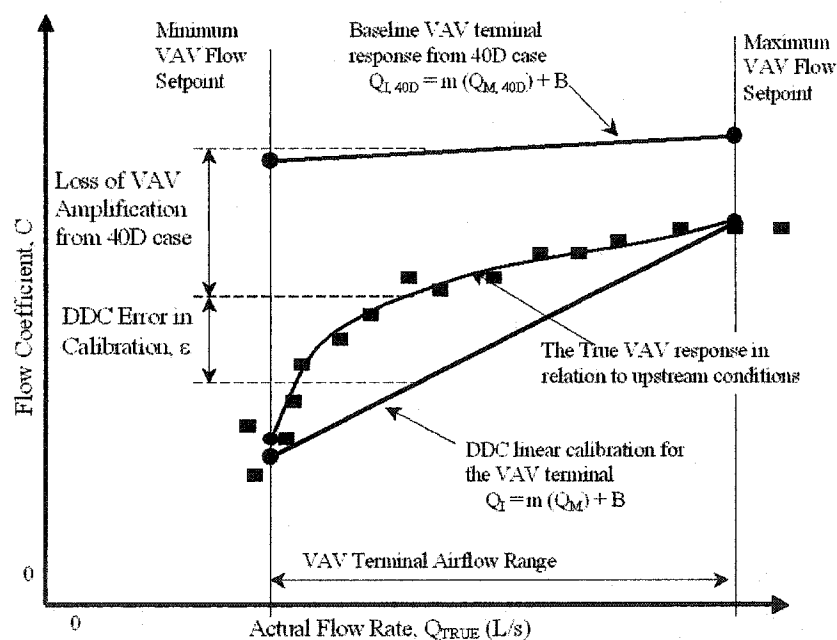


Figure 27: A simple representation of typical laboratory results for the purposes of discussion. The baseline VAV response was experimentally obtained for each VAV terminal from the 40D case (given by a linear equation), the square points are typical for some upstream geometry (note in this case the loss of amplification is quite high). It is also useful to recall that the DDC systems (from the field testing) only allowed for a linear calibration at the setpoints; therefore, there will be a significant DDC airflow calibration error (ϵ). Only the region between the min/max setpoints is of interest.

The results for the baseline tests of the two largest VAV terminals (both 10" in diameter) are also presented graphically in Figure 28 for added clarity.

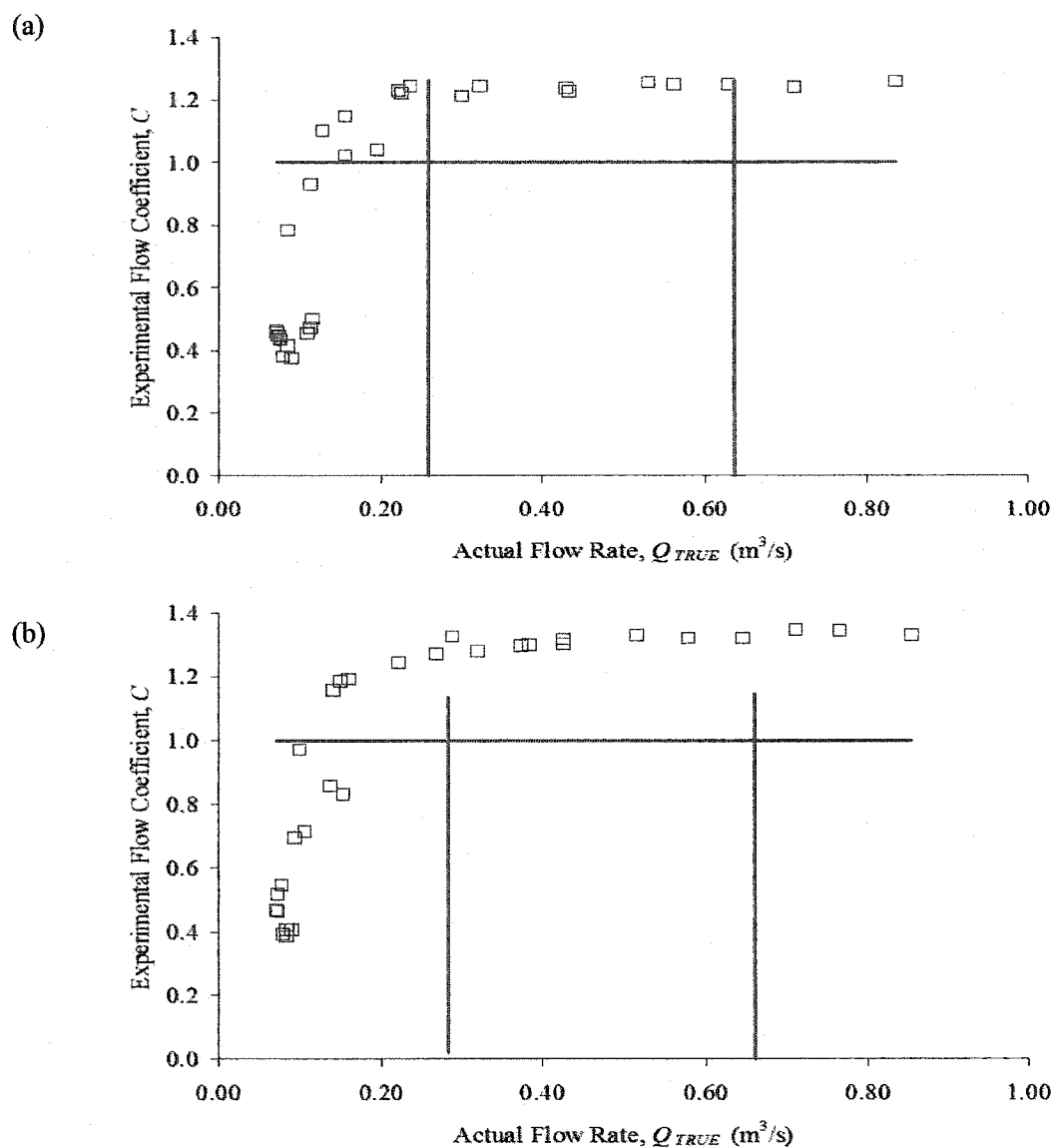


Figure 28: The sample base line results for the first (a) and second (b) brand of VAV terminal (designated as Type A and B in Table 18, respectively) in the 10" size, these results were taken when the terminals were located after 40D of unobstructed straight ductwork. The vertical lines refer to the minimum and maximum VAV operation range recommended by the manufacturer, thus only the portion between the vertical lines are of interest. Note that the flow coefficients (C_{40D}) are nearly constant in this range (and in this case, outside the vertical lines as well), indicating a reliable amplified signal with an average flow coefficient of 1.23 and 1.30 for (a) and (b), respectively.

The baseline response between the maximum and minimum flow setpoints was used to form a series of linear equations that related C to the actual flow rate (Q_{TRUE}) for each of the six VAV terminals considered (recall the discussion of Figure 27). These linear equations were used to standardize the results for the following non-ideal duct geometries by comparing the loss in amplification from the baseline (40D) flow coefficients.

7.2 Non-Ideal Geometry observed in the Field Tests

The VAV terminals that responded the worst to recommissioning during the field tests were typically located after “poor” upstream duct geometries. The most common upstream geometries that seemed to cause problems included concentric reducers, 90° elbows, S-shaped geometries (which are commonly used to account for elevation changes), and inadequate unobstructed duct lengths prior to the VAV terminal. The laboratory results indicate the loss of amplification and precision that can be expected with these upstream conditions. The change in amplification is significant because the pressure sensors used to measure the VAV flow rate typically require the amplification, while scatter throughout the useful range will have negative consequences on the IAQ, thermal control and energy efficiency of the VAV terminal. The data tables to support the results presented in this section are located in Appendix C, Section 1.

7.2.1 Two 90° Elbows in Series

The use of 90° elbows is common in many HVAC systems. Fluid will flow fastest along the outside of the curve and, depending on the velocity profile, there may well be a recirculation region and secondary flow. Therefore, it was expected that both the accuracy and precision (which refers to the scatter within the VAV useful range) would be affected by the inclusion of 90° elbows. The duct was set up to resemble Figure 25 (c), with 40D of straight, unobstructed duct (where the true flow measurement, Q_{TRUE} , was made) prior to a 90° elbow, followed by 10D of straight duct and a second 90° elbow. Various section lengths were then used (10D, 5D, 3D and 2D) prior to the VAV terminals.

The amplification of the VAV pressure signal decreased in each case (except for the Type B, 8” unit which showed a minor increase in amplification) for this duct geometry. However, it is also evident that the decrease in amplification is not significant in either the 8” or 10” sized terminals within this duct configuration, where the loss of amplification (ΔC) varied between only -0.02 and 0.07 (-1.5% and 5.6% , respectively). By comparison, the 6” sized terminals showed a more dramatic reduction in amplification that varied between 0.09 and 0.19 (5.3% and 12.0% ,

respectively). The standard deviations (or scatter) associated with the flow measurements increased in every case, indicating that the precision of the flow meters decreased with the addition of the two 90° elbows, as expected³¹. The loss of amplification and precision was most significant within the 6" cases where the maximum standard deviation was as high as 0.107 (7.6 % of the actual C value). The loss of precision (or the scatter associated with the results) is evident from Figure 29, which corresponds to the results from the Type B, 6" VAV terminal after two 90° elbows.

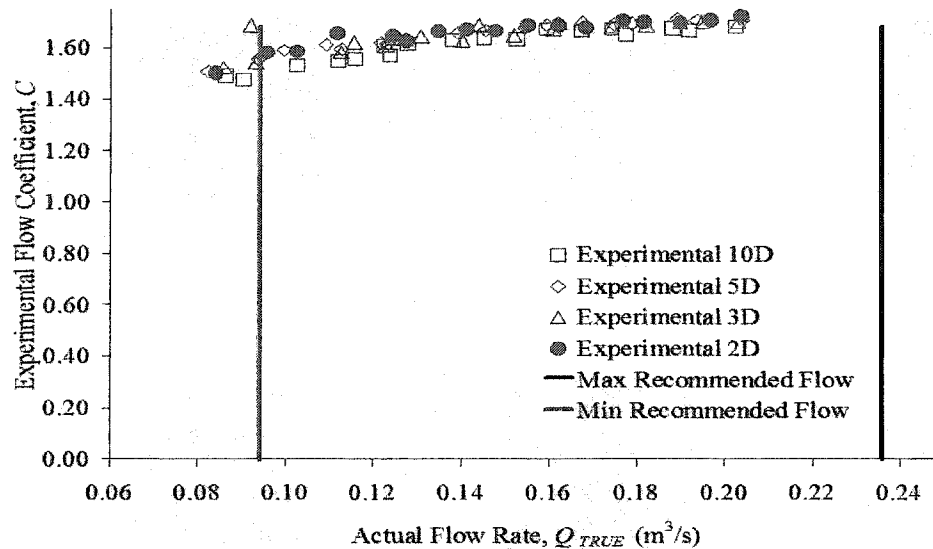


Figure 29: Experimental flow coefficients for the Type B, 6" VAV terminal after two 90° elbows, note the imprecision (the high amount of scatter associated with each of the duct lengths) and the loss of amplification at the low end of the range.

7.2.2 S-Shaped Bends (Two 45° Elbows in Series)

S-shaped bends, are commonly used within HVAC systems to make elevation changes, and are comprised of two 45° elbows in series. Again, it was expected that the amplification and precision of the VAV airflow sensors would be affected, likely in a similar manner as the previous configuration. To test this hypothesis the duct was setup to resemble (b), with 40D of straight, unobstructed duct (where the true flow measurement, Q_{TRUE} , was made) prior to two 45° elbows in series with 2D of duct between them. Various section lengths were then used (10D, 5D, 3D and 2D) after the S-section and prior to the VAV terminals. The results of the testing, including the change in the amplification and precision, respectively, are summarized in Appendix C and discussed below. The Type A, 10" Terminal showed the greatest loss in

³¹ Recall that it was hypothesized that the non-uniform velocity profile would result in a loss of sensor amplification and precision.

precision, which is presented graphically in Figure 30 for additional clarity. Note also there is increased scatter compared to the results presented in Figure 28 (b), which refers to the same VAV terminal in the baseline case.

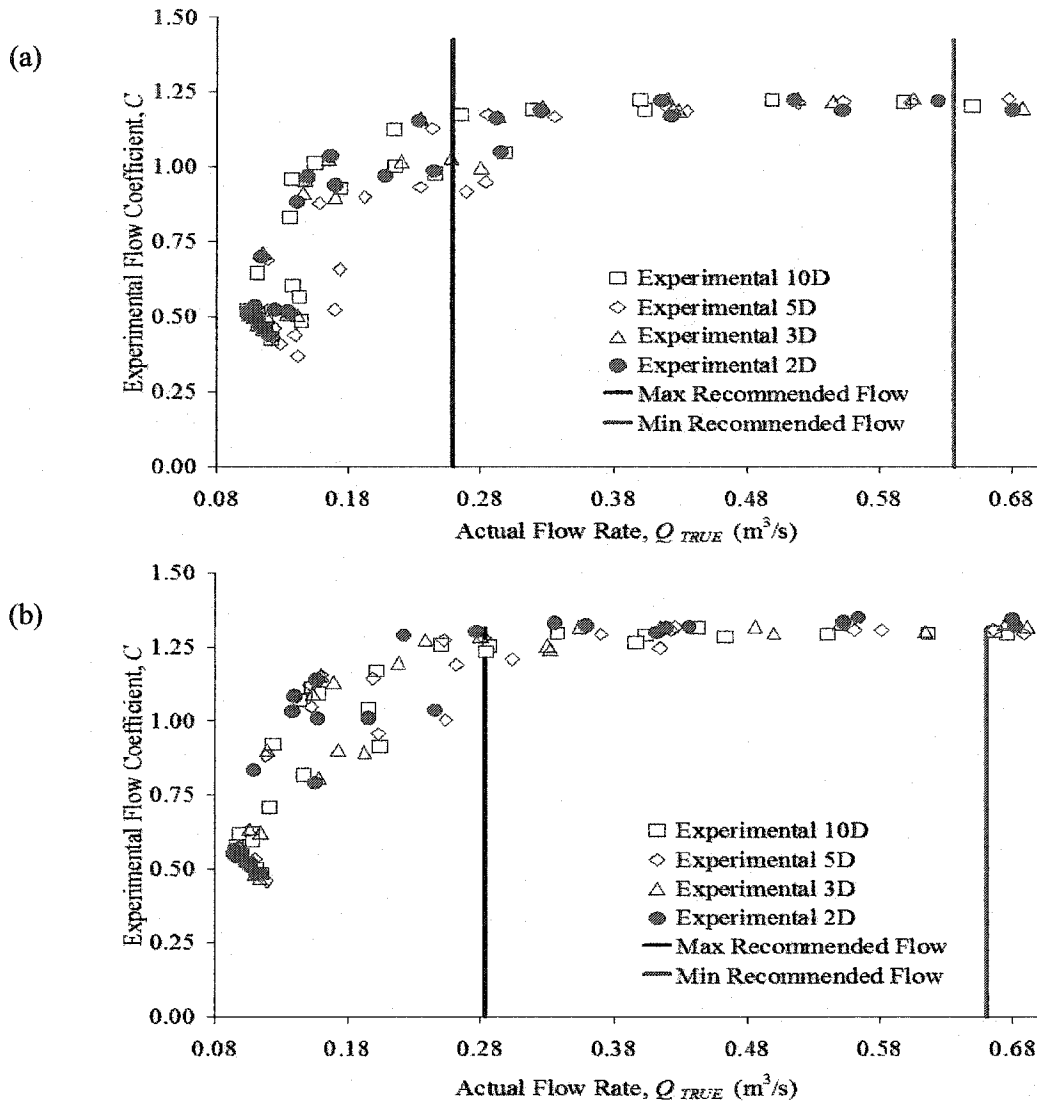


Figure 30: Results for the Type A and B, 10" VAV terminal for the S-Shape Geometry (which is two 45° elbows in series), designated as (a) and (b), respectively. The data for the 10D, 5D, 3D and 2D cases refers to the length of straight unobstructed duct between the S-shape geometry and the VAV terminal. Note how the curves from (a) have shifted to the right when compared to Figure 28 (b). The precision of this (a) VAV terminal is reduced, especially at the lower end of the flow range. The loss of precision at (b) is milder and more inline with the other observed results.

Once again, the amplification associated with nearly all of the VAV terminals was reduced with the addition of the S-shaped geometry and the reduction was more dramatic in the smaller VAV

terminals. The Type B, 6" VAV terminals provided a reduced flow signal with C values that varied between -0.01 and 0.02 lower than the baseline values (C_{40D}) for the correct flow rate. However, the Type A 6" VAV terminals consistently showed an increased amplification that varied between 0.01 and 0.03 . In either case, the addition of the S-shaped geometry did not significantly affect the sensor amplification. The precision associated with each VAV terminal decreased in every case, and remained relatively consistent (again) regardless of the number of straight duct lengths between the obstruction and the terminals. Despite the results collected for the Type A, 10" VAV terminal the majority of the S-shape elevation tests produced results that were quite consistent with the 90° elbow tests: a slight reduction in C values and a small decrease in precision.

7.2.3 Concentric Reducers and Expanders (with and without Elbows)

The most common ductwork identified prior to "poor" VAV terminals during the field tests were concentric reducers. Recall Figure 24 (a) and (c), which are often used to combine large ducts to a smaller sized VAV terminal. Unfortunately, concentric reducers were also often used immediately prior to the VAV terminal. This results in both a significant static pressure loss and high velocity airflow that can dramatically affect the precision and amplification of VAV airflow sensors. The fluid mechanics of air moving through a concentric reducer (or an expander for that matter) is well known, the basic behavior for both are provided in Figure 31.

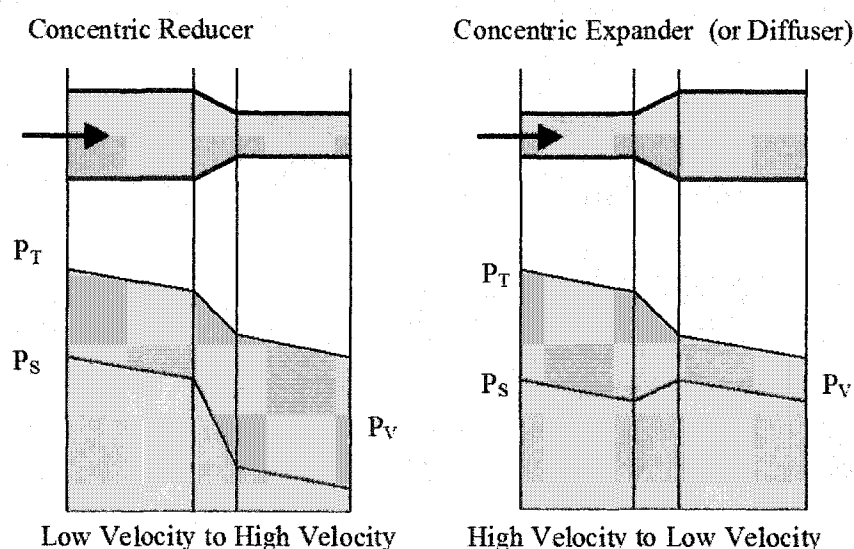


Figure 31: Simple representation of expected airflow behavior through a concentric reducer (a) and a concentric expander (b). Note that the total pressure (P_T) drops in both cases; however, the static pressure (P_S) decreases within the reducer and increases within the expander. Thus, the velocity pressure ($P_V = P_T - P_S$) will increase within a reducer and decrease within an expander.

There is an industry misconception that VAV airflow sensors are compensated for the use of concentric reducers; however, several “poorly” behaving VAV terminals were identified during the course of the field tests. To test the true effects of concentric reducers and expanders on these airflow sensors the laboratory apparatus was set up so that 40D of straight duct entered either a reducer or expander (of assorted sizes). Test sections that varied between 10D, 5D, 3D, 2D and in some cases 0D were placed between the reducers/expanders and the VAV terminals; however, it was expected that only a slight dependence on duct length would be encountered. The results of the reducer tests are available in Appendix C; the sizes that were tested include a 10” to 8”, 10” to 6”, and 8” to 6”.

The results of the concentric reducer experiments have indicated the largest reduction in VAV flow rate amplification, and once again, the greatest loss in amplification occurred for the 6” sized VAV terminals. The amplification of the 10” to 8” VAV terminals was also reduced, although to a far less extent, at a ΔC of 0.05 to 0.13 (4.0 % to 10.0%, respectively). The results of the 10” to 6” VAV terminal trials showed an extreme loss of amplification with a ΔC that ranged from 0.58 to 0.65 (36.7% and 38.7%, respectively). The experimental results for the 6” Type A VAV terminal with the 10” to 6” reducer are displayed graphically in Figure 32 for added clarity.

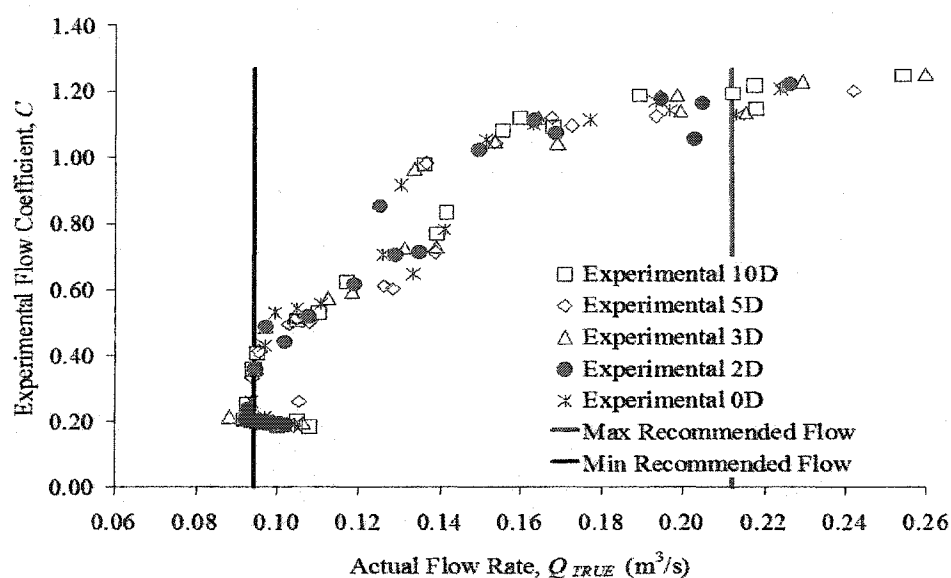


Figure 32: Results for the Type A, 6” VAV terminal for the 10” to 6” reducer geometry. The data for the 10D, 5D, 3D, 2D and 0D cases refer to the length of straight unobstructed duct between the geometry and the VAV terminal. Note the extremely high loss of amplification, especially near the minimum recommended flow setpoint. For instance, C at the minimum is $\sim 1/3$ of the value at the maximum, 0.4 compared to 1.2.

The results (again) were only mildly affected by adequate duct lengths prior to the VAV terminal. The lost sensor amplification was generally as high with 10D as it was with only 2D or even 0D. The loss of precision within the VAV operational range was also quite significant for the 10" to 6" and the 8" to 6" configurations, although the scatter remained reasonable in the 10" to 8" case, or at least consistent with the other flow obstructions observed. In a similar manner, a concentric expander was also tested (in only the 8" to 10" size); the results of these tests are available in Appendix C and are quite different from the other configurations that were tested. There is a negligible change in the amplification on the VAV airflow signal with a ΔC that is always less than 0.04. The results of 8" to 10" expander trials for the Type B VAV terminal are also displayed graphically in Figure 33. In addition, the loss of VAV airflow sensor precision, while present, is quite low in comparison to the other flow obstructions. Once again, it is also evident that adequate duct lengths does not significantly change the results associated with this transition.

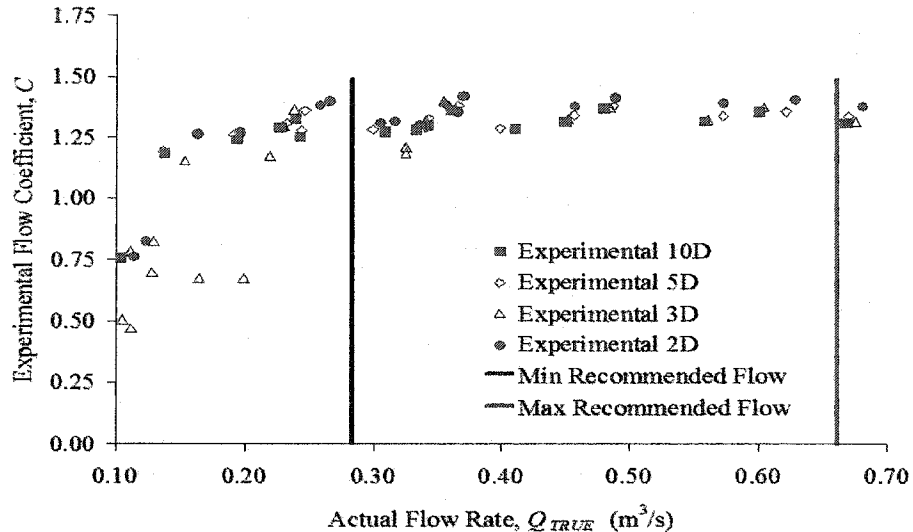


Figure 33: Experimental results for the 8" to 10" expander, Type B VAV terminal. It is evident that the amplification and precision are only mildly affected by this type of duct geometry. The case presented here is actually the "worst" set of results for this geometry and the sensor still provided reasonable response.

The results of the concentric reducer trials indicated the most dramatic loss of signal amplification and precision of all of the configurations tested. Meanwhile, the use of concentric expanders had only a very mild effect. The final duct configuration that was considered included a 90° elbow immediately prior to a concentric reducer or expander, sample results are provided below in Figure 34.

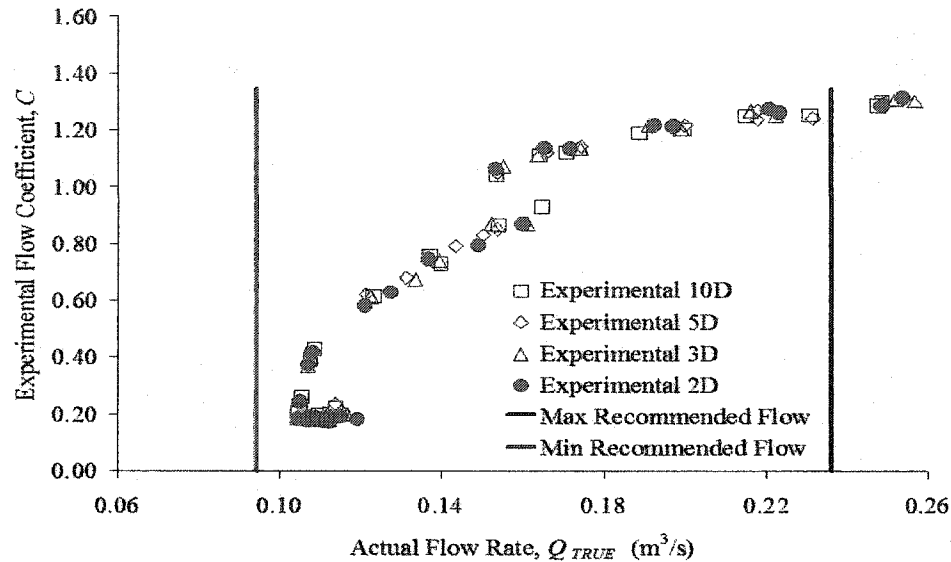


Figure 34: Results for the Type B, 6" VAV terminal for the 10" to 6" reducer geometry with a 90° elbow. The data for the 10D, 5D, 3D, and 2D cases refer to the length of straight unobstructed duct between the geometry and the VAV terminal. Note the extremely high loss of amplification (again) especially near the minimum recommended flow setpoint. There is also a noticeable "dip" at midrange that will greatly lower the precision of this terminal.

The setup for this duct geometry was otherwise identical to the previous tests. The results of the reducer and expander tests with a 90° elbow included just prior to the reducer/expander are available in Appendix C. As expected the amplification of the VAV airflow sensor is affected slightly by the inclusion of a 90° elbow prior to the concentric reducer or expander but not to a great degree. The reducer, expander, elbow (or whatever other type of flow obstruction) was dominant in all cases, over duct length for instance, and will significantly lower the VAV sensor amplification and precision.

7.3 Discussion of Duct Length Prior to the Sensor

Despite the differing results that were encountered with the various flow obstructions (elbows, reducers etc.), it was evident that the accuracy and precision of the flow coefficients were independent of duct length in relatively every test. In each case, there was very little difference between the results for the 10D test and the 2D test, which directly contradicts current industry practices. The HVAC industry generally believes, with some justification, after 10D of straight, unobstructed ductwork an accurate reading can be taken. This belief likely follows the procedure for completing a pitot tube traverse, where 7.5D downstream and 3d upstream is considered

adequate.³² However, the results of the laboratory experiments indicate that duct length is not nearly as significant as the type of obstruction. In all cases, the industry accepted value of 10D was insufficient to improve the response of these sensors. Further tests would be required to determine exactly what would constitute an adequate duct length prior to a VAV airflow sensor to minimize the scatter and maximize the amplification. It is also expected that the adequate duct length should be dependent on the volume flow rate, where the required duct length for a uniform velocity profile will increase with the velocity. It can be concluded from the laboratory experiments that the adequate duct length lies between 10D and 40D for the range of flow rates considered.

7.4 Discussion of Greater Flow Errors near the Minimum Flow Setpoint

It was also experimentally verified that VAV flow sensors errors, when they did occur, were far more likely to happen near the low end of the VAV operational range. Recall the results that were presented graphically in Figure 28 and Figure 31; the greatest loss of sensor precision was focused around the low end of the VAV operational range. The accuracy of VAV flow sensors near the low end of their operational range can be related to the pressure independence of VAV terminals, which is still a topic that is debated within the literature. It is agreed by many sources that VAV terminals require a minimum pressure to operate (typically a number like 25 Pa or 0.1” H₂O); however, this minimum amount of pressure does not ensure accurate or reliable operation. For instance, Avery (1989) states that: “...improperly sized VAV terminals furnished with pressure independent controls...[are] a “black eye” on our industry, an industry that almost universally assumes that the pressure independent feature will atone for oversized terminals, poor duct design, and sloppy supply duct pressure controls.”

The loss of amplification at the minimum flow setpoint can be related to the nature of VAV flow control, namely the use of a circular damper. Avery (1989) states that VAV sensors ensure that the effective range of the sensor usually begins when the damper is 50° open (where 90° is fully open); however, he does this mathematically without the benefit of experimental data. Therefore, the actual VAV pressure requirement for an accurate signal is near the 50° damper positions, according to Avery, and not at the minimum flow setpoint. The experimental results from the laboratory tests verify the inability of VAV terminals to provide a full usable range of flow rates. For instance, the usable range of the 10” VAV terminals is presented graphically in Figure 35.

³² The 7.5D and 3D recommendation was written into ANSI/ASHRAE standard 41.2-1987, which details the correct method for completing a full pitot tube traverse.

For the purposes of this analysis the damper position varies between fully closed (0°) and fully open (90°) while the pressure ratio (P_R) refers to the current VAV pressure differential (P_{VAV}) divided by the maximum VAV pressure differential ($P_{VAV,MAX}$), as shown in [80]. For instance, the maximum pressure differential was 250 Pa or 1" H₂O for both VAV terminals in Figure 35.

$$P_R = \frac{P_{VAV}}{P_{VAV,MAX}} = \frac{P_T - P_S}{P_{VAV,MAX}} \quad [80]$$

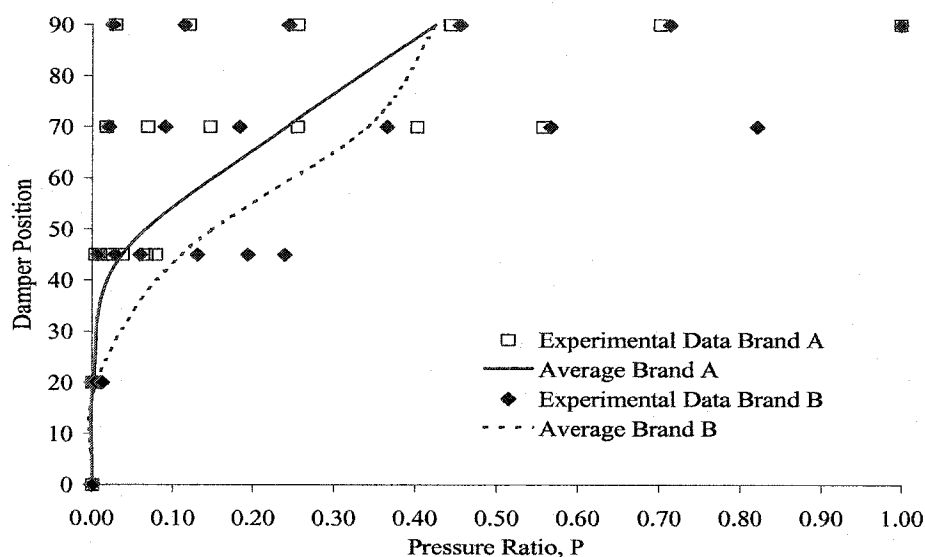


Figure 35: Usable operational range of the 10" VAV Terminals within the 40D ideal base line test for Terminal Type A and B. Note that both terminals provide relatively little airflow until the damper is 30° to 50° open, which is the same behavior discussed by Avery (1989).

The experimental results presented in Figure 35 mirrors the behavior that Avery (1989) predicted, indicating that under sizing terminals or believing that poor upstream conditions can be compensated for by the control system will produce a large amount of system instability. The insensitivity of the airflow response to damper position (near the minimum, as seen in Figure 35) also contributes to greater flow errors near the lower end of the operational range. The flow visualization experiments were completed to support these conclusions.

7.5 Supporting Flow Visualization Results

Smoke wire visualization experiments were undertaken to identify how the wake region (located around the static pressure port, behind the VAV airflow sensor) changed in relation to the upstream geometry and internal damper position. The field tests and laboratory experiments indicated that VAV airflow sensors lose significant amplification at the lower end. The

theoretical calculations and laboratory experiments indicated that the loss in amplification was related to a change in the wake region. The results of the laboratory tests also indicated that the placement of the damper affects the amplification of the airflow sensor by changing the wake region. Recall (from Section 6.3) that three duct geometries were modeled using flow visualization: a straight duct (a base line test), a concentric reducer (which resulted in the greatest loss of amplification according to the laboratory experiments) and a 90° elbow (which resulted in a high loss of signal precision). The airflow speed was maintained at 4.5 m/s and the damper was rotated from fully open (90°), half closed (45°) and nearly closed (30°) for each duct geometry: Only the airflow sensor from the Type B VAV terminals was evaluated with flow visualization. The results are presented in Figure 36 through Figure 38.

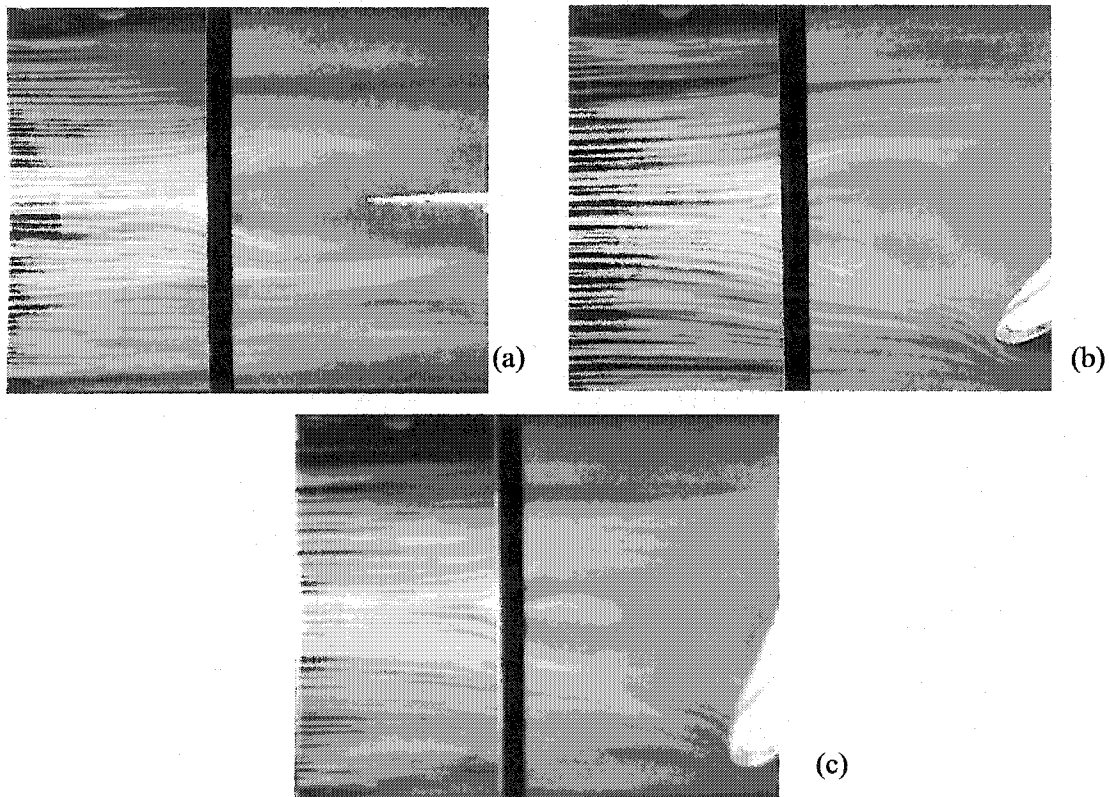


Figure 36: Flow visualization results for the straight duct configuration (or baseline case). Note the wake region following the VAV flow sensor in the middle of the images, where the four arms of the sensor meet. The static pressure port is barely visible within the wake region (a black square). The damper positions are fully open or 90° (a), half closed or 45° (b) and nearly closed or 30° in (c).

As expected, the baseline case verified that the static pressure port was located well within the wake region (producing a negative static pressure), which ensured that the VAV airflow signal

was amplified. It is also evident that the shape of the wake region changes significantly in relation to damper position (consider the changes between the 90° and 30° cases above), even in the presence of ideal upstream conditions (as in Figure 36).

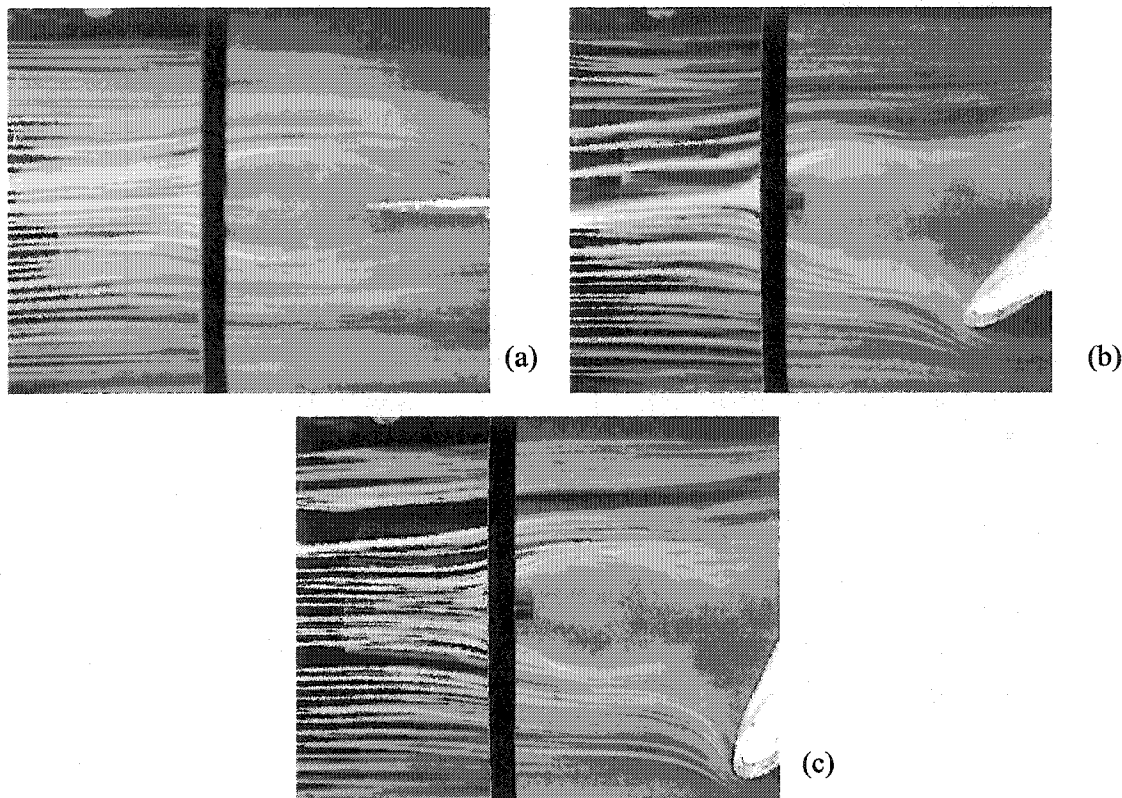


Figure 37: Flow visualization results for the concentric reducer where the damper positions are fully open or 90° (a), half closed or 45° (b) and nearly closed or 30° (c).

Recall that the laboratory experiments indicated that the concentric reducer provided the greatest loss of VAV airflow sensor amplification. The flow visualization provided here still shows a well-developed wake region (similar to the baseline case in Figure 36); however, it is evident that the wake region has decreased in size. Thus, the increased air velocity (which contributes to the total pressure) and the reduced static pressure signal result in a large loss in amplification. Another aspect of the flow visualization tests, which is not apparent from these images, is the increased smoke scatter within the wake region. This likely corresponds to the reduced precision observed for this duct configuration.

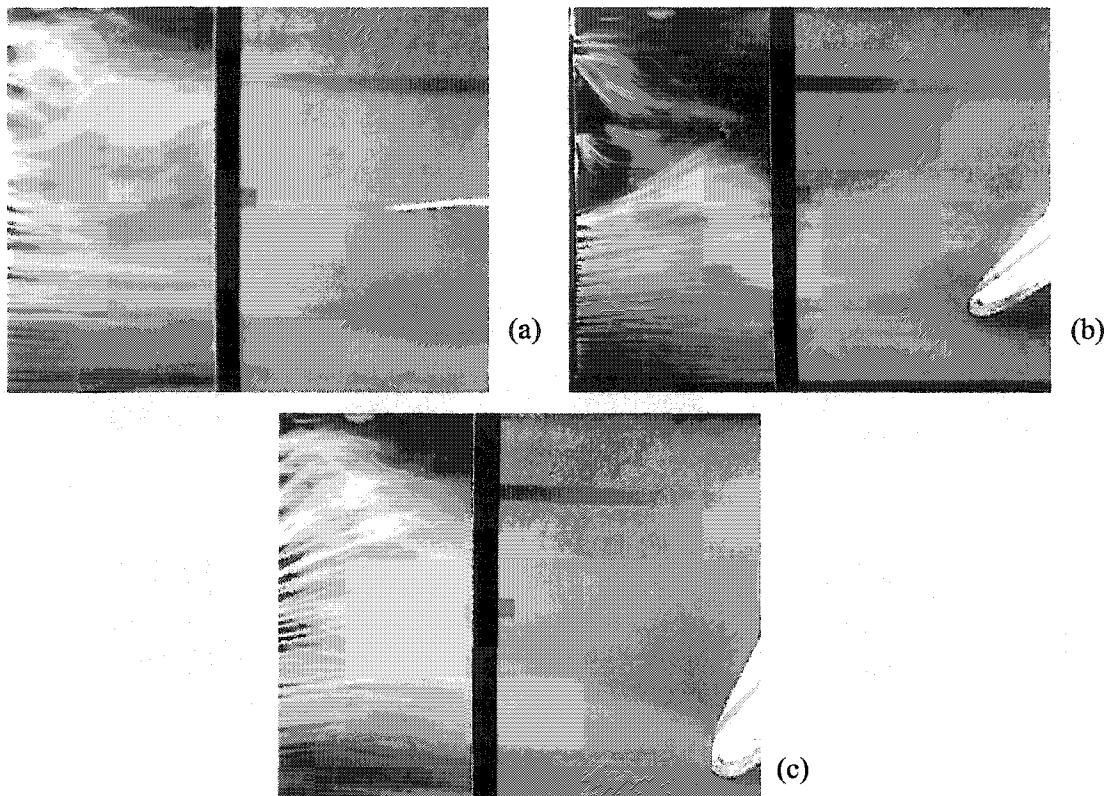


Figure 38: Flow visualization results for the 90° elbow where the damper positions are fully open or 90° (a), half closed or 45° (b) and nearly closed or 30° (c).

The flow visualization results for the 90° elbow test, shown in Figure 38, were quite different than the previous two cases. Note that a clearly defined wake region is no longer visible, even when the damper is fully open, (a). This contributes to a loss in sensor amplification because C_p is less negative as turbulence increases. In addition, note the crossing smoke streams near the top left of each image, which are more pronounced when the damper is closed. This area is a recirculation zone that lowers the precision of the airflow sensor as the varying flow rates cause scatter within the sensor response. The visualization also showed that the majority of airflow passed along the outside diameter of the elbow (along the bottom of the images in Figure 38), this is the expected flow behavior through a 90° elbow but not expected given the damper location. It is important to note these conclusions were also made based on video footage.

The results of the flow visualization experiments led to a few useful conclusions regarding VAV airflow sensor response. The position and size of the wake region does change in response to the upstream geometry, in the case of the 90° elbow this change was quite dramatic. Changes in the wake region size and shape could be partially, or fully, responsible for the decreased sensor

amplification that was observed in flow sensors following either of these obstructions. In addition, the position of the damper within the VAV terminal interferes with the signal from the flow sensors in every case. The current setup mimics the internals of the Type B VAV terminals, where the damper was positioned only 1.5D downstream of the flow sensor. Increasing the distance between the flow sensor and the damper may provide better response in this respect.

7.6 Summary of Coefficients, Independent of Adequate Duct Length

The laboratory testing was useful in that it identified problems associated with both VAV airflow sensors and the placement of VAV terminals in locations that have poor upstream duct geometry. VAV terminals were observed to lose signal amplification near the low end of the flow range, especially when the upstream geometry was not ideal or the terminal was smaller. It was observed that the greatest loss of signal amplification occurred in the 6" VAV terminals; however, it is also interesting to note that the 6" terminals used in the baseline tests (40D) provided the largest original flow amplification ($C = 1.59$ and 1.72 for Type A and B, respectively). It was also concluded that concentric reducers were the worst flow obstruction in terms of lowering the sensor amplification and precision. The 90° elbows and S-Shape geometries provided a moderate loss of precision. It is also evident that duct length will not greatly effect either the amplification or the precision of the flow sensor. The dominant factors are: sensor size, upstream geometry, and terminal design, which are presented in Table 19 and 20.

The ranking presented in Table 19 and Table 20 indicates the "worst" upstream conditions in terms of VAV airflow sensor amplification and precision. The ranking uses descriptors such as "fair" and "worst," which corresponds to a change that occurs on the order of magnitude scale. During the course of identifying the factors that contributed to VAV sensor response a number of recommendations have been developed for an "ideal" flow sensor (which is better compensated for poor upstream conditions). Recall that positioning the damper close to the flow sensor (Section 7.4) and averaging the total pressure ports inside to the duct (Section 3.7.1.2) decreases signal amplification. A discussion of improvements that could be used to design an "ideal" flow sensor has been made throughout the thesis, but the results are also summarized in Section 8.2.

Table 19: Summary of the most significant Amplification Loss, μ (Average)*

Geometries and Sizes		Type A		Type B		Type A	Type B
		C_{40D}	C	C_{40D}	C	ΔC	ΔC
Good	8" S-Shape	1.27	1.26	1.33	1.35	0.01	-0.02
	8" to 10", 90° Elbow	1.23	1.21	1.30	1.33	0.02	-0.03
	8" to 10"	1.23	1.22	1.30	1.31	0.01	-0.01
	8", Two 90° Elbows	1.27	1.23	1.33	1.34	0.04	-0.01
	6", S-Shape	1.59	1.53	1.71	1.71	0.06	0.00
	10" S-Shape	1.23	1.17	1.30	1.29	0.06	0.01
Fair	10", Two 90° Elbows	1.23	1.18	1.30	1.27	0.05	0.03
	10" to 8"	1.27	1.18	1.33	1.26	0.09	0.07
	6", Two 90° Elbows	1.59	1.41	1.71	1.60	0.18	0.11
Worst	10" to 8", 90° Elbow	1.27	1.14	1.34	1.17	0.13	0.17
	8" to 6"	1.58	1.23	1.70	1.34	0.35	0.36
	8" to 6", 90° Elbow	1.58	1.25	1.70	1.32	0.33	0.38
	10" to 6"	1.58	0.97	1.68	1.04	0.61	0.64
	10" to 6", 90° Elbow	1.58	0.93	1.67	0.99	0.65	0.68

* Note that the baseline C values (C_B) were determined from the average of the linear equations (40D), the C values are the average values between the min/max setpoints and the ΔC term is the difference. Decreased amplification is indicated by a positive ΔC . The ranking is based on the absolute average ΔC value for Type A and B, independent of adequate duct length.

Table 20: Summary of the most significant Precision Loss, σ (Standard Deviations)*

Geometries and Sizes		Type A		Type B		Type A	Type B
		C_{40D}	C	C_{40D}	C	ΔC	ΔC
Good	8" S-Shape	0.009	0.028	0.003	0.017	0.019	0.014
	6", S-Shape	0.004	0.028	0.017	0.032	0.024	0.016
	8" to 10", 90° Elbow	0.002	0.038	0.009	0.018	0.036	0.009
	10" to 8"	0.050	0.058	0.003	0.064	0.008	0.061
	8", Two 90° Elbows	0.010	0.046	0.003	0.037	0.036	0.034
	10", Two 90° Elbows	0.002	0.059	0.009	0.038	0.057	0.029
Fair	10" S-Shape	0.002	0.085	0.010	0.029	0.082	0.019
	8" to 10"	0.002	0.066	0.010	0.052	0.064	0.042
	6", Two 90° Elbows	0.004	0.078	0.014	0.051	0.074	0.038
	10" to 8", 90° Elbow	0.010	0.062	0.003	0.086	0.052	0.083
Worst	8" to 6"	0.005	0.117	0.018	0.090	0.112	0.072
	8" to 6", 90° Elbow	0.005	0.113	0.020	0.107	0.108	0.087
	10" to 6"	0.003	0.159	0.033	0.155	0.155	0.122
	10" to 6", 90° Elbow	0.003	0.158	0.012	0.177	0.155	0.165

* Note that these values were determined in a similar manner but refer to the standard deviations of the points instead of the averages, the ΔC value is now reversed as well so that a positive value indicates an increased scatter (or lower precision). In every case, the precision decreased.

8.0 Conclusions

This thesis has fulfilled a need within the building sciences (and the HVAC community) for quantitative experimental research that concerns the recommissioning of VAV systems equipped with DDC. The results can be subdivided into two sections: the first deals with the critical aspects and longevity involved with building recommissioning, the second concerns the response of VAV airflow sensors. The conclusions for both topics are summarized below.

It is also important to note that the reasons why these types of systems require recommissioning was not a focus of this research. The results seem to indicate that both sensor error and changes in space usage (which correspond to different system settings and ranges) play an important role. However, this research was completed based on the assumption that recommissioning was beneficial (and necessary) at unknown, regularly spaced intervals. This assumption was made using past research dealing with recommissioning these systems.

8.1 The Critical Aspect of Building Recommissioning, in Terms of Longevity

Field research was undertaken to determine the effects of recommissioning within facilities that had been operational for several years. The primary focus of the field research was determining what critical factors were responsible for system longevity. Key performance indicators used for this comparison included DDC system accuracy, IAQ, energy/economic efficiency, and thermal comfort. This research was significant because the longevity of recommissioning VAV systems with DDC had not been previously investigated. Secondary objectives included the documentation of the recommissioning process and the development of analysis tools for these types of system.

It was originally hypothesized that the improvement of individual VAV terminal accuracy was the most significant aspect of building recommissioning (which is why the laboratory tests were initiated). The experimental field results have since verified this assumption. Field-testing was completed at three facilities in the Edmonton area. The system performance at each location was monitored prior to recommissioning, immediately after recommissioning and after the system had been allowed to deviate (which lasted between 8 and 21 months). The exact system performance was established by applying the DDC system trend logs to the recommissioning data to evaluate the various performance indicators. For instance, the improvement of DDC system accuracy was quite significant, where all three DDC systems were initially indicating excessive ventilation (by ~18%, ~10% and ~9% at the Cross Cancer Institute, Timms Center and Yellowhead Library,

respectively). Each DDC system was improved substantially with recommissioning (as expected) but it was interesting that the systems did not deviate much over time. Recall that the total DDC system accuracy at the Timms Center deviated by ~1% in 21 months, while the system at the Yellowhead Library deviated by only ~0.5% in 8 months. These results were further verified with an energy evaluation. For instance, recall that the Timms Center was originally wasting ~74% of the supply fan energy at the minimum flow setpoint, after recommissioning this value was reduced to ~14%. After the system was allowed to drift (for the longest time period considered in the field, a full 21 months) the system was wasting ~38% of the supply fan power at the minimum flow setpoint (in heating mode). Thus, even after nearly 2 years the benefits of recommissioning remained significant.

The field experiments indicate that although the energy, and thus economic, benefits may be greater for other portions of the recommissioning process³³ (as opposed to VAV flow sensor calibration) but the improvements to IAQ and DDC system accuracy were more substantial. Although the energy efficiency of VAV systems with DDC is desirable, the primary objective of any HVAC systems is to provide a healthy, comfortable environment, preferably with excellent individual zone control. The improvement of VAV airflow accuracy satisfies all of these requirements by improving IAQ (by accurately monitoring the O/A), thermal response, and DDC system accuracy for greater zone control. Thus, the improvement of VAV terminal accuracy is the most significant portion of building recommissioning. The field research was also able to provide an estimate for the longevity associated with recommissioning VAV systems with DDC. Unfortunately, the results could not be used to define the exact longevity of recommissioning since that point was not reached in the field research. However, it can be concluded that the effects of building recommissioning will remain beneficial for at least the maximum length considered in the field tests, which was 21 months. Recommendations for a research plan that could determine the average longevity of recommissioning VAV systems with DDC are provided in Section 9.0.

Finally, the process of recommissioning VAV systems with DDC was documented to add to the current collection of research on this topic. The recommissioning of systems is hardly a static process, thus the continued improvement of recommissioning techniques is both inevitable and

³³ Recall the large amount of supply fan energy saved by calibrating the EOL static sensors, which is a relatively simple procedure when compared to many other aspects of the recommissioning process.

desirable. Techniques such as the identification of misaligned dampers without intrusive testing³⁴ or the real-time estimation of DDC system accuracy in response to recommissioning (without the use of trend data)³⁵ are both good examples of unique improvements to the recommissioning procedure. Hopefully, these analysis tools will be beneficial to the HVAC industry and can be used to further improve the recommissioning process for these types of systems.

8.2 The Response of VAV Airflow Sensors

It was also hypothesized that poor upstream conditions were the limiting factors when making improvements to VAV sensor calibrations. Laboratory experiments were undertaken to determine the effects of upstream conditions on VAV airflow sensor response. It was determined that current industry practices during the design phase often contribute to inaccurate VAV airflow sensors and system wide instability. Common industry misconceptions state that VAV terminals are compensated for concentric reducers and that 10D of straight ducting is adequate to provide a uniform VAV differential pressure signal. Recall that the use of concentric reducers resulted in extreme amplification losses during the laboratory experiments, which varied between $\Delta C = 0.35$ to 0.64 (or ~22% to ~38% of the baseline amplification with no obstructions). It was also found that there is virtually no difference in the VAV differential pressure signal between the 10D and 2D duct lengths, which was consistently shown in each geometry. This directly contradicts the current industry practice of leaving 10D of unobstructed ducting prior to the VAV terminal.

The “worst” upstream conditions that were observed during the field tests were recreated in the laboratory and ranked in terms of amplification and precision loss³⁶. The experiments provided an insight into VAV airflow sensor response: although the results are limited to the worst conditions observed in the field tests and only two common VAV terminal designs. Theoretical fluid mechanics and flow visualization experiments were further used to formulate a list of recommendations to improve VAV airflow sensor response to “poor” upstream conditions.

A brief summary of key recommendation/findings are provided:

1. Increase the distance between the airflow sensor and damper (inside the VAV terminal). Currently the distance varies between 1.5D to 2D (internally) and flow visualization shows excessive damper interference that lowers signal amplification by interacting with the wake region when the dampers are partially opened.

³⁴ Recall Section 4.5, as well as Figures 15 and 16, which outline this technique.

³⁵ Recall Section 5.2, which discussed this analysis in detail for the Yellowhead Library.

³⁶ Recall Tables 19 and 20, which ranked each geometry in terms of amplification and precision loss.

2. Use a concentric damper, such as an Iris. This will lower the impact on the wake region, providing more signal amplification. Another positive side effect may also be improved flow control at low flow rates (recall that the VAV terminals tested provide negligible control at damper angles of 0 to 50° and 30°, respectively).
3. The most obvious improvement that can be made is to limit duct obstructions prior to the VAV terminal. The laboratory tests show that 10D of straight ducting is generally insufficient, while 40D is more than adequate. Further testing would be required to specify the exact allowable distance for each upstream duct geometry (especially in a universal manner for all VAV terminals) but a value ~30D of straight ducting would seem prudent. Although this is the most obvious solution, it is also the most impractical. Providing 30D of straight duct prior to a VAV terminal would be quite difficult (and costly) within the majority of HVAC systems.
4. The last solution, which is also obvious, is to sacrifice the amplification provided by placing the static pressure port in the wake region in order to improve signal accuracy (especially at the low end of the sensors range). Unfortunately, accuracy will only be improved in this manner if the quality of the pressure transducer is also upgraded, which directly contradicts one of the primary goals of the HVAC industry: cost efficiency. The results of this research have shown that the improvement of VAV sensor accuracy is extremely important. Therefore, the improvement of VAV pressure transducers seems justified.

It is the intent of the author that this research be used to further reduce the energy consumption of VAV systems while improving the response of DDC systems and the accuracy of VAV airflow sensors. This thesis has also focused on relating the experiences gained with VAV systems and DDC to supplement the current experimental research that is available.

9.0 Recommendations for Future Work

Despite the successful completion of the objectives, the results of this research have led to a number of other interesting questions. In a perfect world, time constraints and budgets would allow me to explore these problems; nonetheless, it is my hope that someone else is able to continue with this work at a later date.

- 1) True Longevity of Recommissioning VAV systems with DDC: The field research was limited to a period of 21 months. It was impossible to complete longer field tests due to the budget constraints of ASHRAE RP 1137 (which funded all field experiments), the personnel constraints of Stantec Consulting Ltd. (who provided support personnel to assist in data collection) and the constraints imposed by the operators of the various buildings. Unfortunately, the absolute longevity of recommissioning VAV systems with DDC has not been identified from the field results. It was determined that the longevity at the three buildings considered was at least equal to the maximum period (again, this was 21 months in our case). The solution to the longevity question may be that these types of systems cannot be categorized into a common time frame, perhaps the longevity of recommissioning is dependent on other factors that did not materialize in the time allowed. The simplest answer may still be best: recommissioning should not be completed until the simple payback period has elapsed from the last recommissioning procedure. The field research has provided a starting point for future work (recall that no one had been able to estimate this time period) but ideally we would be able to continue monitoring the facilities until deviations occurred. It is recommended that a smaller study be considered instead: monitor a group of VAV terminals (say 10 or so) in a large facility and continue collecting data for a far longer time-period, say in the range of five or more years. Focus on zone requirements during that time (what part of the range does the terminal operate in and what accuracy does this correspond to). The deviation of the system is only a function of accuracy at whatever space use is needed for that zone, and monitoring how it changes (over a longer time) will allow for a true estimate of longevity. If this were completed simultaneously in a large number of buildings (say 20 at least) it may even be possible to create an experimental estimate of longevity for all of these types of systems.
- 2) The laboratory tests (which focus on VAV accuracy and amplification) can also be expanded to become more useful to the HVAC industry. The effects of poor upstream duct geometry on VAV flow accuracy is usually ignored; however, this research has

shown that a significant amplification loss can result from certain duct geometries. It is also troubling that the industry accepted value of 10D of straight ducting has been found to be insufficient for VAV airflow sensors. It is recommended that the laboratory tests be repeated (to build a more detailed table of common loss coefficients), which ideally would include a greater variety of both VAV manufacturers and upstream conditions. There are several ways that VAV airflow accuracy can be improved. This research has identified some good recommendations, but further work could also focus on developing the “ideal” VAV airflow sensor. VAV flow sensors are typically designed to provide an amplified signal in an economical fashion. Further research could focus on the ideal response for the lowest price.

10.0 Bibliography

A. J. Smits and T. T. Lim (2000), Flow Visualization: Techniques and Examples, Imperial College Press, London.

ANSI/ASHRAE Guideline 2-1986 (1986), "Guide for Engineering Analysis of Experimental Data", ANSI/ASHRAE Standard.

ANSI/ASHRAE Standard 111-1988 (1988) "Practices for Measurement, Testing, Adjusting and Balancing of Building Heating, Ventilation, Air-Conditioning and Refrigeration Systems", ANSI/ASHRAE Standard

ANSI/ASHRAE Standard 41.1-1974 (1974), "Standard Measurements Guide: Section on Temperature Measurements", ANSI/ASHRAE Standard.

ANSI/ASHRAE Standard 41.2-1987 (1987), "Standard Methods for Laboratory Airflow Measurement", ANSI/ASHRAE Standard.

ANSI/ASHRAE Standard 41.3-1989 (1989), "Standard Method for Pressure Measurement", ANSI/ASHRAE Standard.

ASHRAE (1995), HVAC Applications Handbook: SI Edition, 1791 Tullie Circle, N.E., Atlanta, GA 30329: ASHRAE.

ASHRAE (2000), Systems and Equipment Handbook: SI Edition, 1791 Tullie Circle, N.E., Atlanta, GA 30329: ASHRAE.

ASHRAE (2001), Fundamentals Handbook: SI Edition, 1791 Tullie Circle, N.E., Atlanta, GA 30329: ASHRAE.

ASHRAE (2002), Refrigeration Handbook: SI Edition, 1791 Tullie Circle, N.E., Atlanta, GA 30329: ASHRAE.

ASHRAE (2003), HVAC Applications Handbook: SI Edition, 1791 Tullie Circle, N.E., Atlanta, GA 30329: ASHRAE.

B. Freese, R. Coleman, D. Aldag, B. Dutton, J. Brue, E.P. Howard (2002), HVAC Systems Testing, Adjusting and Balancing, 3rd Edition, Sheet Metal and Air Conditioning Contractors National Association Inc., Chantilly, VA, 20151-1209.

C. Kjellman, R. Haasl and C. Chappell (1996), "Evaluating Commissioning as an Energy-Saving Measure", ASHRAE Transactions 1996 (1), pp. 492 – 501.

C. Norberg (1993), "Flow around rectangular cylinders: Pressure forces and wake frequencies", *Journal of Wind Engineering and Industrial Aerodynamics* 49 (1993), pp .87-196.

C. Schroeder, M. Krarti, and M. J. Brandemuehl (2000), "Error analysis of measurement and control techniques of outside air intake rates in VAV systems", ASHRAE Transaction: Research, V106, Pt. 2, pp. 26.

- C.A. Walker (1984), "Application of Direct Digital Control to a Variable Air Volume System" ASHRAE Transactions 1984 (3), pp. 846 –855.
- C. Y. Han, Y. Xiao and C. Ruther (1990), "Fault Detection and Diagnosis of HVAC Systems" ASHRAE Transactions 1990 (1), pp. 568 – 578.
- D. C. Hittle (1999), "Controlling Variable-Volume Systems", ASHRAE Journal, April 22, 1999.
- D. W. Bearg (1999), "The Use of Multipoint Monitoring as a Tool for Commissioning Buildings for IAQ" ASHRAE Transaction 1999 (1), pp. 1101 –1108.
- D. J. Herzig and F. F. Wajcs (1993), "Lessons Learned from Monitored Office Building Data" ASHRAE Transactions 1993, pp. 851 –856.
- F. C. McQuiston, J. D. Parker and J. D. Spitler (2000), Heating, Ventilation and Air Conditioning: Analysis and Design, 5th Edition, John Wiley & Sons Inc., New York.
- F. White, Fluid Mechanics, 4th Edition, McGraw-Hill Companies Inc., 1999.
- G. Avery (1989), "The Myth of Pressure Independent VAV Terminals", ASHRAE Journal, August, 1989.
- G. J. Janu, J.D. Wenger and C. G. Nestler (1995), "Strategies for Outdoor Airflow Control from a System Perspective" ASHRAE Transactions 1995, pp. 631 –643.
- H. K. W. Mui, D. W. T. Chan and J. Burnett (2003). "Dynamic evaluation of airflow rates for a variable air volume system serving an open-plan office", Blackwell Munksgaard Publishing, Denmark, *Indoor Air* 2003; 13: pp. 311-323.
- H. Sauer Jr., R. Howell and W. Coad (2001), Principles of Heating Ventilating and Air Conditioning, 1791 Tullie Circle, N.E., Atlanta, GA 30329: ASHRAE.
- I. Taylor and M. Vezza (1999), "Prediction of unsteady flow around square and rectangular section cylinders using a discrete vortex method", *Journal of Wind Engineering and Industrial Aerodynamics* 82 (1999), pp. 247 – 269.
- J. A. Roberson and C. T. Crowe (1976), Engineering Fluid Mechanics, Houghton Mifflin Company, 1976.
- J. Diep (2001), Flow Control Reduction of Smokestack Downwash, M.Sc. Thesis, Department of Mechanical Engineering, University of Alberta, 2001.
- J. P. Kettler (1995), "Minimum Ventilation Control for VAV Systems: Fan Tracking vs. Workable Solutions: ASHRAE Transactions (1995), pp. 613 –618.
- J. Stewart (1995), Calculus: Early Transcendentals, 3rd Edition, Brooks/Cole Publishing Company, 1995.
- J. F. Busch, (1992) "A tale of two populations: Thermal comfort in air-conditions and naturally ventilated offices in Thailand", *Energy and Buildings*, chapter 18, pp. 235-249.

- K. LauBauve, R. Pachikara, K. Pandit, S. Powell, S. Shade and J. Sivak (2003) "Temperature, Humidity and Worker Productivity Analysis of Constant Air Volume and Variable Air Volume Underfloor Air Conditioning systems", www.rhsmith.umd.edu/quest/senior20practicum%20projects/2002/york/york_final_paper_120402_1211am.doc, August 26, 2003
- K. Maki, G. Chamberlin, Z. Li and L. L. Christianson (1997), "VAV System Performance - Field Characterization of Airflow, System Diagnosis Tools, and Operation Design Implications" ASHRAE Transactions 1997 (2), pp. 830 – 842.
- K. M. Elovitz (1992), "Commissioning Building Mechanical Systems", ASHRAE Transactions 1992 (2), pp. 543 – 552.
- K. N. Ghia, T. J. Mueller and B. R. Patel (1981), Computers in Flow Predictions and Fluid Dynamics Experiments, Fluid Engineering Division of ASME, 345 East 47th Street, New York, N.Y. 10017, 1981.
- K. W. Roth, D. Westphalen and D. Brodrick (2003), "Saving Energy with Building Commissioning", ASHRAE Journal, November, 2003.
- M. A. Piette and B. Nordman (1996), "Costs and Benefits from Utility-Funded Commissioning of Energy-Efficiency Measures in 16 Buildings", ASHRAE Transactions 1996 (1), pp. 482- 491.
- Moncef Krarti, Michael J. Brandemuehl, Chris Schroeder and Erik Jeannette, RP 980 Final Report: Techniques for Measuring and Controlling Outside Air Intake Rates in Variable Air Volume Systems, ASHRAE, Final Report JCEM TR/99/03, 1791 Tullie Circle, N.E., Atlanta, GA 30329: ASHRAE.
- M. Krarti, C. C. Schroeder, E. Jeanette, and M. J. Brandemuehl (2000), "Experimental Analysis of Measurements and Control Techniques of Outside Air Intake Rates in VAV Systems" ASHRAE Transactions 2000 (2), pp. 39 – 52.
- N. P. Fleming, Passive Ventilation for Combustion Air Supply, M.Sc Thesis, Department of Mechanical Engineering, University of Alberta, 1996.
- P. Chang (1976), Control of Flow Separation: Energy Conservation, Operational Efficiency and Safety, Hemisphere Publishing Corporation, McGraw-Hill Book Company.
- P.O. Fanger (1972), Thermal Comfort: Analysis and Applications in Environmental Engineering, McGraw-Hill Book Company, 1972.
- R. de Dear, K. Leow and A. Ameen (1997), "Thermal Comfort in the Humid Tropics", ASHRAE Transactions 1997 (1), pp. 874-879.
- R. L. Daugherty, J. B. Franzini and E. J. Finnemore (1985), Fluid Mechanics with Engineering Applications, 8th Edition, McGraw-Hill Book Company, 1985.
- R. T. Ellis (1996), "Commissioning a Museum and Archival Storage Facility" ASHRAE Transactions 1996 (1), pp. 476 – 481.
- R. V. Hogg and A. T. Craig (1970), Introduction to Mathematical Statistics, 3rd Edition, MacMillan Publishing Co. Inc., 1970

S. J. Hayter and R. Judkoff (1999), " Optimizing Building and HVAC Systems", ASHRAE Journal, December, 1999.

S. A. Mumma and R. J. Bolin (1994), "Real-time, On-line Optimization of VAV System Control to Minimize the Energy Consumption Rate and to Satisfy ASHRAE Standard 62-1989 for all Occupied Zones" ASHRAE Transactions 1994 (1), pp. 168 – 177.

S. W. Churchill (1977), "Friction Factor Equation Spans All Fluid Flow Regimes", Chemical Engineering, November 1977, pp. 91-92.

T. E. Cappellin (1997), "VAV Systems - What Makes them Succeed? What Makes the Fail?" ASHRAE Transactions 1997 part 2, pp. 814 –822.

W. J. Fisk and D. Faulkner (1992), "Air Exchange Effectiveness in Office Buildings Measurement Techniques and Results," LBL-33103, Presented at the International Symposium on Room Air Convection and Ventilation Effectiveness, University of Tokyo, July 22 -24, 1992.

W. J. Fisk, W. Delp, R. Diamond, D. Dickerhoff, R. Levinson, M. Modera, M. Nematollahi, D. Wang (1999), "Duct systems in large commercial buildings: physical characterization, air leakage, and heat conduction gains", Energy and Buildings 32 2000 109-119, Elsevier, Received 1 April 1999; accepted 10 November 1999.

W. C. L Shih, C. Wang, D. Coles and A. Roshko (1993), "Experiments on flow past rough circular cylinders at large Reynold Numbers", Journal of Wind Engineering and Industrial Aerodynamics 49 (1993), pp. 351 – 368.

Y. A. Cengel and M. A. Boles (1998), Thermodynamics An Engineering Approach, 3rd Edition, WCB McGraw-Hill, 1998.

Y. Nakayama (1988), Visualized Flow: Fluid Motion in Basic and Engineering Situations Revealed by Flow Visualization, the Japan Society of Mechanical Engineers, Pergamon Press, Hiratsuka, Japan, 1988.

Z. Gu and T. Sun (1999), "On Interference between two circular cylinders in staggered arrangement at high subcritical Reynolds numbers", Journal of Wind Engineering and Industrial Aerodynamics 80 (1999), pp. 287-309.

Appendix A

Contents: Theoretical Calculations

- | | | |
|----|--|-----|
| 1) | Fluid Mechanics for the Case of Three Total Pressure ports | 117 |
| 2) | Sample Calculations for the VAV airflow sensor Model | 123 |

1) Fluid Mechanics for the Case of Three Total Pressure ports

It is desirable to predict the total pressure signal that will result from the VAV airflow sensor in response to varying upstream conditions, thus it was necessary create a simple model. The primary model (which was discussed in detail within the main body) was for a simplistic 2-port case. The following calculations are for the more complex case where 3 forward facing pressure ports are required, as detailed in Figure A1 (which was also presented in the main body).

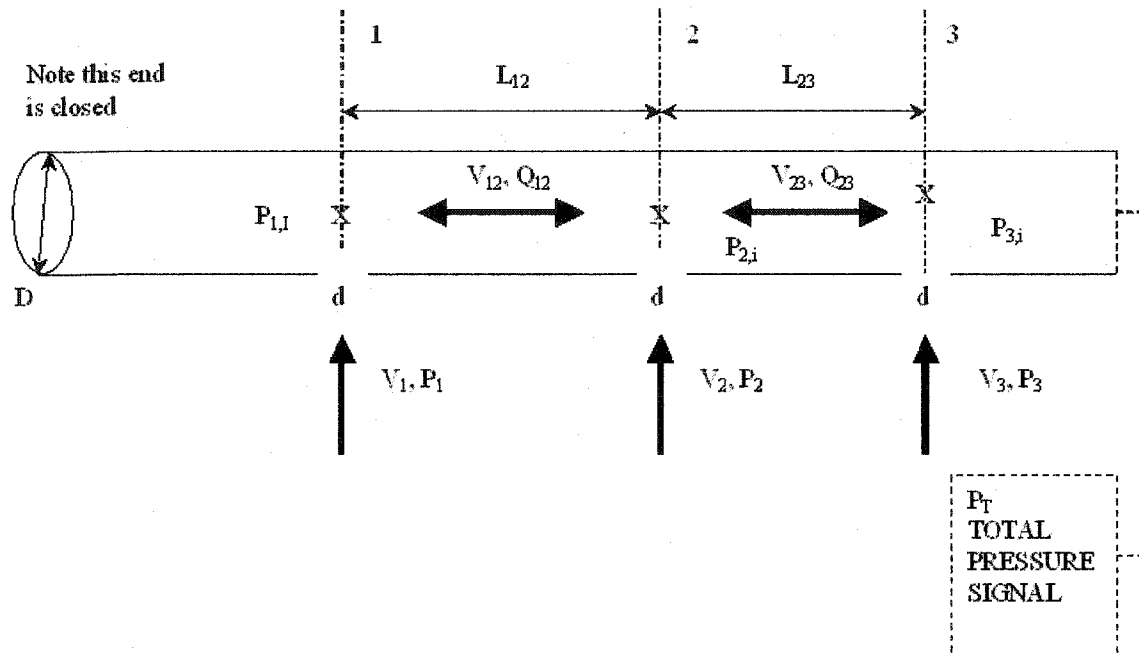


Figure A1: More realistic representation of a typical VAV airflow sensor with three forward facing velocity pressure ports, this diagram will be used in the following calculations to determine the total pressure signal as a function of the velocity at each port (V_1, V_2, V_3).

As a starting point it is once more useful to consider the conservation of mass equation, which leads to the conservation of volume equation due to the fact that the area and the density considered at points 1, 2 and 3 are all equal. This is summarized below in [A1] and [A2], along with the relationships describing the flow into the airflow sensor (for instance, from P_i to $P_{i,i}$) using the orifice equations that were used in the previous analysis.

$$\frac{\partial m}{\partial t} = 0 \text{ so that } \dot{m}_1 = \dot{m}_2 + \dot{m}_3 \quad [\text{A1}]$$

$$\rho V_1 A_1 = \rho V_2 A_2 + \rho V_3 A_3 \quad [\text{A2}]$$

These relationships are built on assumptions that $V_1 \gg V_2, V_3$ and thus $Q_1 \gg Q_2, Q_3$, or that, simply put, the velocity profile is steep enough that backflow is occurring that will force air into the port at location 1 and out the ports at location 2 and 3. Note that a simple factor will later be introduced to account for the fact that Q_2 does not necessarily have to equal Q_3 , although it is certainly possible and perhaps even likely given this physical system. In either case, the following orifice equations are used to further describe the system.

$$Q_1 = kA_1 \left[\frac{2(P_1 - P_{1,i})}{\rho} \right]^{1/2} \quad [\text{A3}]$$

$$Q_2 = kA_2 \left[\frac{2(P_{2,i} - P_2)}{\rho} \right]^{1/2} \quad [\text{A4}]$$

$$Q_3 = kA_3 \left[\frac{2(P_{3,i} - P_3)}{\rho} \right]^{1/2} \quad [\text{A5}]$$

By introducing the orifice equations into the previous volume balance (recall that $Q = VA$ for the substitution) it is possible to determine the following relationship. It is also important to note that a different form of the loss coefficient ($k=K^{-0.5}$) is used here when compared to the 2-hole case. The form presented here is more convenient to work with and since the coefficient only refers to some constant value the results are not affected in this case.

$$\rho(kA_1) \left[\frac{2(P_1 - P_{1,i})}{\rho} \right]^{1/2} = \rho(kA_2) \left[\frac{2(P_{2,i} - P_2)}{\rho} \right]^{1/2} + \rho(kA_3) \left[\frac{2(P_{3,i} - P_3)}{\rho} \right]^{1/2} \quad [\text{A6}]$$

Where the loss coefficient, surface area, and density terms are equal then the relation can be further simplified, with some additional manipulation, to the following form.

$$\Delta P = (P_1 + P_3) = (P_{1,i} + P_{3,i}) + (P_{2,i} - P_2) + 2(P_{2,i} - P_2)^{1/2} (P_{3,i} - P_3)^{1/2} \quad [\text{A7}]$$

The majority of the terms in the previous Equation have already been defined, for instance, the 2nd and 3rd terms on the RHS can simple be determined from the orifice Equations that were previously provided in Equations [A3] – [A6], recall that $Q = VA$ for the following two equations.

$$(P_{2,i} - P_2) = \left(\frac{\rho}{2} \right) \left(\frac{Q_2}{kA_2} \right)^2 = \left(\frac{\rho}{2} \right) \left(\frac{V_2}{k} \right)^2 \quad [\text{A8}]$$

$$(P_{3,i} - P_3) = \left(\frac{\rho}{2} \right) \left(\frac{Q_3}{kA_3} \right)^2 = \left(\frac{\rho}{2} \right) \left(\frac{V_3}{k} \right)^2 \quad [\text{A9}]$$

To determine the other relations necessary it is once more useful to consider Bernoulli's standard pipe flow equation between points 1 and 2 (internally) as shown in the following relation.

$$\frac{P_{1,i}}{\rho} + 0 = \frac{P_{2,i}}{\rho} + gL_{12} + f \frac{L_{12}}{D} \frac{1}{2} (V_{12})^2 \quad [\text{A10}]$$

Then with some simplification it is possible to reduce the previous equation to the following:

$$(P_{1,i} - P_{2,i}) = f \left(\frac{\rho}{2} \right) \frac{L_{12}}{D} (V_{12})^2 \quad [\text{A11}]$$

Note that to achieve the previous equation the hydrostatic term was neglected (the hydrostatic gL_{12} term, which should have been included on the RHS of the previous equation). Recall that hydrostatic pressure forces are typically insignificant based on an order of magnitude basis, and can be safely neglected. In a very similar manner, the Bernoulli pipe flow equation was used to consider the internal pressure losses between points two and three, for the following relation.

$$(P_{2,i} - P_{3,i}) = f \left(\frac{\rho}{2} \right) \frac{L_{23}}{D} (V_{23})^2 \quad [\text{A12}]$$

In this manner, the resistance analogy can once again be used to model the flow throughout the system, as shown by the Figure A2. Note that the flow resistance R_1 , R_2 and R_3 were obtained from the orifice equations and the resistances R_4 and R_5 are simply obtained from Bernoulli's equation.

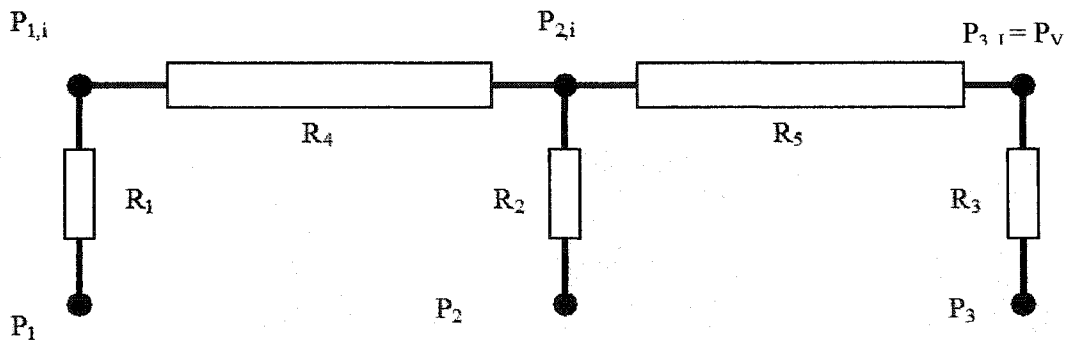


Figure A2: Resistance Analogy for the 3 port case, the P_v pressure corresponds to the P_T signal that we are interested in.

The resistance terms for each branch of Figure A2 are provided below.

$$R_1 = \frac{P_1 - P_{1,i}}{Q_1} = \frac{Q_1}{(kA_d)^2} \rho/2 = \left(\frac{V_1}{k}\right)^2 \rho/2 \left(\frac{1}{Q_1}\right) \quad [\text{A13}]$$

$$R_2 = \frac{P_{2,i} - P_2}{Q_2} = \frac{Q_2}{(kA_d)^2} \rho/2 = \left(\frac{V_2}{k}\right)^2 \rho/2 \left(\frac{1}{Q_2}\right) \quad [\text{A14}]$$

$$R_3 = \frac{P_{3,i} - P_3}{Q_3} = \frac{Q_3}{(kA_d)^2} \rho/2 = \left(\frac{V_3}{k}\right)^2 \rho/2 \left(\frac{1}{Q_3}\right) \quad [\text{A15}]$$

$$R_4 = \frac{\Delta P_{12}}{Q_{12}} = \frac{P_{1,i} - P_{2,i}}{Q_{12}} = \left(\frac{1}{Q_{12}}\right) \rho/2 f\left(\frac{L_{12}}{D}\right) (V_{12})^2 = \left(\frac{2\rho}{\pi}\right) f\left(\frac{L_{12}}{D^3}\right) V_{12} \quad [\text{A16}]$$

$$R_5 = \frac{\Delta P_{23}}{Q_{23}} = \frac{P_{2,i} - P_{3,i}}{Q_{23}} = \left(\frac{1}{Q_{23}}\right) \rho/2 f\left(\frac{L_{23}}{D}\right) (V_{23})^2 = \left(\frac{2\rho}{\pi}\right) f\left(\frac{L_{23}}{D^3}\right) V_{23} \quad [\text{A17}]$$

It is then possible to consider the results in terms of the Arms associated with Figure A2, for added simplicity. In this manner, it was possible to combine the resistance associated with Arm 1 (R_1 and R_4), Arm 2 (R_2) and Arm 3 (R_3 and R_5), as shown below.

$$Q_1 = \frac{P_1 - P_{2,i}}{R_1 + R_4} \quad [\text{A18}]$$

$$Q_2 = \frac{P_2 - P_{2,i}}{R_2} \quad [\text{A19}]$$

$$Q_3 = \frac{P_3 - P_{2,i}}{R_3 + R_5} \quad [\text{A20}]$$

Recall that conservation of mass has provided that ($Q_1 + Q_2 + Q_3 = 0$), therefore:

$$\frac{P_1 - P_{2,i}}{R_1 + R_4} + \frac{P_2 - P_{2,i}}{R_2} + \frac{P_3 - P_{2,i}}{R_3 + R_5} = 0 \quad [\text{A21}]$$

Now when the R terms are substituted into [A21] it is possible to obtain the following:

$$\frac{P_1 - P_{2,i}}{\left(\frac{V_1}{k}\right)^2 \rho/2 \left(\frac{1}{Q_1}\right) + \left(\frac{1}{Q_{12}}\right) \rho/2 f\left(\frac{L_{12}}{D}\right) (V_{12})^2} + Q_2 + \frac{P_3 - P_{2,i}}{\left(\frac{V_3}{k}\right)^2 \rho/2 \left(\frac{1}{Q_3}\right) + \left(\frac{1}{Q_{23}}\right) \rho/2 f\left(\frac{L_{23}}{D}\right) (V_{23})^2} = 0$$

or that

$$\frac{P_1 - P_{2,i}}{\left(\frac{V_1}{k}\right)^2 \rho/2 \left(\frac{1}{Q_1}\right) + \left(\frac{1}{Q_{12}}\right) \rho/2 f\left(\frac{L_{12}}{D}\right) (V_{12})^2} + \frac{\rho/2 V_2 A_d + \dots}{\left(\frac{V_3}{k}\right)^2 \rho/2 \left(\frac{1}{Q_3}\right) + \left(\frac{1}{Q_{23}}\right) \rho/2 f\left(\frac{L_{23}}{D}\right) (V_{23})^2} = 0 \quad [\text{A22}]$$

Recall that it is desirable to obtain $P_{3,i} = f(V_1, V_2, V_3 \text{ etc.})$ with no pressure terms, thus it is necessary to recall that the numerators of [A22] can simply be represented by terms from [A11] and [A12]. Therefore, it is possible to further substitute variables into [A22] to obtain the following:

$$\frac{\left(\frac{\rho}{2}\right)f\left(\frac{L_{12}}{D}\right)(V_{12})^2 + \left(\frac{V_1}{k}\right)^2 \frac{\rho}{2}}{\left(\frac{V_1}{k}\right)^2 \frac{\rho}{2} \left(\frac{1}{Q_1}\right) + \left(\frac{1}{Q_{12}}\right) \frac{\rho}{2} f\left(\frac{L_{12}}{D}\right)(V_{12})^2} + \frac{\rho}{2V_2 A_d} + \dots$$

$$\frac{P_3 - P_{2,i} - \left(\frac{V_3}{k}\right)^2 \frac{\rho}{2}}{\left(\frac{V_3}{k}\right)^2 \frac{\rho}{2} \left(\frac{1}{Q_3}\right) + \left(\frac{1}{Q_{23}}\right) \frac{\rho}{2} f\left(\frac{L_{23}}{D}\right)(V_{23})^2} = 0 \quad [\text{A23}]$$

Now, there are a number of terms that cancel out, $(\rho/2)$ for instance, and when the area terms are further substituted into [A23] it is possible to obtain, with some algebra, the following relationship. It is also useful to recall that the flow within the duct is laminar, thus the friction factor (f) can be described by the following:

$$f = f_{\text{LAMINAR}} = \frac{64}{\text{Re}_D} = 64 \left(\frac{\pi \mu D}{4 \rho Q} \right) = \frac{16 \pi \mu D}{\rho Q} \quad [\text{A24}]$$

$$P_{3,i} = P_2 - \frac{\rho}{2} \left[\frac{V_2}{k} \right]^2 + \frac{\rho}{2} \left[\frac{V_3}{k} \right]^2 - \frac{\rho}{2} \left[V_2 \frac{\pi}{4} d^2 + \frac{\frac{16 \pi \mu D}{\rho Q_{12}} \left(\frac{L_{12}}{D} \right) (V_{12})^2 + \left[\frac{V_1}{k} \right]^2}{\left(\frac{1}{Q_1} \right) \frac{16 \pi \mu D}{\rho Q_{12}} \left(\frac{L_{12}}{D} \right) (V_{12})^2 + \left(\frac{1}{Q_1} \right) \left[\frac{V_1}{k} \right]^2} \right] \times \dots$$

$$\left[\frac{1}{Q_{23}} \frac{16 \pi \mu D}{\rho Q_{23}} \left(\frac{L_{23}}{D} \right) (V_{23})^2 + \frac{1}{Q_3} \left[\frac{V_3}{k} \right]^2 \right] \quad [\text{A25}]$$

Now it is possible to get rid of the Q terms by subbing in the appropriate relationships for velocity and area, as shown below. Note that the diameter term will be either d or D in this case, depending on whether the flowrate refers to the velocity at a port (d) or within the sensor (D).

$$Q = VA = V \frac{\pi}{4} (\text{diameter})^2 \quad [\text{A26}]$$

Thus, by subbing [A26] into [A25] with [A24] it is possible to further reduce the relation to achieve the following:

$$P_v = P_2 - \rho/2 \left[\frac{V_2}{k} \right]^2 + \rho/2 \left[\frac{V_3}{k} \right]^2 - \rho/2 \left[V_2 \frac{\pi}{4} d^2 + \frac{\frac{16\pi\mu D}{\rho Q_{12}} \left(\frac{L_{12}}{D} \right) (V_{12})^2 + \left[\frac{V_1}{k} \right]^2}{\left(\frac{4}{\pi D^2} \right) \frac{16\pi\mu D}{\rho Q_{12}} \left(\frac{L_{12}}{D} \right) (V_{12}) + \left(\frac{4}{\pi D^2} \right) \left[\frac{V_1}{k} \right]^2} \right] \times \dots$$

$$\left[\left(\frac{4}{\pi D^2} \right) \frac{16\pi\mu D}{\rho Q_{23}} \left(\frac{L_{23}}{D} \right) (V_{23}) + \frac{4}{\pi D^2} \left(\frac{V_3}{k} \right)^2 \right]$$

[A27]

The relationship provided in [A25] represents the conclusion of this analysis that was passed over in the body of the thesis. The final relationship used to describe this system, which is provided as equation [29] in Section 3.7.1.2, was obtained by considering a simple order-of-magnitude analysis. Where $d < D$ for all VAV airflow sensors considered, then it can be concluded that $d^2 \ll D^2$ thus its is possible to neglect all of the d^2 terms in the numerators and all of the D^2 terms in the denominators of [A27].

Where:

$$d^2 \ll 1$$

$$\frac{1}{D^2} \text{ or } \frac{1}{D^3} \ll 1$$

Then [A27] can be further reduced to:

$$P_T = P_{3,i} = P_2 - \frac{\rho}{2k^2} \left[\left(\frac{V_3}{V_1} \right) (V_1)^2 + (V_2)^2 - (V_3)^2 \right] - \frac{\rho}{2} \left(\frac{16\pi\mu D}{\rho Q_{12}} \right) \frac{L_{12}}{D} \left(\frac{V_3}{V_1} \right) V_{12}^2 \quad [A28]$$

This is the exact form presented in the main body of the thesis. Note that the method used here directly follows the technique used in the simplistic, 2 hole case, which was presented and discussed directly within the thesis.

2) Sample Calculations for the VAV airflow sensor Model

It was shown in the main body of the thesis that VAV airflow sensor response can be described with the following equation when used with the simplistic, 2 hole case (the calculations to justify the fluid mechanics for the 2 hole case are provide directly in [46], Section 3.7.3):

$$V_{VAV} = \left[V_1^2 + \frac{(V_1)^2 - (V_2)^2}{2} - C_P (U_C)^2 \right]^{1/2} \quad [A29]$$

As a side note: in a similar manner, the equation used to model the response of the 3-hole case would simply involve substituting the P_T term from [A27] into:

$$V_{VAV} = \left(\frac{2\Delta P}{\rho} \right)^{1/2} = \left(\frac{2(P_T - P_S)}{\rho} \right)^{1/2} \quad [A30]$$

where the static pressure term (PS) is simply provided by:

$$C_P = \frac{\text{Static Pressure}}{\text{Dynamic Pressure}} = \frac{P_S}{1/2 \rho U_\infty^2} \quad [A31]$$

For the purposes of evaluating the relative importance of each term, it is more beneficial to use the results for the 2-hole case. The goal is to determine the amplification coefficient (C) for the 2-hole model when it is used to describe a situation that is quite similar to the 40D benchmark tests used to provide the true response of the VAV flow sensors. A turbulent case is represented graphically in Figure A3, on the following page.

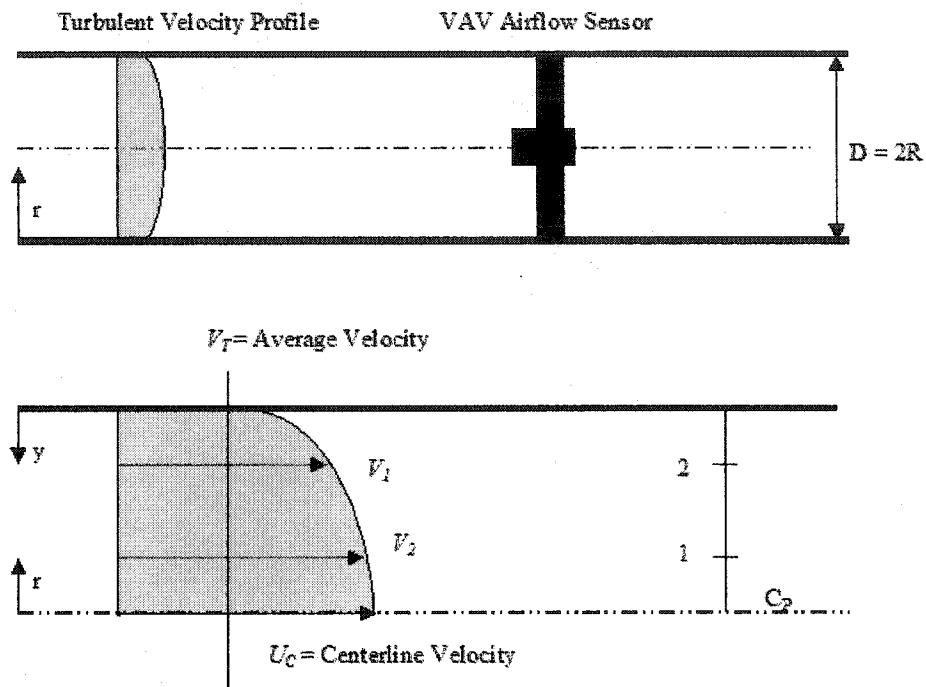


Figure A3: Simple representation of an exaggerated (logarithmic) turbulent velocity profile within a circular duct. The black shape in the top duct is meant to represent a VAV airflow sensor, where 2 total pressure ports are located along the front (at 1 and 2) and the static pressure signal is achieved in the wake region at the center (behind the sensor) using the centerline velocity (U_C).

It is first necessary to consider a likely case for a known VAV airflow sensor to carry out some sample calculations. For that reason, let the diameter of the duct equal 0.203 m (8") and let the air have standard properties at 20°C. Thus for this problem, let $\rho = 1.2 \text{ kg/m}^3$ and $\nu = 1.5 \cdot 10^{-5} \text{ m}^2/\text{s}$. In addition, for this simplistic case let the 2 total pressure ports (located at 1 and 2, respectively) be equally spaced along the duct. Therefore, let there be $R/3$ distance (or 0.068m) between the centerline to 1, 1 to 2 and 2 to the duct edge.

It is possible to use the logarithmic law to determine the velocity profile³⁷ as a function of the radius (r) of the duct, as shown in Figure A3. Note that [A32] is a common approximation of a regular turbulent velocity profile in a circular duct.

$$\frac{u(r)}{u^*} = \frac{1}{\kappa} \ln \frac{(R-r)u^*}{\nu} + B \quad [\text{A32}]$$

The constants in [A32] are $\kappa = 0.41$ and $B = 5.0$ for this simple case, and the u^* term can be determined with [A33].

³⁷ Frank White, "Fluid Mechanics" 4th Edition, McGraw-Hill, page 344-346

$$\frac{V_T}{u^*} = \sqrt{\frac{8}{f}} \quad [A33]$$

The final step needed to predict the response of this VAV airflow sensor is to specify both the average velocity (V_T) and pressure coefficient (C_p) for the case. However, since it is desirable to evaluate the response, namely the amplification (C), which results from varying V_T and C_p it is beneficial to leave these functions open.

Therefore, the response is first obtained by evaluating the Reynolds number based on diameter (d) and the true average velocity (V_T), as provided below.

$$\text{Re}_D = \frac{V_T D}{\nu} \quad [A34]$$

It is then possible to estimate the friction factor (f) for the problem with the Blasius Approximation³⁸, which is summarized below in [A35].

$$f = \frac{0.316}{\text{Re}_D^{0.25}} \quad [A35]$$

In this manner, the u^* term can be determined using [A33] and then it is possible to determine the velocity profile at any point along the duct radius (r) using [A32]. The velocity at both locations 1 and 2 can be determined in this manner and the centerline velocity (U_C) can be determined using the following relationship, [A36], where the friction factor (f) comes from [A35]:

$$U_C = V_T (1 + \frac{4}{3} \sqrt{f}) \quad [A36]$$

In this manner the velocity signal from the VAV airflow sensor (V_{VAV}) can be estimated for any sized circular duct that is experiencing turbulent flow conditions using [A29] – recall that this is for the 2 port case. For our purposes, it was beneficial to leave the pressure coefficients (C_p) and true average velocity (V_T) as variables and to evaluate their effect on the amplification coefficient (C) for the airflow sensor.

Using this procedure the graph presented as Figure 12 in the main body was created, the theoretical numbers used to create this Figure are presented below in Table A1 for a typical average flow range (V_T) of 0.1 m/s to 8 m/s (which match the range of the 8" VAV terminals considered in the laboratory experiments (limited, in this case, to the range of $4000 < \text{Re}_D < 10^5$ corresponds to the Blasius approximation we have chosen to use). As well as

³⁸ Ibid, Note that the Blasius approximation is only accurate within the range of $4000 < \text{Re}_D < 10^5$

for a pressure coefficient (C_p) that varies between -0.5 to -1.7 (which match the range of predicted C_p values from the literature review) that were considered with arbitrary values of $C_p = -1.7, -1.3, -1.0, -0.8$ and -0.5 .

This concludes the sample calculations for the theoretical VAV airflow sensor response.

Table A1: Summary of VAV Airflow Sensor Response (C) in relation to V_T and C_p^*

Average Velocity	Reynolds Number	Friction Factor				Centerline Velocity		Amp. Coeff.
V_T	Re_D	f	u^*	V_1 (at $r = R/3$)	V_2 (at $r = 2R/3$)	U_C	C_p	C
(m/s)	(dim)	(dim)	(m/s)	(m/s)	(m/s)	(m/s)	(dim)	(dim)
0.10	1,355	0.05	0.01	0.11	0.10	0.13	-1.3	1.89
0.50	6,773	0.03	0.03	0.57	0.51	0.62	-1.3	1.85
1.00	13,547	0.03	0.06	1.13	1.03	1.23	-1.3	1.83
1.50	20,320	0.03	0.09	1.69	1.54	1.83	-1.3	1.81
2.00	27,093	0.02	0.11	2.24	2.05	2.42	-1.3	1.80
2.50	33,867	0.02	0.13	2.78	2.56	3.01	-1.3	1.79
3.00	40,640	0.02	0.16	3.33	3.06	3.60	-1.3	1.79
3.50	47,413	0.02	0.18	3.87	3.56	4.18	-1.3	1.78
4.00	54,187	0.02	0.20	4.40	4.06	4.77	-1.3	1.77
4.50	60,960	0.02	0.23	4.94	4.56	5.35	-1.3	1.77
5.00	67,733	0.02	0.25	5.47	5.05	5.93	-1.3	1.77
5.50	74,507	0.02	0.27	6.00	5.55	6.51	-1.3	1.76
6.00	81,280	0.02	0.29	6.53	6.04	7.09	-1.3	1.76
6.50	88,053	0.02	0.31	7.06	6.53	7.67	-1.3	1.75
7.00	94,827	0.02	0.33	7.58	7.02	8.25	-1.3	1.75
7.50	101,600	0.02	0.35	8.11	7.51	8.83	-1.3	1.75
8.00	108,373	0.02	0.37	8.63	8.00	9.41	-1.3	1.74
0.10	1,355	0.05	0.01	0.11	0.10	0.13	-1	1.75
0.50	6,773	0.03	0.03	0.57	0.51	0.62	-1	1.72
1.00	13,547	0.03	0.06	1.13	1.03	1.23	-1	1.70
1.50	20,320	0.03	0.09	1.69	1.54	1.83	-1	1.69
2.00	27,093	0.02	0.11	2.24	2.05	2.42	-1	1.68
2.50	33,867	0.02	0.13	2.78	2.56	3.01	-1	1.67
3.00	40,640	0.02	0.16	3.33	3.06	3.60	-1	1.66
3.50	47,413	0.02	0.18	3.87	3.56	4.18	-1	1.66
4.00	54,187	0.02	0.20	4.40	4.06	4.77	-1	1.65
4.50	60,960	0.02	0.23	4.94	4.56	5.35	-1	1.65
5.00	67,733	0.02	0.25	5.47	5.05	5.93	-1	1.64
5.50	74,507	0.02	0.27	6.00	5.55	6.51	-1	1.64
6.00	81,280	0.02	0.29	6.53	6.04	7.09	-1	1.63
6.50	88,053	0.02	0.31	7.06	6.53	7.67	-1	1.63

7.00	94,827	0.02	0.33	7.58	7.02	8.25	-1	1.63
7.50	101,600	0.02	0.35	8.11	7.51	8.83	-1	1.62
8.00	108,373	0.02	0.37	8.63	8.00	9.41	-1	1.62
0.10	1,355	0.05	0.01	0.11	0.10	0.13	-0.8	1.65
0.50	6,773	0.03	0.03	0.57	0.51	0.62	-0.8	1.63
1.00	13,547	0.03	0.06	1.13	1.03	1.23	-0.8	1.61
1.50	20,320	0.03	0.09	1.69	1.54	1.83	-0.8	1.60
2.00	27,093	0.02	0.11	2.24	2.05	2.42	-0.8	1.59
2.50	33,867	0.02	0.13	2.78	2.56	3.01	-0.8	1.58
3.00	40,640	0.02	0.16	3.33	3.06	3.60	-0.8	1.57
3.50	47,413	0.02	0.18	3.87	3.56	4.18	-0.8	1.57
4.00	54,187	0.02	0.20	4.40	4.06	4.77	-0.8	1.56
4.50	60,960	0.02	0.23	4.94	4.56	5.35	-0.8	1.56
5.00	67,733	0.02	0.25	5.47	5.05	5.93	-0.8	1.55
5.50	74,507	0.02	0.27	6.00	5.55	6.51	-0.8	1.55
6.00	81,280	0.02	0.29	6.53	6.04	7.09	-0.8	1.55
6.50	88,053	0.02	0.31	7.06	6.53	7.67	-0.8	1.54
7.00	94,827	0.02	0.33	7.58	7.02	8.25	-0.8	1.54
7.50	101,600	0.02	0.35	8.11	7.51	8.83	-0.8	1.54
8.00	108,373	0.02	0.37	8.63	8.00	9.41	-0.8	1.53
0.10	1,355	0.05	0.01	0.11	0.10	0.13	-0.5	1.49
0.50	6,773	0.03	0.03	0.57	0.51	0.62	-0.5	1.48
1.00	13,547	0.03	0.06	1.13	1.03	1.23	-0.5	1.46
1.50	20,320	0.03	0.09	1.69	1.54	1.83	-0.5	1.45
2.00	27,093	0.02	0.11	2.24	2.05	2.42	-0.5	1.44
2.50	33,867	0.02	0.13	2.78	2.56	3.01	-0.5	1.44
3.00	40,640	0.02	0.16	3.33	3.06	3.60	-0.5	1.43
3.50	47,413	0.02	0.18	3.87	3.56	4.18	-0.5	1.42
4.00	54,187	0.02	0.20	4.40	4.06	4.77	-0.5	1.42
4.50	60,960	0.02	0.23	4.94	4.56	5.35	-0.5	1.41
5.00	67,733	0.02	0.25	5.47	5.05	5.93	-0.5	1.41
5.50	74,507	0.02	0.27	6.00	5.55	6.51	-0.5	1.41
6.00	81,280	0.02	0.29	6.53	6.04	7.09	-0.5	1.40
6.50	88,053	0.02	0.31	7.06	6.53	7.67	-0.5	1.40
7.00	94,827	0.02	0.33	7.58	7.02	8.25	-0.5	1.40
7.50	101,600	0.02	0.35	8.11	7.51	8.83	-0.5	1.39
8.00	108,373	0.02	0.37	8.63	8.00	9.41	-0.5	1.39
0.10	1,355	0.05	0.01	0.11	0.10	0.13	-1.7	2.07
0.50	6,773	0.03	0.03	0.57	0.51	0.62	-1.7	2.02
1.00	13,547	0.03	0.06	1.13	1.03	1.23	-1.7	1.99
1.50	20,320	0.03	0.09	1.69	1.54	1.83	-1.7	1.97
2.00	27,093	0.02	0.11	2.24	2.05	2.42	-1.7	1.96
2.50	33,867	0.02	0.13	2.78	2.56	3.01	-1.7	1.95
3.00	40,640	0.02	0.16	3.33	3.06	3.60	-1.7	1.94
3.50	47,413	0.02	0.18	3.87	3.56	4.18	-1.7	1.93

4.00	54,187	0.02	0.20	4.40	4.06	4.77	-1.7	1.93
4.50	60,960	0.02	0.23	4.94	4.56	5.35	-1.7	1.92
5.00	67,733	0.02	0.25	5.47	5.05	5.93	-1.7	1.92
5.50	74,507	0.02	0.27	6.00	5.55	6.51	-1.7	1.91
6.00	81,280	0.02	0.29	6.53	6.04	7.09	-1.7	1.91
6.50	88,053	0.02	0.31	7.06	6.53	7.67	-1.7	1.91
7.00	94,827	0.02	0.33	7.58	7.02	8.25	-1.7	1.90
7.50	101,600	0.02	0.35	8.11	7.51	8.83	-1.7	1.90
8.00	108,373	0.02	0.37	8.63	8.00	9.41	-1.7	1.90

*Note: In this case the numbers correspond to airflow at 20°C, a logarithmic turbulent velocity profile and 2 total pressure ports spaced evenly in a 8" circular duct where the true average velocity (V_T) and the pressure coefficient (C_p) are the control variables (both highlighted in grey) and the amplification coefficient (C) is the dependent variable.

Appendix B

Contents: Sample Calculations and Results of Field Testing

1)	DDC system accuracy Tables	130
2)	Degree-Day Analysis	142

1) DDC System Accuracy Tables

The methodology for the DDC accuracy analysis has already been presented for the Yellowhead Regional Library (recall Section 5.2), similar results from the other two test facilities (the Timms Center and Cross Cancer Institute) are included here. The results from all three facilities were quite similar, thus only the results of from the Yellowhead Regional Library were directly discussed, in the interest of brevity.

Table B1: BC Calibrations taken from the Timms Center, note that Terminal 3, 12, 27 and 42 were not available

Tag #	Min (L/s)	Max (L/s)	BC				Exist. F	New F
			Measured 1 (l/s)	Measured 2 (l/s)	Indicated 1 (l/s)	Indicated 2 (l/s)		
1	100	225	316	177	263	145	18.7	12.6
2	110	280	127	281	102	236	18.7	15.58
3	110	250						
4	150	325	158	260	139	251	17.8	19.3
5	0	300	296	272	275	247		
6	50	115	122	56	110	50		
7	80	180	479	124	233	76	24.7	7.46
8	160	350	417	152	406	157	11	11
9	350	800	1037	380	970	385	15	14.24
10	110	240	282	110	247	102	18.7	16.92
11	110	240	252	95	242	100	18.7	18.7
12	350	800						
13	190	420	486	237	420	184	17.8	11.96
14	190	420	218	96	166	137		
15	200	450	279	425	219	381	17.8	15.98
16	130	300	137	365	133	317	17.8	16.35
17	45	100	143	44	130	45	19.7	18.44
18	65	150	60	227	58	205	18.7	16.34
19	175	400	191	409	194	457	17.8	14.26
20	30	70	101	35	79	32	19.7	14.34
21	500	500	626	0	534	0	16.7	12.14
22	500	500	614	0	729	0	15	21.14
23	760	760	618	0	535	0	16.7	12.52
24	760	760	736	0	901	0	15	10.01
25	450	450	465	0	496	0	17.8	20.23
26	0	1700						
27	50	115	51	119	53	118	19.7	19.7
28	175	400	148	338	169	353	12	13.23
29	175	400	464	187	409	175	16.8	13.59
30	220	440	511	228	445	210	17.8	14.31
31	220	510	690	768	580	663	16.17	12.14
32	110	250	81		100			
33	45	100	135	49	121	46	19.7	16.48
34	45	100	244	104	210	88	18.7	13.64
35	90	210	377	917	337	834	15	12.18
36	370	640	114	38	104	38	19.7	16.4
37	35	80	37	107	34	93	19.7	15.75
38	35	80	271	117	280	119	18.7	18.7
39	35	80	85	43	82	58	19.7	18.25
40	175	400	478	195	452	170	17.8	14.72
41	30	50	56	0	50	0		
42	130	300						
43	130	300	256	135	302	203	17.8	22.5
44	1000	1000	1242	0	1057	0	20	14.48
45	1000	1000	1175	0	1064	0	20	16.42
46	1000	1000	1249	0	1225	0	20	15.17
47	1000	1000	1284	0	1073	0	20	13.98
48	310	700	800	387	746	375	15	13.57
49	440	1000	1254	468	1008	468	20	20
50	440	1000	1231	548	973	443	20	12.78
51	45	100	128.6	47	124	43	21.7	19.16

Table B2: AC Calibrations taken from the Timms Center

AC						
Measured1 N	Measured 2 n	Indicated1 N	Indicated 2 N	Tstat Ind	Tstat Meas	
108	320	109	314	19.9	19.9	
108	262	100	278	23.8	22	
203	315	194	350	19.5	20.7	
				32.8	31.5	
47	144	56	152	24.8	23.6	
195	428	189	471	21.4	21.4	
				21.4	20.5	
1019	0	998	0	19.4	19.8	
110	260	107	284 X			
			X		X	
				22.7	22.2	
225	510	228	474	22.2	21.8	
				22.6	21.8	
101	386	118	387	21.4	22.1	
355	150	327	150 X		X	
53	113	50	128	22.6	24.9	
66	223	70	227	21		
241	456	255	458	21.7	21.1	
32	92	31	101	22.1	21.2	
614	0	615	0	20.7	20	
666	0	619	0 X		X	
622	0	617	0 X		X	
892	0	841	0 X		X	
455	0	466	0 X		X	
			X		X	
			X		X	
342	177	341	166	23.1	23.2	
164	445	173	459	21.5	20.4	
216	496	222	519	20.7	20.6	
449	687	454	695 N		N	
				21.2	20.7	
43	131	43	134	20.1	19.9	
237	109	235	107	20.6	20.4	
383	925	380	917	21.6	20.4	
82	42	80	36	21.7	21.3	
44	105	44	109.5	21.3	21	
				22.6	21.9	
28	112	27	113 X		X	
182	500	181	478	21.1	20	
				21.7	21.5	
137	297	136	322	21.7	21.1	
1372	0	1278	0 X		X	
1251	0	1188	0 X		X	
1249	0	1225	0 X		X	
1272	0	1235	0 X		X	
362	707	388	751	23.1	23.3	
992	842	986	851	22.8	23	
1231	553	1223	572 X		X	
128.6	50	132	51	21.1	20.9	

Table B3: AAC Calibrations taken from the Timms Center

AAC							
Tag #	Min	Max	Measured 1 (l/s)	Measured 2 (l/s)	Indicated 1 (l/s)	Indicated 2 (l/s)	F coef
1	100	225	114	214	117	219	12.6
2	110	280	114	203	114	206	16
5	0	300	299	0	280	0	18.7
7	80	180	106	117	98	176	7.46
8	160	350	154	358	159	361	11
9	350	800	348	836	370	830	14.24
12	350	800	359	870	364	827	15
13	190	420	181	401	200	437	11.96
16	130	300	129	317	134	308	16.35
30	200	440	176	440	203	440	14.3
31	220	510	205	539	226	520	12.14
32	45	100	50	121	45	95	19.7
33	45	100	48	105	46	104	
34	90	210	96	207	95	218	13.64
35	370	840	355	858	352	840	12.18
36	35	80	24	72	35	78	16.4
38	110	250	107	232	115	256	18.7
40	175	400	183	411	181	409	14.72
41	30	50	24.6	54	21	53	19.7
42	130	300	62	294	121	299	17.8
43	130	300	136	298	144	375	22.5
44	1200	1200	1160	0	1143	0	14.48
45	1200	1200	1228	0	1288	0	16.42
46	1200	1200	1181	0	1161	0	15.17
47	1200	1200	1121	0	1166	0	13.98
49	440	1000	493	985	474	985	20
50	440	1000	422	1060	450	1017	12.78
51	45	100	51	100	48	96	19.6

Table B4: Linear BC, AC and AAC Calibration Equations for the Timms Center

BC		AC		AAC	
Qind = A (Qmeas) + B		Qind = A (Qmeas) + B		Qind = A (Qmeas) + B	
A	B	A	B	A	B
(slope)	(y intercept)	(slope)	(y intercept)	(slope)	(y intercept)
0.85	-5.26	0.97	4.57	1.02	0.72
0.87	-8.51	1.16	-24.83	1.03	-3.84
NO DATA	NO DATA	NO DATA	NO DATA	NO DATA	NO DATA
1.10	-34.49	1.39	-88.75	NO DATA	NO DATA
1.17	-70.33	1.17	-70.33	0.94	0.00
0.91	-0.91	0.99	9.48	NO DATA	NO DATA
0.44	21.16	1.21	-47.01	7.09	-653.64
0.94	14.18	0.94	14.18	0.99	6.51
0.89	46.64	0.98	0.00	0.94	41.97
0.84	9.27	1.18	-22.80	NO DATA	NO DATA
0.90	14.08	0.90	14.08	NO DATA	NO DATA
NO DATA	NO DATA	NO DATA	NO DATA	0.91	38.72
0.95	-40.63	0.86	33.79	1.08	5.01
0.24	114.18	0.24	114.18	NO DATA	NO DATA
1.11	-90.58	0.94	22.67	NO DATA	NO DATA
0.81	22.44	0.86	20.49	0.93	14.61
0.86	7.22	1.30	-18.90	NO DATA	NO DATA
0.88	5.19	1.00	4.00	NO DATA	NO DATA
1.21	-36.43	0.94	27.45	NO DATA	NO DATA
0.71	7.08	1.17	-6.33	NO DATA	NO DATA
0.85	0.00	1.00	0.00	NO DATA	NO DATA
1.19	0.00	0.93	0.00	NO DATA	NO DATA
0.87	0.00	0.99	0.00	NO DATA	NO DATA
1.22	0.00	0.94	0.00	NO DATA	NO DATA
1.07	0.00	1.02	0.00	NO DATA	NO DATA
NO DATA	NO DATA	NO DATA	NO DATA	NO DATA	NO DATA
0.96	4.25	0.96	4.25	NO DATA	NO DATA
0.97	25.67	1.06	-21.73	NO DATA	NO DATA
0.84	17.03	1.02	6.08	NO DATA	NO DATA
0.83	20.67	1.06	-7.11	0.90	45.00
1.06	-154.23	1.01	-0.66	0.88	45.55
NO DATA	NO DATA	NO DATA	NO DATA	0.70	9.79
0.87	3.27	1.03	-1.47	1.02	-2.84
0.87	-2.63	1.00	-2.00	1.11	-11.38
0.92	-9.98	0.99	0.53	0.97	7.59
0.87	5.00	1.10	-10.20	0.90	13.50
0.84	2.81	1.07	-3.25	NO DATA	NO DATA
1.05	-3.32	1.05	-3.32	1.13	-5.70
0.57	33.43	1.02	-1.67	NO DATA	NO DATA
1.00	-24.31	0.93	11.02	1.00	-2.00
0.89	0.00	0.89	0.00	1.09	-5.78
NO DATA	NO DATA	NO DATA	NO DATA	0.77	73.43
0.82	92.55	1.16	-23.26	1.43	-49.93
0.85	0.00	0.93	0.00	0.99	0.00
0.91	0.00	0.95	0.00	1.05	0.00
0.98	0.00	0.98	0.00	0.98	0.00
0.84	0.00	0.97	0.00	1.04	0.00
0.90	27.36	1.05	7.11	NO DATA	NO DATA
0.69	146.47	0.90	93.20	1.04	-38.04
0.78	17.76	0.96	41.02	0.89	74.96
0.99	-3.65	1.03	-0.53	0.98	-1.96

Table B5: Simplified DDC Accuracy analysis for BC, AC and AAC, note that the midpoint is assumed in each case thus the values will not be a true representation of system behavior – only an indication.

Mid Value of RANGE for typical Point MIN + (0.5)(MAX-MIN) (L/s)	BC ACTUAL Qm = (Qi - B)/A (L/s)	BC ERROR ABS(Mid-Act)/Act (%)	AC ACTUAL Qm = (Qi - B)/A (L/s)	AC ERROR ABS(Mid-Act)/Act (%)	AAC ACTUAL Qm = (Qi - B)/A (L/s)	ACC ERROR ABS(Mid-Act)/Act (%)
162.50	197.61	-17.8%	163.33	-0.5%	158.61	2.5%
195.00	233.88	-16.6%	190.19	2.5%	192.36	1.4%
180.00	NO DATA	NO DATA	NO DATA	NO DATA	NO DATA	NO DATA
237.50	247.71	-4.1%	234.23	1.4%	NO DATA	NO DATA
150.00	188.86	-20.6%	188.86	-20.6%	160.18	-6.4%
82.50	91.75	-10.1%	73.78	11.8%	NO DATA	NO DATA
130.00	246.10	-47.2%	146.25	-11.1%	110.51	17.6%
255.00	256.30	-0.5%	256.30	-0.5%	250.95	1.6%
575.00	593.38	-3.1%	587.10	-2.1%	565.48	1.7%
175.00	196.59	-11.0%	167.63	4.4%	NO DATA	NO DATA
175.00	177.92	-1.6%	177.92	-1.6%	NO DATA	NO DATA
575.00	NO DATA	NO DATA	NO DATA	NO DATA	591.87	-2.9%
305.00	364.67	-16.4%	314.21	-2.9%	278.47	9.5%
305.00	802.76	-62.0%	802.76	-62.0%	NO DATA	NO DATA
325.00	374.53	-13.2%	320.31	1.5%	NO DATA	NO DATA
215.00	238.61	-9.9%	225.28	-4.6%	216.52	-0.7%
72.50	76.03	-4.6%	70.31	3.1%	NO DATA	NO DATA
107.50	116.23	-7.5%	103.50	3.9%	NO DATA	NO DATA
287.50	268.50	7.1%	275.42	4.4%	NO DATA	NO DATA
50.00	60.28	-17.0%	48.29	3.6%	NO DATA	NO DATA
500.00	586.14	-14.7%	499.19	0.2%	NO DATA	NO DATA
500.00	421.12	18.7%	537.96	-7.1%	NO DATA	NO DATA
760.00	877.91	-13.4%	766.16	-0.8%	NO DATA	NO DATA
760.00	620.82	22.4%	806.09	-5.7%	NO DATA	NO DATA
450.00	421.88	6.7%	439.38	2.4%	NO DATA	NO DATA
850.00	NO DATA	NO DATA	NO DATA	NO DATA	NO DATA	NO DATA
82.50	81.86	0.8%	81.86	0.8%	NO DATA	NO DATA
287.50	270.36	6.3%	291.56	-1.4%	NO DATA	NO DATA
287.50	320.17	-10.2%	276.50	4.0%	NO DATA	NO DATA
330.00	372.51	-11.4%	317.82	3.8%	317.47	3.9%
365.00	487.95	-25.2%	361.11	1.1%	362.91	0.6%
180.00	NO DATA	NO DATA	NO DATA	NO DATA	241.70	-25.5%
72.50	79.39	-8.7%	71.53	1.4%	74.04	-2.1%
72.50	86.21	-15.9%	74.50	-2.7%	75.70	-4.2%
150.00	173.82	-13.7%	150.86	-0.6%	146.79	2.2%
505.00	575.76	-12.3%	468.36	7.8%	548.65	-8.0%
57.50	64.88	-11.4%	56.57	1.6%	NO DATA	NO DATA
57.50	58.17	-1.2%	58.17	-1.2%	56.02	2.6%
57.50	42.13	36.5%	57.79	-0.5%	NO DATA	NO DATA
287.50	312.92	-8.1%	296.03	-2.9%	289.50	-0.7%
40.00	44.80	-10.7%	44.80	-10.7%	42.06	-4.9%
215.00	NO DATA	NO DATA	NO DATA	NO DATA	184.52	16.5%
215.00	149.67	43.7%	204.96	4.9%	185.79	15.7%
1000.00	1175.02	-14.9%	1073.55	-6.9%	1014.87	-1.5%
1000.00	1104.32	-9.4%	1053.03	-5.0%	953.42	4.9%
1000.00	1019.59	-1.9%	1019.59	-1.9%	1017.23	-1.7%
1000.00	1196.64	-16.4%	1029.96	-2.9%	961.41	4.0%
505.00	531.72	-5.0%	473.20	6.7%	NO DATA	NO DATA
720.00	834.80	-13.8%	696.44	3.4%	729.85	-1.4%
720.00	904.96	-20.4%	707.14	1.8%	725.81	-0.8%
72.50	76.72	-5.5%	70.86	2.3%	76.01	-4.6%

Table B6: Results from DDC Accuracy analysis for AC and AAC Trends relative to BC, note that the midpoint is assumed in each case thus the values will not be a true representation of system behavior – only an indication. These percentages refer to the Percentage improvement due to commissioning from BC to AC and from BC to AAC, as expected these values are generally quite similar

IMPROVEMENT	
AC	AAC
ABS(BC) - ABS(AC) ERROR (%)	ABS(BC) - ABS(AAC) ERROR (%)
17.3%	15.3%
14.1%	15.3%
NO DATA	NO DATA
2.7%	NO DATA
0.0%	14.2%
-1.7%	NO DATA
36.1%	29.5%
0.0%	-1.1%
1.0%	1.4%
6.6%	NO DATA
0.0%	NO DATA
NO DATA	NO DATA
13.4%	6.8%
0.0%	NO DATA
11.8%	NO DATA
5.3%	9.2%
1.5%	NO DATA
3.6%	NO DATA
2.7%	NO DATA
13.5%	NO DATA
14.5%	NO DATA
11.7%	NO DATA
12.6%	NO DATA
16.7%	NO DATA
4.2%	NO DATA
NO DATA	NO DATA
0.0%	NO DATA
4.9%	NO DATA
6.2%	NO DATA
7.6%	7.5%
24.1%	24.6%
NO DATA	NO DATA
7.3%	6.6%
13.2%	11.7%
13.1%	11.5%
4.5%	4.3%
9.7%	NO DATA
0.0%	-1.5%
36.0%	NO DATA
5.2%	7.4%
0.0%	5.8%
NO DATA	NO DATA
38.8%	27.9%
8.0%	13.4%
4.4%	4.6%
0.0%	0.2%
13.5%	12.4%
-1.7%	NO DATA
10.4%	12.4%
18.6%	19.6%
3.2%	0.9%

Table B6: BC Calibrations taken from the Cross Cancer Institute

Tag #	Min (L/s)	Max (L/s)	BC						Exist. F	New F
			Measured 1 (l/s)	Measured 2 (l/s)	Measured 3 (l/s)	Indicated 1 (l/s)	Indicated 2 (l/s)	Indicated 3 (l/s)		
71	241	505	248	373	518	241	373	499	0.86	0.88
72	244	489	235	360	489	240	366	485	0.82	0.81
73	180	365	188	273	345	183	270	351	0.8	0.82
74	81	163	81	122	161	80	121	163	0.8	0.8
75	244	489	470	411	0	391	398	0	0.84	0.88
76	210	480	219	439	0	228	456	0	0.85	0.82
77	0	603	568	701	0	490	600	0	0.78	0.91
78	228	452	234	345	465	228	338	452	0.82	0.84
79	145	290	148	220	294	145	218	290	0.79	0.8
80	0	791	768	0	0	787	0	0	0.8	0.78
81	200	399	199	301	401	195	301	395	0.8	0.82
82	70	145	70	144	0	70	144	0	0.75	0.75
83	80	160	96	188	0	81	160	0	0.65	0.76
86	156	306	158	161	294	147	153	303	0.8	0.8
87	0	663	720	667	0	664	664	0	0.81	0.88
88	153	306	154	304	0	153	310	0	0.75	0.75
89	153	420	165	425	414	150	413	420	0.77	0.81
90	0	473	503	477	0	477	474	0	0.8	0.84
91	0	111	111	114	0	112	114	0	1.1	1.1
92	145	290	144	282	0	140	290	0	0.83	0.81
93	154	305	153	311	315	153	303	305	0.8	0.8
94	156	306	160	311	0	153	306	0	0.8	0.82
1	249	985	266	248	237	249	249	249	0.84	0.9
2	52	985	283	537	1037	249	529	995	0.8	0.83
3	301	1078	270	1042	0	310	1099	0	0.83	0.79
4	0	496	111	230	415	102	212	391	0.76	0.82
5	0	386	360	382	0	354	392	0	0.87	0.89
6	79	862	882	885	0	878	870	0	0.82	0.83
7	40	424	430	0	0	424	0	0	0.58	0.58
8	271	1025	991	0	0	967	0	0	0.91	0.74
9	0	330	273	335	0	270	332	0	0.78	0.78
10	20	356	35	370	199	30	366	193	0.78	0.78
11	30	424	228	231	405	228	232	425	0.82	0.8
12	9	275	154	288	274	143	275	276	0.55	0.58
13	34	425	238	437	0	235	436	0	0.79	0.79
14	21	212	15	135	239	26	120	214	0.73	0.82
15	0	85	69	114	87	51	85	85	0.78	1
16	19	120	76	126	126	70	121	123	0.78	0.81
17	79	615	323	645	619	307	617	614	0.85	0.88
18	47	249	264	255	0	250	247	0	0.78	0.83
19	23	115	63	125	0	60	117	0	0.76	0.76
22	10	283	38	148	280	28	139	284	0.78	0.78
23	85	115	44	86	0	43	85	0	0.94	0.95
24	40	249	61	122	236	60	124	249	0.78	0.76
25	43	211	44	221	212	44	211	211	0.72	0.72
26	45	222	51	238	0	45	220	0	0.71	0.76
27	15	211	91	129	168	109	158	213	0.78	0.64
28	43	211	67	217	209	43	211	211	0.74	0.77
29	19	170	86	172	173	85	170	172	0.71	0.75
30	79	392	81	423	0	77	395	0	0.75	0.8
31	42	211	112	220	0	105	211	0	0.71	0.74

Table B7: AC Calibrations taken from the Cross Cancer Institute

AC							
Measured 1 (l/s)	Measured 2 (l/s)	Measured 3 (l/s)	Indicated 1 (l/s)	Indicated 2 (l/s)	Indicated 3 (l/s)	Tstat Ind	Tstat Meas
0	0	0	0	0	0	21.9	21.6
366	0	0	362	0	0	21.9	22.3
0	0	0	0	0	0	24.1	24.2
0	0	0	0	0	0	23.6	22.3
245	372	486	240	366	480	22.6	22.5
220	445	0	216	452	0	23.4	23.2
590	0	0	604	0	0	23.7	23.6
343	0	0	342	0	0	22.8	22.4
0	0	0	0	0	0	23.2	23.2
750	0	0	748	0	0	22.9	23.3
403	0	0	399	0	0	23.4	23.2
0	0	0	0	0	0	23.1	23.2
161	0	0	160	0	0	23.7	23.1
305	0	0	303	0	0	23	23.2
600	0	0	600	0	0	23.3	23.9
0	0	0	0	0	0	22.6	21.3
155	0	0	150	0	0	22.8	20.3
0	0	0	0	0	0	23	22.7
100	0	0	100	0	0	23.7	24
144	287	0	140	288	0	23.3	23.5
0	0	0	0	0	0	25	25.1
158	311	0	153	306	0	23	23.3
1046	0	0	995	0	0	20.1	21.3
270	1008	0	249	995	0	22.8	22.5
1106	0	0	1099	0	0	23.7	23.3
109	389	0	106	399	0	0	0
0	0	0	0	0	0	22.9	23.7
0	0	0	0	0	0	22.3	22.8
0	0	0	0	0	0	23	23.2
516	0	0	552	0	0	23	23.1
0	0	0	0	0	0	23	21.9
0	0	0	0	0	0	22	21.8
426	0	0	424	0	0	22.5	22.1
0	0	0	0	0	0	24.5	24.7
0	0	0	0	0	0	23.7	23.2
117	216	0	120	214	0	22.2	22.8
54	0	0	52	0	0	23.4	25
77	0	0	73	0	0	23.1	23
0	0	0	0	0	0	24	23.6
247	0	0	249	0	0	23.6	23.2
60	116	0	58	115	0	23.2	23.3
0	0	0	0	0	0	0	0
42	81	0	43	84	0	23.4	22.6
62	121	240	64	125	249	23.4	23.3
0	0	0	0	0	0	22.1	22.3
48	216	0	45	222	0	23.1	23
57	105	147	52	105	150	23	23.3
105	0	0	105	0	0	23.4	23.5
0	0	0	0	0	0	22.6	23.2
81	399	0	79	392	0	22.5	22.8
211	0	0	211	0	0	23.1	23.4

Table B8: AAC Calibrations taken from the Cross Cancer Institute

AAC							
Tag #	Min	Max	Measured 1 (l/s)	Measured 2 (l/s)	Indicated 1 (l/s)	Indicated 2 (l/s)	F coef
71	241	505					
72	244	489	501	1116	492	1130	
73	180	365	380	970	385	981	
74	81	163	172	420	173	436	
75	244	489					
76	210	480	468	964	482	960	
77	0	603	0	1377	0	1429	
78	228	452	497	1061	492	1078	
79	145	290					
80	0	791					
81	200	399					
82	70	145					
83	80	160	187	425	163	336	
86	156	306					
87	0	663					
88	153	306					
89	153	420	348	958	318	889	
90	0	473					
91	0	111	182	264	130	238	
92	145	290					
93	154	305					
94	156	306	349	1001	332	981	
1	249	985	518	3063	505	3075	
2	52	985					
3	301	1078					
4	0	496					
5	0	386	396	823	427	825	
6	79	862					
7	40	424	506	895	499	899	
8	271	1025					
9	0	330					
10	20	356	0	763	0	748	
11	30	424					
12	9	275	312	600	304	586	
13	34	425	472	906	498	900	
14	21	212					
15	0	85					
16	19	120	157	278	141	257	
17	79	615	667	1358	656	1308	
18	47	249					
19	23	115	490	948	500	1008	
22	10	283	453	883	420	835	
23	85	115					
24	40	249					
25	43	211					
26	45	222					
27	15	211	8	369	12	370	
28	43	211					
29	19	170	197	402	196	384	
30	79	392					
31	42	211					

Table B9: Linear BC, AC and AAC Calibration Equations from the Cross Cancer

BC Qind = A (Qmeas) + B		AC Qind = A (Qmeas) + B		AAC Qind = A (Qmeas) + B	
A (slope)	B (y intercept)	A (slope)	B (y intercept)	A (slope)	B (y intercept)
0.95	9.08	NO DATA	NO DATA	NO DATA	NO DATA
0.96	15.22	0.99	0.00	1.04	-27.74
1.07	-19.12	NO DATA	NO DATA	1.01	1.14
1.04	-4.51	NO DATA	NO DATA	1.06	-9.40
0.88	3.95	1.00	-4.12	NO DATA	NO DATA
1.04	0.17	1.02	-2.51	0.96	30.98
0.86	0.43	1.02	0.00	1.04	0.00
0.97	1.97	1.00	0.00	1.04	-24.39
0.99	-1.47	NO DATA	NO DATA	NO DATA	NO DATA
1.02	0.00	1.00	0.00	NO DATA	NO DATA
0.99	-0.41	0.99	0.00	NO DATA	NO DATA
1.00	0.00	NO DATA	NO DATA	NO DATA	NO DATA
0.85	-0.23	0.99	0.00	0.73	27.07
1.14	-31.50	0.99	0.00	NO DATA	NO DATA
0.95	1.93	1.00	0.00	NO DATA	NO DATA
1.02	-1.33	NO DATA	NO DATA	NO DATA	NO DATA
1.04	-21.99	0.97	0.00	0.94	-7.75
0.97	0.59	NO DATA	NO DATA	NO DATA	NO DATA
1.00	0.01	1.00	0.00	1.32	-109.71
1.03	-2.64	1.00	-1.50	NO DATA	NO DATA
0.94	8.66	NO DATA	NO DATA	NO DATA	NO DATA
0.98	-1.43	0.98	-0.81	1.00	-15.39
0.00	249.00	0.95	0.00	1.01	-18.09
0.98	-16.48	0.99	-7.98	NO DATA	NO DATA
1.05	11.57	0.99	0.00	NO DATA	NO DATA
0.95	-4.94	1.03	-2.62	NO DATA	NO DATA
1.01	-0.47	NO DATA	NO DATA	0.93	57.89
0.99	0.02	NO DATA	NO DATA	NO DATA	NO DATA
0.99	0.00	NO DATA	NO DATA	1.03	-21.31
0.98	0.00	1.07	0.00	NO DATA	NO DATA
0.99	-0.06	NO DATA	NO DATA	NO DATA	NO DATA
1.00	-5.61	NO DATA	NO DATA	0.98	0.00
1.11	-25.01	1.00	0.00	NO DATA	NO DATA
1.03	-15.27	NO DATA	NO DATA	0.98	-1.50
1.00	-0.74	NO DATA	NO DATA	0.93	60.80
0.84	11.36	0.99	1.24	NO DATA	NO DATA
0.70	11.04	0.96	0.00	NO DATA	NO DATA
1.04	-9.04	0.95	0.00	0.96	-9.51
0.99	-13.01	NO DATA	NO DATA	0.94	26.65
0.96	0.10	1.01	0.00	NO DATA	NO DATA
0.94	0.34	0.99	-0.48	1.11	-43.49
1.06	-14.19	NO DATA	NO DATA	0.97	-17.20
0.99	-0.16	1.04	-0.18	NO DATA	NO DATA
1.08	-6.80	1.04	-0.60	NO DATA	NO DATA
0.97	1.72	NO DATA	NO DATA	NO DATA	NO DATA
0.93	-1.01	1.03	-2.04	NO DATA	NO DATA
1.35	-14.72	1.09	-9.86	0.99	4.07
1.15	-33.67	1.00	0.00	NO DATA	NO DATA
0.99	-0.52	NO DATA	NO DATA	0.92	15.34
0.93	0.65	0.98	-0.28	NO DATA	NO DATA
0.96	-0.79	1.00	0.00	NO DATA	NO DATA

Table B10: Simplified DDC Accuracy analysis for BC, AC and AAC, note that the midpoint is assumed in each case thus the values will not be a true representation of system behavior – only an indication.

Mid Value of RANGE for typical Point MIN + (0.5)(MAX-MIN) (L/s)	BC ACTUAL Qm = (Qi - Bj)/A (L/s)	BC ERROR ABS(Mid-Act)/Act (%)	AC ACTUAL Qm = (Qi - Bj)/A (L/s)	AC ERROR ABS(Mid-Act)/Act (%)	AAC ACTUAL Qm = (Qi - Bj)/A (L/s)	ACC ERROR ABS(Mid-Act)/Act (%)
373.00	381.76	-2.3%	NO DATA	NO DATA	NO DATA	NO DATA
366.50	364.27	0.6%	370.55	-1.1%	380.02	-3.6%
272.50	272.88	-0.1%	NO DATA	NO DATA	268.63	1.4%
122.00	121.98	0.0%	NO DATA	NO DATA	123.91	-1.5%
366.50	411.00	-10.8%	372.19	-1.5%	NO DATA	NO DATA
345.00	331.97	3.9%	342.09	0.9%	325.84	5.9%
301.50	350.93	-14.1%	294.51	2.4%	290.53	3.8%
340.00	348.69	-2.5%	340.99	-0.3%	350.71	-3.1%
217.50	220.50	-1.4%	NO DATA	NO DATA	NO DATA	NO DATA
395.50	385.95	2.5%	396.56	-0.3%	NO DATA	NO DATA
299.50	302.86	-1.1%	302.50	-1.0%	NO DATA	NO DATA
107.50	107.50	0.0%	NO DATA	NO DATA	NO DATA	NO DATA
120.00	141.28	-15.1%	120.75	-0.6%	127.84	-6.1%
231.00	230.70	0.1%	232.52	-0.7%	NO DATA	NO DATA
331.50	345.72	-4.1%	331.50	0.0%	NO DATA	NO DATA
229.50	226.39	1.4%	NO DATA	NO DATA	NO DATA	NO DATA
286.50	295.27	-3.0%	296.05	-3.2%	314.35	-8.9%
236.50	243.56	-2.9%	NO DATA	NO DATA	NO DATA	NO DATA
55.50	55.25	0.5%	55.50	0.0%	125.44	-55.8%
217.50	214.15	1.6%	218.24	-0.3%	NO DATA	NO DATA
229.50	234.05	-1.9%	NO DATA	NO DATA	NO DATA	NO DATA
231.00	236.30	-2.2%	235.61	-2.0%	247.53	-6.7%
617.00	#DIV/0!	#DIV/0!	648.63	-4.9%	628.91	-1.9%
518.50	545.13	-4.9%	530.66	-2.3%	NO DATA	NO DATA
689.50	647.20	6.5%	693.89	-0.6%	NO DATA	NO DATA
248.00	265.65	-6.6%	243.36	1.9%	NO DATA	NO DATA
193.00	192.07	0.5%	NO DATA	NO DATA	144.95	33.1%
470.50	475.61	-1.1%	NO DATA	NO DATA	NO DATA	NO DATA
232.00	235.28	-1.4%	NO DATA	NO DATA	246.34	-5.8%
648.00	664.08	-2.4%	605.74	7.0%	NO DATA	NO DATA
165.00	166.66	-1.0%	NO DATA	NO DATA	NO DATA	NO DATA
188.00	193.03	-2.6%	NO DATA	NO DATA	191.77	-2.0%
227.00	226.80	0.1%	228.07	-0.5%	NO DATA	NO DATA
142.00	152.21	-6.7%	NO DATA	NO DATA	146.55	-3.1%
229.50	230.85	-0.6%	NO DATA	NO DATA	182.13	26.0%
116.50	125.49	-7.2%	116.21	0.3%	NO DATA	NO DATA
42.50	45.21	-6.0%	44.13	-3.7%	NO DATA	NO DATA
69.50	75.52	-8.0%	73.31	-5.2%	82.42	-15.7%
347.00	362.29	-4.2%	NO DATA	NO DATA	339.52	2.2%
148.00	154.54	-4.2%	146.81	0.8%	NO DATA	NO DATA
69.00	73.35	-5.9%	70.10	-1.6%	101.42	-32.0%
146.50	151.71	-3.4%	NO DATA	NO DATA	169.61	-13.6%
100.00	101.35	-1.3%	96.62	3.5%	NO DATA	NO DATA
144.50	139.82	3.3%	139.56	3.5%	NO DATA	NO DATA
127.00	129.67	-2.1%	NO DATA	NO DATA	NO DATA	NO DATA
133.50	145.03	-8.0%	131.02	1.9%	NO DATA	NO DATA
113.00	94.54	19.5%	112.79	0.2%	109.85	2.9%
127.00	139.95	-9.3%	127.00	0.0%	NO DATA	NO DATA
94.50	95.56	-1.1%	NO DATA	NO DATA	86.32	9.5%
235.50	251.81	-6.5%	239.86	-1.8%	NO DATA	NO DATA
126.50	132.74	-4.7%	126.50	0.0%	NO DATA	NO DATA

Table B11: Results from DDC Accuracy analysis for AC and AAC Trends relative to BC, note that the midpoint is assumed in each case thus the values will not be a true representation of system behavior – only an indication. These percentages refer to the Percentage improvement due to commissioning from BC to AC and from BC to AAC

IMPROVEMENT	
AC ABS(BC) - ABS(AC) ERROR (%)	AAC ABS(BC) - ABS(AAC) ERROR (%)
NO DATA	NO DATA
-0.5%	-2.9%
NO DATA	-1.3%
NO DATA	-1.5%
9.3%	NO DATA
3.1%	-2.0%
11.7%	10.3%
2.2%	-0.6%
NO DATA	NO DATA
2.2%	NO DATA
0.1%	NO DATA
NO DATA	NO DATA
14.4%	8.9%
-0.5%	NO DATA
4.1%	NO DATA
NO DATA	NO DATA
-0.3%	-5.9%
NO DATA	NO DATA
0.5%	NO DATA
1.2%	NO DATA
NO DATA	NO DATA
0.3%	-4.4%
NO DATA	NO DATA
2.6%	NO DATA
5.9%	NO DATA
4.7%	NO DATA
NO DATA	-32.7%
NO DATA	NO DATA
NO DATA	-4.4%
-4.6%	NO DATA
NO DATA	NO DATA
NO DATA	0.6%
-0.4%	NO DATA
NO DATA	3.6%
NO DATA	-25.4%
6.9%	NO DATA
2.3%	NO DATA
2.8%	-7.7%
NO DATA	2.0%
3.4%	NO DATA
4.4%	NO DATA
NO DATA	-10.2%
-2.2%	NO DATA
-0.2%	NO DATA
NO DATA	NO DATA
6.1%	NO DATA
19.3%	16.7%
9.3%	NO DATA
NO DATA	-8.4%
4.7%	NO DATA
4.7%	NO DATA

2) Degree-Day Analysis

An estimate of the energy use associated with the heating of outdoor air was completed for each of the three facilities using a variation of the degree-day method. However, there are questions about whether this approach was valid for the field research. Therefore, although the results are consistent with other data they are only discussed within the Appendix. This analysis was completed by determining the annual energy requirements for the heated air that was previously being wasted at each facility, as each of the spaces were originally over ventilated. The process is outlined in [B1] – [B4].

$$q_{O/A} = \dot{m}_{O/A} (c_p) \Delta T \quad [B1]$$

Where:

$$\begin{aligned} q_{O/A} &= \text{outdoor air energy consumption to heat the air (kJ)} \\ \dot{m}_{O/A} &= \text{mass flow rate of the outdoor air (kg/s)} \\ c_p &= \text{specific heat of air (assuming dry air) = 1.005 kJ/kg}^\circ\text{K} \\ \Delta T &= \text{temperature difference between the outdoors and indoors (}^\circ\text{K)} \end{aligned}$$

The degree-day method offers an approximation of the true energy requirements; however, several assumptions were required. For instance, it was assumed that for winter conditions the VAV systems will operate at the minimum volume flow rates (in full heating mode) while, in reality, the system is expected to operate at some intermediate value. Cooling energy required for the summer months was also neglected, which may be acceptable given that the local climate calls primarily for heating³⁹. This analysis also assumes that the main air handler will operate at the minimum O/A within each facility, where the system will naturally allow more O/A (on average) to satisfy mixed air temperature control.

$$V_{MIN} = \sum_{Terminal\#1}^N (V_{MIN,sept}) \quad [B2]$$

Where:

$$V_{MIN} = \text{sum of the minimum air volume set points for each terminal}$$

$$\Delta V_{MIN} = \left(\frac{Q_1}{Q_2} - 1.0 \right) V_{MIN} \quad [B3]$$

Where:

$$\Delta V_{MIN} = \text{minimum flow rate savings (L/s or m}^3\text{/s)}$$

³⁹ The degree-day method is not recommended for the determination of cooling loads. This is because the degree-day method cannot account for any system components that are dependent on outdoor ambient conditions. This is a serious limitation of the technique; however, for the purposes of this analysis the method remains adequate.

$$\left(\frac{Q_1}{Q_2} - 1.0 \right) = \text{the percentage over ventilation between 2 trends, for instance between the BC to AC or the BC to AAC in this analysis}$$

The minimum design O/A of 15% was used for all three of the field test locations. In this manner, the total heated air volume savings are estimated from [C4], as shown below:

$$Q_{SAVINGS} = \rho(O/A)(c_p)(DegD)\Delta V_{MIN} \quad [B4]$$

Where:

$Q_{SAVINGS}$	= energy savings due to reduced outside air (kJ)
ρ	= air density (kg/m ³)
ΔV_{MIN}	= minimum flow rate savings (L/s or m ³ /s)
O/A	= design percentage outdoor air for the space (15% at each facility)
c_p	= specific heat of air (assuming dry air) = 1.005 kJ/kg ^o K
$DegD$	= degree days, 5500 ^o K days for Edmonton, 18 ^o C, 65F Base

The determination of energy savings using the degree-day technique provides a secondary measure that can be used to quantify the improvement due to recommissioning. The results of this analysis agree quite well with the previous calculations where the recommissioning process is clearly beneficial from an energy savings perspective. The results can also be used to gauge the longevity of the calibration process in terms of an energy efficiency standpoint, which was obviously one of the chief goals of the field research. The results of the degree-day analysis are summarized in Table C12.

Table B12: Results of the Degree-Day Analysis

	Minimum Flow Rate Savings ΔV_{MIN} (L/s)		Annual Energy Savings $Q_{SAVINGS}$ (GJ)	
	BC to AC	BC to AAC	BC to AC	BC to AAC
Cross Cancer Institute 51 VAV Terminals	716	404	56.4	31.8
Timms Center for the Arts 51 VAV Terminals	769	685	60.6	54.0
Yellowhead Regional Library 17 VAV Terminals	281	405	22.1	31.9

The BC to AC and the BC to AAC trends correspond quite well; this is expected since the airflow accuracy improvements were also quite consistent. For instance, the estimated annual energy savings for the Timms Center for the Arts were ~61 GJ and ~54 GJ (a difference of only ~12%), even with an extremely long 21 month period separating the BC to AAC trend periods. This relatively simple analysis verifies that the longevity of the recommissioning process remains consistent over the range tested within this research.

Unfortunately, the degree-days analysis requires a large amount of assumptions that may (or may not) be appropriate for the field research. Therefore, the conclusions are only included as supplementary material. Although the results are very consistent with the other data (and our expectations), there are simply too many assumptions to justify the inclusion of this material within the main body of the thesis.

Appendix C

Contents: Sample Calculations and Results of Laboratory Experiments

- | | | |
|----|-------------------------------|-----|
| 1) | Summary of Laboratory Results | 146 |
|----|-------------------------------|-----|

1) Summary of Laboratory Results

The results of the laboratory experiments are presented in the following section, usually in tabular form. The results refer to the loss of sensor amplification that was measured in relation to duct geometry. The methodology for these results has been explained in the main body of the thesis but will be briefly discussed here for clarity. The flow amplification coefficients (C) were determined for several upstream duct geometries, where the flow amplification coefficient has been defined as the ratio of the VAV indicated flowrate (Q_{VAV}) divided by the true flowrate (Q_{TRUE}).

All of the results are compared to the baseline response (C_{40D}) for each of the six VAV terminals that were considered. The baseline response, as the name implies, refers to the amplification coefficients that were measured when the VAV terminal was located downstream of 40D of straight ductwork, which represents the ideal case. The baseline response was used to form linear equations that provided the amplification coefficient (C) as a function of the true flowrate (Q_{TRUE}). The linear equations, and the graphical results of the two 10" sized VAV terminals, are already presented in the main body of the report.

The graphical results for the remaining four VAV terminals are presented in Figures C1 - C4.

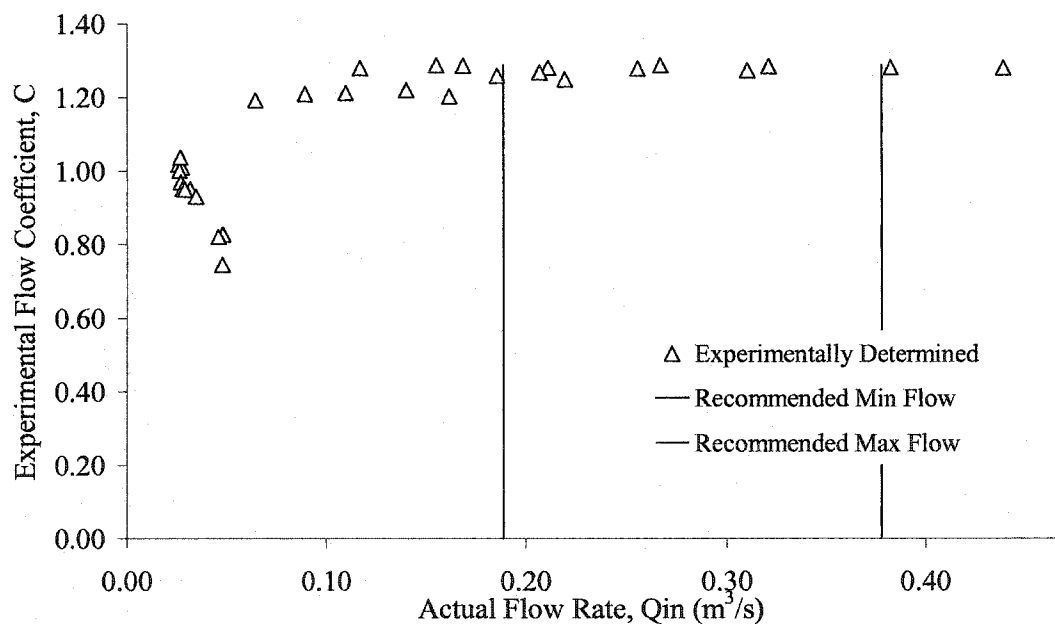


Figure C1: Baseline Response for the Type A, 8" VAV Terminal

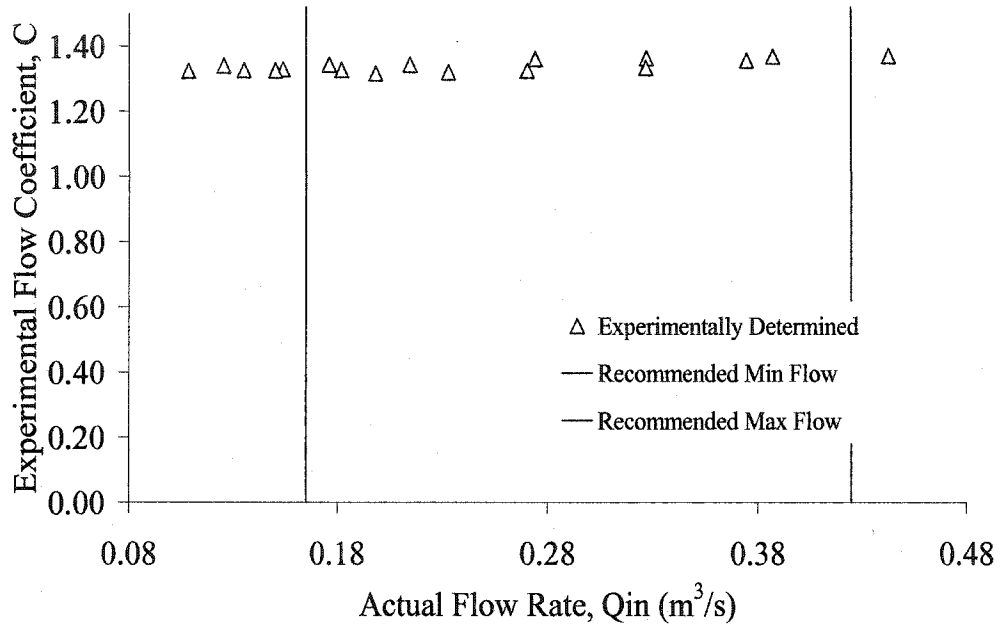


Figure C2: Baseline Response for the Type B, 8" VAV Terminal

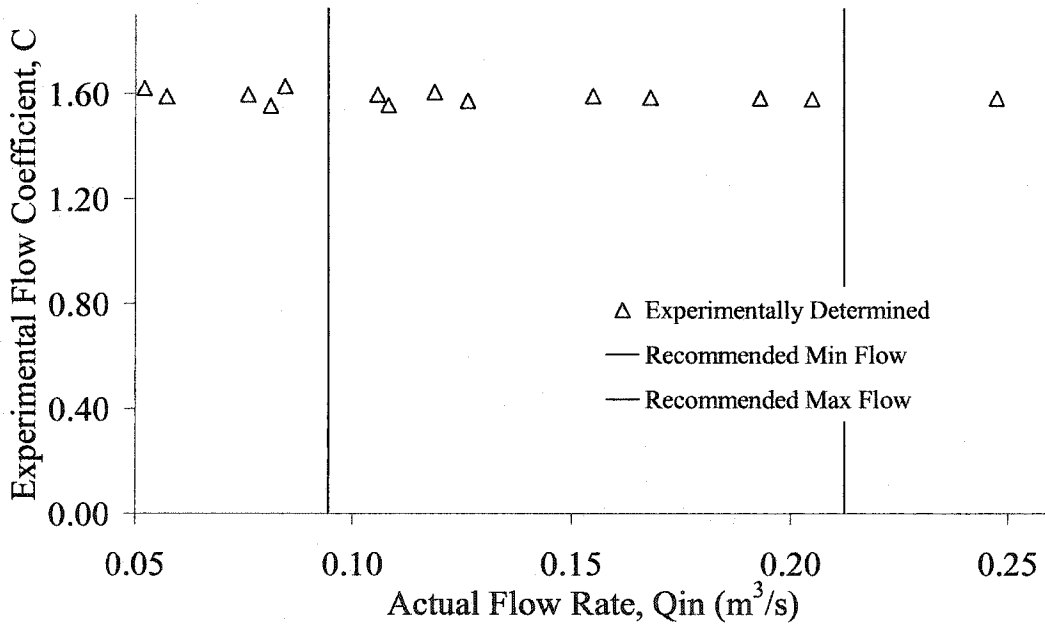


Figure C3: Baseline Response for the Type A, 6" VAV Terminal

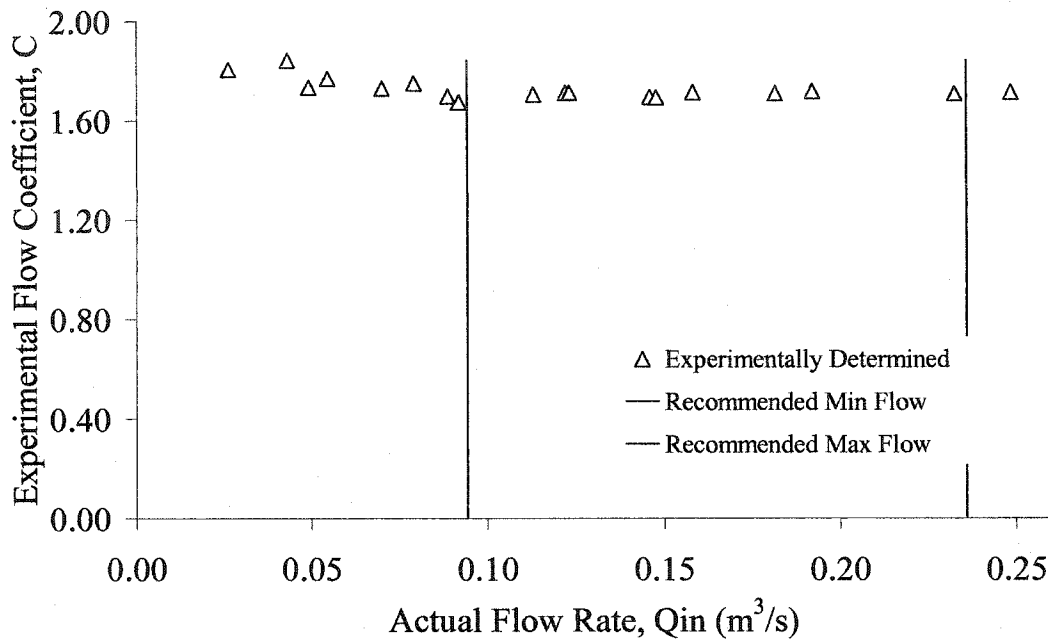


Figure C4: Baseline Response for the Type B, 6” VAV Terminal

As expected, the amplification provided between the minimum and maximum flow setpoints (recall that this is the only region of interest in this case) is remarkably constant. The linear equations that can be fitted from the data presented in the last few figures (and the 10” calibration curves that are located in the main body of the thesis) are provided in Table C1.

Table C1: Baseline Linear Equation (C_{40D}) results for Laboratory test of the VAV Terminals*

	Type “A” VAV Units		Type “B” VAV Units	
	m	b	m	b
6”	-0.195	1.607	-0.731	1.787
8”	0.227	1.220	0.058	1.322
10”	0.020	1.227	0.126	1.256

*Note that these linear equations are of the form “ $C_{40D} = m(Q_{TRUE}) + b$ ”, where C is the amplification coefficient for the 40D baseline cases and m and b are the slope and y-intercept, respectively.

In a similar manner, the average (and in this case standard deviations) for the C_{40D} values between the minimum and maximum setpoints for each terminal was determined, and provided in the main body of the thesis (the results are also presented below for clarity)

Table C2: Baseline (C_{40D}) results for Laboratory test of the VAV Terminals*

	Type "A" VAV Units		Type "B" VAV Units	
	μ of C_{40D}	σ of C_{40D}	μ of C_{40D}	σ of C_{40D}
6"	1.587	0.028	1.719	0.030
8"	1.267	0.028	1.333	0.013
10"	1.233	0.013	1.300	0.019

*Note that the C term is simply the ratio of the indicated VAV volume flow rate (Q_{VAV}) divided by the true volume flow rate (Q_{TRUE}). These are the average (μ) and standard deviations (σ) of the C values between the minimum and maximum recommended range for each VAV terminal, from the manufacturer. A low standard deviation and a high average C value are desirable.

In actuality the C_{40D} was calculated for the appropriate true flowrate (Q_{TRUE}) for every point that was considered, thus the results presented in Table C2 are only provided for interest. Thus, when a true flowrate (Q_{TRUE}) is located within the appropriate range (between the minimum/maximum flow setpoint) the linear equations are used to estimate what the C_{40D} value should be at that point (note, obviously the C_{40D} values will not change much so this may be an unnecessary step, but it was completed for the sake of completeness). The difference between the actual coefficient of amplification C and the predicted baseline response C_{40D} is determined to be ΔC , where the C_{40D} will always be the larger value (amplification, and thus the flow coefficient, is always reduced with the addition of flow obstructions).

The average ΔC between the flow setpoints is a measure of signal amplification, while the standard deviation of the ΔC is a measure of precision. The results (average and standard deviations) for each of the duct geometries and duct lengths are provided in the following tables.

Table C3: Results of two 90° Elbows: μ (Average) Values*

Size, Duct Lengths		VAV Terminal Unit Type A			VAV Terminal Unit Type B		
		C_{40D}	C	$\Delta C = (C_B - C)$	C_{40D}	C	$\Delta C = (C_B - C)$
10"	10D	1.23	1.19	0.05	1.30	1.26	0.04
	5D	1.23	1.20	0.04	1.30	1.27	0.03
	3D	1.23	1.16	0.07	1.30	1.28	0.02
	2D	1.23	1.18	0.06	1.30	1.28	0.02
8"	10D	1.27	1.25	0.02	1.33	1.31	0.02
	5D	1.27	1.24	0.03	1.33	1.35	-0.01
	3D	1.27	1.23	0.04	1.34	1.35	-0.02
	2D	1.27	1.22	0.05	1.34	1.35	-0.02
6"	10D	1.58	1.42	0.16	1.70	1.56	0.15
	5D	1.59	1.41	0.18	1.71	1.60	0.11
	3D	1.59	1.41	0.18	1.70	1.61	0.10
	2D	1.59	1.40	0.19	1.70	1.62	0.09

*A positive ΔC value indicates a loss in VAV flow signal amplification.

Table C4: Results of two 90° Elbows: σ (Standard Deviations)*

Size, Duct Lengths		VAV Terminal Unit Type A			VAV Terminal Unit Type B		
		C_{40D}	C	$\Delta C = (C - C_B)$	C_{40D}	C	$\Delta C = (C - C_B)$
10"	10D	0.002	0.035	0.033	0.009	0.034	0.025
	5D	0.002	0.039	0.037	0.009	0.038	0.029
	3D	0.002	0.094	0.092	0.009	0.042	0.033
	2D	0.002	0.068	0.066	0.010	0.039	0.029
8"	10D	0.010	0.051	0.041	0.003	0.049	0.046
	5D	0.010	0.047	0.037	0.003	0.036	0.033
	3D	0.010	0.042	0.032	0.003	0.028	0.025
	2D	0.010	0.045	0.035	0.003	0.035	0.032
6"	10D	0.004	0.052	0.048	0.013	0.053	0.040
	5D	0.004	0.087	0.083	0.013	0.044	0.031
	3D	0.004	0.062	0.058	0.014	0.051	0.037
	2D	0.004	0.111	0.107	0.014	0.056	0.042

*A positive ΔC value indicates an increased scatter (or lower precision).

Table C5: Results for the S-Shaped Geometry: μ (Average) Values*

Size, Duct Lengths	VAV Terminal Unit Type A			VAV Terminal Unit Type B			
	C_{40D}	C	$\Delta C = (C_B - C)$	C_{40D}	C	$\Delta C = (C_B - C)$	
10"	10D	1.23	1.21	0.03	1.30	1.28	0.03
	5D	1.23	1.15	0.09	1.30	1.27	0.03
	3D	1.23	1.15	0.08	1.30	1.29	0.01
	2D	1.23	1.17	0.07	1.30	1.31	-0.01
8"	10D	1.27	1.25	0.02	1.33	1.33	0.00
	5D	1.27	1.25	0.02	1.33	1.34	-0.01
	3D	1.27	1.25	0.02	1.33	1.36	-0.03
	2D	1.27	1.29	-0.02	1.33	1.37	-0.04
6"	10D	1.59	1.59	0.00	1.71	1.72	-0.01
	5D	1.59	1.58	0.01	1.72	1.71	0.01
	3D	1.59	1.58	0.01	1.72	1.70	0.02
	2D	1.59	1.56	0.03	1.72	1.72	0.00

*A positive ΔC value indicates a loss in VAV flow signal amplification.

Table C6: Results for the S-Shaped Geometry: σ (Standard Deviations)*

Size, Duct Lengths	VAV Terminal Unit Type A			VAV Terminal Unit Type B			
	C_{40D}	C	$\Delta C = (C - C_B)$	C_{40D}	C	$\Delta C = (C - C_B)$	
10"	10D	0.002	0.105	0.103	0.010	0.026	0.016
	5D	0.002	0.091	0.089	0.009	0.046	0.037
	3D	0.002	0.084	0.082	0.012	0.030	0.018
	2D	0.003	0.058	0.055	0.010	0.014	0.004
8"	10D	0.012	0.029	0.017	0.003	0.007	0.004
	5D	0.007	0.026	0.019	0.003	0.022	0.019
	3D	0.008	0.030	0.022	0.003	0.018	0.015
	2D	0.007	0.025	0.018	0.003	0.022	0.019
6"	10D	0.004	0.026	0.022	0.022	0.037	0.015
	5D	0.004	0.032	0.029	0.017	0.041	0.024
	3D	0.004	0.035	0.031	0.013	0.020	0.007
	2D	0.004	0.019	0.015	0.014	0.030	0.016

*A positive ΔC value indicates an increased scatter (or lower precision).

Table C7: Results for Concentric Reducers: μ (Average Values)*

Size, Duct Lengths	VAV Terminal Unit Type A			VAV Terminal Unit Type B			
	C_{40D}	C	$\Delta C = (C_B - C)$	C_{40D}	C	$\Delta C = (C_B - C)$	
10" to 8" Reducer	10D	1.27	1.22	0.05	1.33	1.26	0.07
	5D	1.27	1.19	0.08	1.34	1.27	0.07
	3D	1.27	1.15	0.13	1.34	1.26	0.08
	2D	1.27	1.15	0.12	1.33	1.25	0.08
10" to 6" Reducer	10D	1.58	0.98	0.59	1.68	1.06	0.61
	5D	1.58	0.99	0.58	1.68	1.03	0.65
	3D	1.58	0.94	0.64	1.68	1.03	0.65
	2D	1.58	0.96	0.62	1.68	1.06	0.62
	0D	1.58	1.00	0.58	1.67	1.03	0.64
8" to 6" Reducer	10D	1.58	1.27	0.32	1.70	1.35	0.36
	5D	1.59	1.22	0.36	1.70	1.34	0.36
	3D	1.59	1.23	0.35	1.70	1.34	0.35
	2D	1.59	1.21	0.38	1.70	1.34	0.36
	0D	1.58	1.23	0.36	1.71	1.33	0.37

*A positive ΔC value indicates a loss in VAV flow signal amplification.

Table C8: Results for Concentric Reducers: σ (Standard Deviations)*

Size, Duct Lengths	VAV Terminal Unit Type A			VAV Terminal Unit Type B			
	C_{40D}	C	$\Delta C = (C - C_B)$	C_{40D}	C	$\Delta C = (C - C_B)$	
10" to 8" Reducer	10D	0.011	0.050	0.039	0.003	0.066	0.063
	5D	0.090	0.065	-0.025	0.003	0.062	0.059
	3D	0.090	0.065	-0.025	0.003	0.071	0.068
	2D	0.010	0.052	0.042	0.003	0.056	0.053
10" to 6" Reducer	10D	0.003	0.147	0.144	0.100	0.156	0.056
	5D	0.003	0.165	0.162	0.013	0.169	0.156
	3D	0.003	0.171	0.168	0.014	0.170	0.156
	2D	0.004	0.168	0.164	0.013	0.136	0.123
	0D	0.004	0.142	0.138	0.025	0.144	0.119
8" to 6" Reducer	10D	0.005	0.084	0.079	0.019	0.090	0.071
	5D	0.005	0.120	0.115	0.019	0.098	0.079
	3D	0.005	0.120	0.115	0.020	0.090	0.070
	2D	0.004	0.142	0.138	0.016	0.095	0.079
	0D	0.005	0.117	0.112	0.015	0.076	0.061

*A positive ΔC value indicates an increased scatter (or lower precision).

Table C9: Results for Concentric Expanders: μ (Average) Values

Size, Duct Lengths	VAV Terminal Unit Type A			VAV Terminal Unit Type B			
	C_{40D}	C	$\Delta C = (C_B - C)$	C_{40D}	C	$\Delta C = (C_B - C)$	
8" to 10" Expander	10D	1.23	1.23	0.00	1.30	1.31	-0.01
	5D	1.23	1.20	0.04	1.30	1.32	-0.02
	3D	1.23	1.23	0.01	1.31	1.26	0.05
	2D	1.23	1.24	-0.01	1.30	1.36	-0.06

*A positive ΔC value indicates a loss in VAV flow signal amplification.

Table C10: Results for Concentric Expanders: σ (Standard Deviations)*

Size, Duct Lengths	VAV Terminal Unit Type A			VAV Terminal Unit Type B			
	C_{40D}	C	$\Delta C = (C - C_B)$	C_{40D}	C	$\Delta C = (C - C_B)$	
8" to 10" Expander	10D	0.002	0.035	0.033	0.011	0.038	0.027
	5D	0.002	0.084	0.082	0.010	0.037	0.027
	3D	0.002	0.074	0.072	0.010	0.090	0.080
	2D	0.002	0.070	0.068	0.008	0.043	0.035

*A positive ΔC value indicates an increased scatter (or lower precision).

Table C11: Results for Concentric Reducers (with a 90° Elbow): μ (Average) Values

Size, Duct Lengths	VAV Terminal Unit Type A			VAV Terminal Unit Type B			
	C_{40D}	C	$\Delta C = (C_B - C)$	C_{40D}	C	$\Delta C = (C_B - C)$	
10" to 8" Reducer	10D	1.27	1.13	0.14	1.34	1.16	0.18
	5D	1.28	1.16	0.12	1.34	1.16	0.17
	3D	1.28	1.13	0.15	1.34	1.20	0.14
	2D	1.27	1.13	0.14	1.34	1.17	0.16
10" to 6" Reducer	10D	1.58	0.92	0.65	1.67	0.97	0.70
	5D	1.57	0.97	0.60	1.67	1.00	0.67
	3D	1.58	0.92	0.65	1.67	1.00	0.66
	2D	1.58	0.90	0.68	1.67	1.00	0.67
8" to 6" Reducer	10D	1.59	1.24	0.35	1.70	1.32	0.38
	5D	1.58	1.25	0.33	1.71	1.31	0.39
	3D	1.58	1.27	0.32	1.71	1.32	0.38
	2D	1.58	1.24	0.34	1.70	1.33	0.38
	0D	1.58	1.26	0.33	1.70	1.32	0.39

*A positive ΔC value indicates a loss in VAV flow signal amplification.

Table C12: Results for Concentric Reducers (with a 90° Elbow): σ (Standard Deviations)

Size, Duct Lengths		VAV Terminal Unit Type A			VAV Terminal Unit Type B		
		C_{40D}	C	$\Delta C = (C - C_B)$	C_{40D}	C	$\Delta C = (C - C_B)$
10" to 8" Reducer	10D	0.008	0.062	0.054	0.003	0.097	0.094
	5D	0.010	0.042	0.032	0.003	0.099	0.096
	3D	0.011	0.074	0.063	0.002	0.060	0.058
	2D	0.009	0.069	0.060	0.003	0.087	0.084
10" to 6" Reducer	10D	0.003	0.143	0.140	0.012	0.173	0.161
	5D	0.003	0.148	0.145	0.012	0.172	0.160
	3D	0.003	0.172	0.169	0.012	0.175	0.163
	2D	0.003	0.170	0.167	0.013	0.188	0.175
8" to 6" Reducer	10D	0.004	0.123	0.119	0.018	0.115	0.097
	5D	0.005	0.116	0.111	0.018	0.115	0.097
	3D	0.005	0.096	0.091	0.021	0.101	0.080
	2D	0.005	0.113	0.108	0.021	0.105	0.084
	0D	0.005	0.115	0.110	0.020	0.098	0.078

*A positive ΔC value indicates an increased scatter (or lower precision).

Table C13: Results for Concentric Expanders (with a 90° Elbow): μ (Average) Values*

Size, Duct Lengths		VAV Terminal Unit Type A			VAV Terminal Unit Type B		
		C_{40D}	C	$\Delta C = (C_B - C)$	C_{40D}	C	$\Delta C = (C_B - C)$
8" to 10" Expander	10D	1.233	1.210	0.02	1.297	1.306	-0.01
	5D	1.233	1.223	0.01	1.298	1.328	-0.03
	3D	1.234	1.170	0.06	1.299	1.329	-0.03
	2D	1.234	1.154	0.08	1.298	1.331	-0.03
	0D	1.233	1.277	-0.04	1.292	1.351	-0.06

*A positive ΔC value indicates a loss in VAV flow signal amplification.

Table C14: Results for Concentric Expanders (with a 90° Elbow): σ (Standard Deviations)*

Size, Duct Lengths		VAV Terminal Unit Type A			VAV Terminal Unit Type B		
		C_{40D}	C	$\Delta C = (C - C_B)$	C_{40D}	C	$\Delta C = (C - C_B)$
8" to 10" Expander	10D	0.002	0.035	0.033	0.010	0.015	0.005
	5D	0.002	0.043	0.041	0.010	0.019	0.009
	3D	0.002	0.035	0.033	0.010	0.017	0.007
	2D	0.002	0.029	0.027	0.011	0.021	0.010
	0D	0.002	0.047	0.045	0.006	0.018	0.012

*A positive ΔC value indicates an increased scatter (or lower precision).

It was determined that the majority of these results are independent of "adequate" duct length, thus the ΔC values were averaged together to get a real representation of only the duct geometry. The results are provided, and discussed, in the main body of the thesis.